

# DIPLOMARBEIT / DIPLOMA THESIS

Titel der Diplomarbeit / Title of the Diploma Thesis

„Synthesis and characterization of a novel bifunctional,  
bidentate fluorescent iron chelator“

verfasst von / submitted by

Carmen Rainer

angestrebter akademischer Grad / in partial fulfilment of the requirements for the degree of

Magistra der Pharmazie (Mag.pharm.)

Wien, 2015 / Vienna, 2015

Studienkennzahl lt. Studienblatt /  
degree programme code as it appears on  
the student record sheet:

A 449

Studienrichtung lt. Studienblatt /  
degree programme as it appears on  
the student record sheet:

Diplomstudium Pharmazie

Betreut von / Supervisor:

Univ.-Prof. Dr. Gerhard F. Ecker



## Acknowledgements

First I would like to sincerely thank Univ.-Prof. Dr. Gerhard F. Ecker from the University of Vienna for establishing the contact to Prof. Hider and thereby giving me the opportunity to work on this research project at King's College London (KCL). I appreciate very much that he encouraged me from the very beginning in my idea to go abroad and that he supervised my thesis.

Likewise, I am deeply grateful to Prof. Robert C. Hider from the Medicinal Chemistry group of the Institute of Pharmaceutical Sciences of KCL for accepting me as a member of his working group. I greatly enjoyed my work, the academic atmosphere and the weekly talks at KCL. It was a unique chance to experience this scientific environment, where I was able to acquire plenty of knowledge in synthetic and analytical chemistry during these 5.5 months.

A very special thank you goes to Dr. Vincenzo Abbate for his constant support and encouragement during my stay in London. Due to his creative and patient disposition he was the best supervisor I could have gotten throughout my project at KCL. I would like to thank him for introducing me into synthetical work and HPLC, MS, UV/Vis and fluorescence analysis. Furthermore I would especially like to thank him for bringing my NMR samples to Brittainia house. He was always there for me when I needed help and took the time to answer all my questions.

Moreover, I would like to express my gratitude to Dr. Yu-Lin Chen for determining the  $pK_a$  and  $pFe^{3+}$  values for me, which I could not obtain myself, as he was not present at KCL during my stay. I also want to thank PhD student Cinzia Imberti for introducing me into the use of the microwave reactor at St. Thomas' Hospital Campus of KCL. I am very grateful to my Erasmus coordinator from the University of Vienna, Ass.Prof.Dr. Iris Stappen, for providing me the Erasmus placement and scholarship at KCL.

Above all, I would like to express my deep gratitude to my parents and sisters for their continuous and unconditional love and support throughout my studies and my stay at KCL. Furthermore, I would like to thank my friends and study colleagues in Vienna for our mutual moral support. I would particularly like to thank the new friends I made in London for making my stay there as enjoyable and memorable as it was.



# Table of Contents

Acknowledgements .....	i
Table of Contents .....	iii
Abstract .....	vii
Zusammenfassung.....	viii
1. Introduction.....	1
1.1. Iron .....	1
1.2. Iron metabolism .....	2
1.3. Diseases with iron overload .....	3
1.3.1. Neurodegenerative disorders (ND) .....	3
1.3.1.1. Alzheimer's disease (AD) .....	3
1.3.1.2. Parkinson's disease (PD).....	4
1.3.1.3. Amyotrophic Lateral Sclerosis (ALS) .....	5
1.3.1.4. Huntington's disease (HD).....	5
1.3.1.5. Friedreich's ataxia (FA) .....	6
1.3.2. Diseases not involving neurodegeneration .....	6
1.3.2.1. Primary or hereditary haemochromatosis (HH) .....	6
1.3.2.2. Secondary hemochromatosis .....	7
1.4. Iron Chelators .....	7
1.5. Design of Iron Chelators .....	8
1.5.1. Deferrioxamine B (Deferoxamine, DFO, Desferal <sup>®</sup> ) .....	9
1.5.2. Hydroxypyridinones (HPOs).....	10
1.5.3. Deferiprone (DFP, CP 20, L1, Ferriprox <sup>®</sup> ) .....	10
1.5.4. Deferasirox (ICL670, Exjade <sup>®</sup> ).....	11
1.6. Fluorescence based methods.....	11
2. Overview Statement.....	13
3. Synthesis of fluorescent chelators .....	14
3.1. Synthetic schemes .....	14
3.1.1. Synthesis of 5-benzyloxy-2-hydroxymethyl-4H-pyran-4-one (Compound CR 0) .....	15
3.1.2. Synthesis of 5-(benzyloxy)-4-oxo-4H-pyran-2-carboxylic acid; 3-hydroxy-protected comenic acid (Compound CR 4).....	16
3.1.3. Synthesis of 2-(2-aminoethyl)-7-(benzyloxy)-3,4-dihydro-2H-pyrido[1,2-a]pyrazine-1,8-dione (Compound CR 6).....	17

3.1.4. Synthesis of 2-(2-aminoethyl)-7-hydroxy-3,4-dihydro-2H-pyrido[1,2-a]pyrazine-1,8-dione (Compound CR 19).....	19
3.1.5. Synthetic schemes of the attempts of forming the hexadentate, fluorescent iron chelator .....	21
3.1.5.1. Attempted synthesis of N1,N7-bis(2-(7-(benzyloxy)-1,8-dioxo-1,3,4,8-tetrahydro-2H-pyrido[1,2-a]pyrazin-2-yl)ethyl)-4-(3-((2-(7-(benzyloxy)-1,8-dioxo-1,3,4,8-tetrahydro-2H-pyrido[1,2-a]pyrazin-2-yl)ethyl)amino)-3-oxopropyl)-4-(3-(1,3-dioxoisindolin-2-yl)propanamido)heptanediamide (Compound CR 8)	23
3.1.5.2. Attempted synthesis of 4-(3-aminopropanamido)-N1,N7-bis(2-(7-(benzyloxy)-1,8-dioxo-1,3,4,8-tetrahydro-2H-pyrido[1,2-a]pyrazin-2-yl)ethyl)-4-(3-((2-(7-(benzyloxy)-1,8-dioxo-1,3,4,8-tetrahydro-2H-pyrido[1,2-a]pyrazin-2-yl)ethyl)amino)-3-oxopropyl)heptanediamide (Compound CR 11) .....	25
3.1.5.3. Synthesis of di-tert-butyl 4-acetamido-4-(3-(tert-butoxy)-3-oxopropyl)heptanedioate (Compound CR 14).....	26
3.1.5.4. Synthesis of 4-acetamido-4-(2-carboxyethyl)heptanedioic acid (Compound CR 15) .....	28
3.1.5.5. Attempted synthesis of 4-acetamido-N1,N7-bis(2-(7-(benzyloxy)-1,8-dioxo-1,3,4,8-tetrahydro-2H-pyrido[1,2-a]pyrazin-2-yl)ethyl)-4-(3-((2-(7-(benzyloxy)-1,8-dioxo-1,3,4,8-tetrahydro-2H-pyrido[1,2-a]pyrazin-2-yl)ethyl)amino)-3-oxopropyl)heptanediamide (Compound CR 16) .....	29
3.1.5.6. Attempted synthesis of 4-acetamido-N1,N7-bis(2-(7-hydroxy-1,8-dioxo-1,3,4,8-tetrahydro-2H-pyrido[1,2-a]pyrazin-2-yl)ethyl)-4-(3-((2-(7-hydroxy-1,8-dioxo-1,3,4,8-tetrahydro-2H-pyrido[1,2-a]pyrazin-2-yl)ethyl)amino)-3-oxopropyl)heptanediamide (CR 17) .....	31
3.2. Synthetic Details .....	33
3.2.1. Synthesis of 5-Benzyloxy-2-hydroxymethyl-4H-pyran-4-one (Compound CR 0) .....	33
3.2.2. Synthesis of 5-(benzyloxy)-4-oxo-4H-pyran-2-carboxylic acid; 3-hydroxy-protected comenic acid (Compound CR 4).....	33
3.2.3. Synthesis of 2-(2-aminoethyl)-7-(benzyloxy)-3,4-dihydro-2H-pyrido[1,2-a]pyrazine-1,8-dione (Compound CR 6).....	34
3.2.4. Synthesis of 2-(2-aminoethyl)-7-hydroxy-3,4-dihydro-2H-pyrido[1,2-a]pyrazine-1,8-dione (Compound CR 19).....	35
3.2.5. Synthetic details of the attempts of forming the hexadentate, fluorescent iron chelator.....	37
3.2.5.1. Attempted synthesis of N1,N7-bis(2-(7-(benzyloxy)-1,8-dioxo-1,3,4,8-tetrahydro-2H-pyrido[1,2-a]pyrazin-2-yl)ethyl)-4-(3-((2-(7-(benzyloxy)-1,8-dioxo-1,3,4,8-tetrahydro-2H-pyrido[1,2-a]pyrazin-2-yl)ethyl)amino)-3-oxopropyl)-4-(3-(1,3-dioxoisindolin-2-yl)propanamido)heptanediamide (Compound CR 8)	37
3.2.5.2. Attempted synthesis of 4-(3-aminopropanamido)-N1,N7-bis(2-(7-(benzyloxy)-1,8-dioxo-1,3,4,8-tetrahydro-2H-pyrido[1,2-a]pyrazin-2-yl)ethyl)-4-(3-((2-(7-(benzyloxy)-1,8-dioxo-1,3,4,8-tetrahydro-2H-pyrido[1,2-a]pyrazin-2-yl)ethyl)amino)-3-oxopropyl)heptanediamide (Compound CR 11) .....	38
3.2.5.3. Synthesis of di-tert-butyl 4-acetamido-4-(3-(tert-butoxy)-3-oxopropyl)heptanedioate (Compound CR 14).....	39
3.2.5.4. Synthesis of 4-acetylamido-4-(2-carboxyethyl)heptanedioic acid (Compound CR 15).....	40

3.2.5.5. Attempted synthesis of 4-acetamido-N1,N7-bis(2-(7-(benzyloxy)-1,8-dioxo-1,3,4,8-tetrahydro-2H-pyrido[1,2-a]pyrazin-2-yl)ethyl)-4-(3-((2-(7-(benzyloxy)-1,8-dioxo-1,3,4,8-tetrahydro-2H-pyrido[1,2-a]pyrazin-2-yl)ethyl)amino)-3-oxopropyl)heptanediamide (Compound CR 16) .....	40
3.2.5.6. Attempted synthesis of 4-acetamido-N1,N7-bis(2-(7-hydroxy-1,8-dioxo-1,3,4,8-tetrahydro-2H-pyrido[1,2-a]pyrazin-2-yl)ethyl)-4-(3-((2-(7-hydroxy-1,8-dioxo-1,3,4,8-tetrahydro-2H-pyrido[1,2-a]pyrazin-2-yl)ethyl)amino)-3-oxopropyl)heptanediamide (CR 17) .....	41
4. Characterization of 2-(2-aminoethyl)-7-hydroxy-3,4-dihydro-2H-pyrido[1,2-a]pyrazine-1,8-dione (Compound CR 19).....	42
4.1. Basic physicochemical properties .....	44
4.2. High Resolution Mass Spectrometry (HRMS) .....	45
4.3. Nuclear Magnetic Resonance (NMR) .....	47
4.3.1. <sup>1</sup> H-NMR.....	47
4.3.2. <sup>13</sup> C-NMR .....	49
4.4. High Performance Liquid Chromatography (HPLC) .....	51
4.5. UV/Vis spectroscopy.....	52
4.5.1. UV/Vis spectrum.....	52
4.5.2. Molar Extinction Coefficient.....	53
4.6. Fluorescence emission spectroscopy .....	55
4.7. Fluorescence quenching by iron.....	57
4.8. Recording of Fluorescence quantum yield ( $\phi_F$ ).....	59
4.9. pK <sub>a</sub> (ionization constants) .....	65
4.10. pFe <sup>3+</sup> determination.....	66
5. Analytical and Chemicals .....	67
5.1. High performance liquid chromatography (HPLC) .....	67
5.2. Electrospray Ionisation Mass Spectrometry (ESI-MS) .....	67
5.3. Chromatography.....	67
5.4. Nuclear Magnetic Resonance (NMR) .....	67
5.5. High resolution Mass spectrometry (HRMS) .....	68
5.6. UV/Vis spectrometry .....	68
5.7. Fluorescence Emission.....	68
5.8. pK <sub>a</sub> and iron stability constant determinations .....	68
5.9. Chemicals.....	68
6. Discussion .....	69
Appendix.....	I
Table of Images .....	I

Table of Formulas .....	I
Table of Tables: Characterization of 2-(2-aminoethyl)-7-hydroxy-3,4-dihydro-2H-pyrido[1,2-a]pyrazine-1,8-dione .....	I
Table of Figures: Characterization of 2-(2-aminoethyl)-7-hydroxy-3,4-dihydro-2H-pyrido[1,2-a]pyrazine-1,8-dione .....	I
Table of Equitations .....	II
Table of Schemes .....	II
Table of Selected Data .....	IV
MS selected data .....	VI
HRMS selected data .....	IX
NMR selected data .....	XI
HPLC selected data .....	XIX
References .....	XXII
List of Abbreviations .....	XXV
Curriculum Vitae .....	XXVII
To Whom It May Concern by Professor R.C. Hider .....	XXIX



## Abstract

The element iron is essential and indispensable for the correct function of all living cells. But elevated levels of body iron cause serious clinical problems which can be largely prevented by the administration of iron-specific chelators. Thus the design of an orally active, nontoxic, selective iron chelator is one of the goals of the medicinal chemistry group at KCL.

At present they are developing novel iron-chelators for monitoring and adjusting the excess labile iron pool in mitochondria. Recently 10 novel bidentate, iron specific fluorescent probes, where the fluorescent moiety is merged with the chelating entity of the molecule, have been described.

The aim of this Diploma thesis project was to synthesize a compound similar to those mentioned but with a primary amine functional group. It was fully characterized of its physicochemical properties and I could ascertain that it is a fluorescent, bidentate iron chelator.

The starting material of the chelator synthesis was commercially available kojic acid, which was first benzyl-protected in the 5-OH position to 5-benzyloxy-2-hydroxymethyl-4H-pyran-4-one and then oxidized in the 2-OH position to a carboxylic functional group to obtain 5-(benzyloxy)-4-oxo-4H-pyran-2-carboxylic acid. The pyranone was then converted to the bicyclic pyrazine 2-(2-aminoethyl)-7-(benzyloxy)-3,4-dihydro-2H-pyrido[1,2-a]pyrazine-1,8-dione via an amine insertion reaction. The final step was then to deprotect the molecule from the benzyl group via hydrogenation with 10% Pd/C (w/w), in order to obtain the bicyclic, fluorescent, bidentate chelator 2-(2-aminoethyl)-7-hydroxy-3,4-dihydro-2H-pyrido[1,2-a]pyrazine-1,8-dione.

The compound was fully characterized of its physicochemical properties: NMR, HRMS, HPLC, UV/Vis Spectroscopy, Molar extinction coefficient, Fluorescence emission spectroscopy, Fluorescence quenching by iron, Fluorescence quantum yield and the clogP. The results corresponded with similarly synthesized chelators.

The amine functional group of the iron chelator provides us the advantage of later coupling it to peptides or tripodal carboxylic acids to form a very strong hexadentate, iron chelator which fluoresces by itself. This kind of chelator has not been published yet. However, this last step could only be partially achieved due to the limited time available for my project. In future work the chemists at the department of Medicinal Chemistry of KCL will continue to modify the conditions of this last reaction.

## Zusammenfassung

Eisen ist ein essentielles Element, um das Funktionieren aller lebenden Zellen zu gewährleisten. Eisenüberschuss stellt aber ein schwerwiegendes Problem dar und kann mit eisenspezifischen Chelatverbindungen verhindert werden. Das Design eines oralen, aktiven, nicht toxischen, selektiven Chelatbildners ist eines der Ziele der Forschungsgruppe der pharmazeutischen Chemie am King's College London.

Im Moment arbeiten sie an der Entwicklung neuer chelatbildender Verbindungen, um labiles Eisen in Mitochondrien nachzuweisen und überschüssiges Eisen zu binden. Vor kurzem wurden 10 neue zweibindige, eisenspezifische Moleküle, in denen der sich die fluoreszierende und der chelatbildende Teil vereinigen, publiziert.

Das Ziel dieser Diplomarbeit war es, eine dazu ähnliche Verbindung zu synthetisieren, die zusätzlich noch ein primäres Amin als funktionelle Gruppe trägt. Das Molekül wurde dann physikalisch-chemisch charakterisiert, und es wurde bestätigt, dass es sich um einen fluoreszierenden, zweibindigen Eisenchelatkomples handelt.

Das Edukt der Chelatkomplexsynthese war kommerziell verfügbare Kojisäure, deren OH Gruppe in Position 5 im ersten Schritt mit einer Benzylgruppe geschützt wurde um 5-benzyloxy-2-hydroxymethyl-4H-pyran-4-on zu erhalten. Danach wurde die OH Gruppe in Position 2 zu einer Carbonsäure umgewandelt, 5-(benzyloxy)-4-oxo-4H-pyran-2-carboxylsäure, wurde synthetisiert. Das Pyranon wurde dann über ein eingefügtes Amin zum bityklischen Pyrazin 2-(2-aminoethyl)-7-(benzyloxy)-3,4-dihydro-2H-pyrido[1,2-a]pyrazine-1,8-dion umgesetzt. Der letzte Schritt bestand darin, die schützende Benzylgruppe über Hydrolyse mit 10% Pd/C (w/w) vom Molekül abzuspalten, um die fluoreszierende, bityklische, zweibindige Chelatverbindung 2-(2-aminoethyl)-7-hydroxy-3,4-dihydro-2H-pyrido[1,2-a]pyrazine-1,8-dion zu erhalten.

Diese wurde dann vollständig physikochemisch via NMR, HRMS, HPLC, UV/Vis Spektroskopie, Molaren Extinktionskoeffizienten, Fluoreszenzemissionsspektroskopie, Fluoreszenzlöschung über Eisen, Fluoreszenzquantenausbeute und clogP charakterisiert. Die Ergebnisse korrespondieren mit zuvor ähnlich synthetisierten Chelatkomplexen.

Die funktionelle Amingruppe der Verbindung ermöglicht es uns, später über drei Amidbindungen mit einer dreifüßigen Carbonsäure einen sehr starken sechsbindigen, selbst fluoreszierenden Chelatkomplex herzustellen. Diese Art von Chelatkomplex wurde bisher noch nicht publiziert. Dieser letzte Schritt konnte aufgrund der begrenzten Zeit die ich im Labor des KCL zur Verfügung hatte leider nicht vollständig abgeschlossen werden. Chemiker des Departements für Pharmazeutische Chemie am KCL werden die Reaktionsbedingungen in Zukunft optimieren.

# 1. Introduction

Iron is an indispensable metal for the proper biochemical function of all living cells (Liu & Hider, 2002a), but iron overload is a serious clinical condition (Oshiro, Morioka, & Kikuchi, 2011):

Many forms of neurodegenerative diseases, as for example Alzheimer's Disease, Parkinson's Disease, Friederich's Ataxia (Hider, Roy, Ma, Le Kong, & Preston, 2011) and Huntington's Disease (Jomova & Valko, 2011) are linked to elevated levels of iron (Hider et al., 2011). Besides, the most common hereditary disease hemochromatosis, different types of cancer, Fanconi anaemia, Stroke and Aging are associated with excess of iron (Jomova & Valko, 2011).

Thus a logical way of therapy for this diseases is to remove the toxic levels of iron by selective chelation (Hider et al., 2011). The search for a suitable iron chelator has been one of the main goals of medicinal chemists over the past 25 years (Liu, Kayyali, Hider, Porter, & Theobald, 2002).

## 1.1. Iron

The chemical element iron (Fe) plays an essential role in mammalian cells for fundamental biochemical activities such as haemoglobin synthesis of erythrocytes, oxidation–reduction reactions, cellular proliferation (Kohgo, Ikuta, Ohtake, Torimoto, & Kato, 2008), oxygen transport, energy metabolism and DNA synthesis (Oshiro et al., 2011). The majority of iron in mammals is associated with proteins in the form of haem. The most abundant haemoproteins are the oxygen transport proteins haemoglobin and myoglobin, where oxygen forms complexes with the iron of the haem. Other haemoproteins include cytochromes and enzymes (Papanikolaou & Pantopoulos, 2005)

The most abundant transition metal in cellular systems (Fakih et al., 2008) is present in the body with a total amount of normally 3 to 4 g (Gattermann, 2009). Due to its redox activity it can serve both as an electron donor and acceptor (Altamura & Muckenthaler, 2009). Within its wide range of oxidation states in living organisms, iron is present predominantly in its reduced, called ferrous ( $\text{Fe}^{2+}$ ) and its oxidized, ferric ( $\text{Fe}^{3+}$ ) oxidation state, and less frequently in the oxidation state  $\text{Fe}^{4+}$  (Jomova & Valko, 2011). These chemical properties characterize the element as highly versatile in numerous biological functions but can also lead to toxicity if iron is unshielded (non-protein bound) (Altamura & Muckenthaler, 2009). Elevated levels of excess free ferrous iron are oxidized to ferric iron according to the Fenton reaction (see Equation 1) and catalyse the decomposition of hydrogen peroxide to produce reactive oxygen species (ROS) and the free,

highly reactive hydroxyl radical ( $\text{OH}^\cdot$ ) (Altamura & Muckenthaler, 2009; Jomova & Valko, 2011). They are dangerous and induce serious damage to membrane lipids, proteins and nucleic acids (Jomova & Valko, 2011).



**Equation 1 Fenton reaction (Altamura & Muckenthaler, 2009)**

Iron deficiency as in iron deficiency anaemia is also a common clinical problem. In this case the main reasons for the diseases are increased requirements during growth and pregnancy, unbalanced diet, malabsorption or the chronic loss of blood (Camaschella & Strati, 2010).

As iron excess and deficiency are equally detrimental for cells, under normal iron homeostasis conditions biological systems have evolved protection mechanisms to ensure a tightly regulated iron balance with hardly any free intracellular iron capable of participating in catalytic reactions (Altamura & Muckenthaler, 2009; Jomova & Valko, 2011).

## **1.2. Iron metabolism**

Iron metabolism in humans is highly conservative: iron homeostasis is above all regulated by its absorption and the greater part of it is being recycled within the human body, where iron storage, transport and distribution are tightly controlled (Liu & Hider, 2002a). An average daily diet contains about 15 mg of iron, of which healthy humans absorb 1 to 2 mg, which compensates the nonspecific amount of iron lost (Papanikolaou & Pantopoulos, 2005) due to sweat and in shed cutaneous and mucosal epithelial cells (Gattermann, 2009). Mammals lack a physiological mechanism for eliminating iron (Liu & Hider, 2002a), but women lose iron via menstruation (Papanikolaou & Pantopoulos, 2005).

Under physiological conditions, extracellular iron in circulation is usually bound to the plasma iron carrier protein transferrin (Tf), which renders it soluble and nontoxic (Papanikolaou & Pantopoulos, 2005). The level of free, unsaturated protein is controlled by body iron levels: usually only a third of the circulating transferrin binds to iron, which allows it to buffer higher levels of the metal (Gkouvatsos, Papanikolaou, & Pantopoulos, 2012). The transferrin-iron complex then binds to the transferrin receptor 1 (TfR1) and undergoes endocytosis. The iron storage protein ferritin detoxifies excess levels of iron by sequestration (Papanikolaou & Pantopoulos, 2005). Iron responsive elements (IRE) regulate the expression of ferritin and TfR1 (Liu and Hider 2002).

Iron overload saturates the binding capacity of the carrier protein and makes iron circulate as non-Tf-bound iron (NTBI) which leads to the production of ROS and organ damage. The labile plasma iron (LPI), a biologically active fraction of free iron, is the most toxic of the NTBI fractions: it possesses cytotoxic and carcinogenic activity (Kohgo et al., 2008).

The peptide Hepcidin regulates the body iron level by inhibiting both the iron absorption in the intestine and the reticulo-endothelial iron liberation. It is synthesized in the liver, where production is boosted in the presence of excess levels of iron and inflammation (Kohgo, Ikuta, Ohtake, Torimoto, & Kato, 2008).

### **1.3. Diseases with iron overload**

In humans iron overload becomes critical with iron levels above 7 mg/g dry liver weight (Kohgo et al., 2008). As mentioned above, different neurodegenerative diseases are associated with elevated levels of poorly ligated redox active iron, which leads to iron induced oxidative stress (Jomova & Valko, 2011; Papanikolaou & Pantopoulos, 2005). Oxidative stress is triggered by an imbalance between the production of free radicals and the defective antioxidant and detoxifying capacities of cells (Hider et al., 2011). As a consequence of this imbalance, oxidatively modified molecules accumulate and therefore promote neuronal death and neurodegeneration (Hider et al., 2011).

#### **1.3.1. Neurodegenerative disorders (ND)**

Neurodegenerative disorders are characterized by similar pathological conditions as, on the one hand, abnormal protein components and aggregation of these in the brain leading to selective loss of neurons and, on the other, oxidative stress, which have both a connection with metal ions (Hider, Ma, Molina-Holgado, Gaeta, & Roy, 2008; Molina-Holgado, Hider, Gaeta, Williams, & Francis, 2007).

##### **1.3.1.1. Alzheimer's disease (AD)**

Alzheimer's disease is worldwide the most frequent neurodegenerative disorder, followed by Parkinson disease (Gille & Reichmann, 2011). Advanced age is the main risk factor for this slowly progressive disease of the brain. It is characterized by impairment of memory, in generally disturbances in thinking and perception disorders. The classical pathological feature of AD is

increased formation of aggregates of insoluble beta-amyloid protein (amyloid- $\beta$ ) which triggers neuritic degradation (Oshiro et al., 2011). This protein possesses a high affinity for iron and other transition metals, which is shown by an increase in the metal concentration within the plaques compared to the surrounding tissue (Jomova & Valko, 2011). The toxicity of this preventive brain lipoprotein antioxidant is predominantly linked to the presence of these redox active metals (Jomova & Valko, 2011). The second hallmark of the disease are neurofibrillary tangles (NFTs) in the cortex of AD brains, where the redox active iron levels are also elevated. They are precipitates or aggregates of hyperphosphorylated tau protein, to which ferric iron is bound and which is reduced to the ferrous form, which induces NFT production. The amyloid- $\beta$  precursor protein (APP) is a type I transmembrane protein and expressed ubiquitously in cells. It possesses IRE, and a domain of APP has ferrioxidase activity which suggests an association between iron metabolism and AD. Iron mediated oxidative stress causes APP misregulation, which could be the underlying cause of AD. Inflammatory responses within the brain could be another reason for the development of AD, as APP and ceruloplasmin are regulated by proinflammatory cytokines (Oshiro et al., 2011).

### **1.3.1.2. Parkinson's disease (PD)**

The main clinical symptoms of patients with PD are tremors in hands and feet, postural instability (Oshiro et al., 2011), bradykinesia, dyskinesia and rigidity (Altamura & Muckenthaler, 2009). These symptoms are caused by selective dopaminergic neuronal cell death in the pars compacta of the substantia nigra (SN) (Altamura & Muckenthaler, 2009) and an increase in acetylcholine levels in the striatum (Oshiro et al., 2011).

At the beginning of the disease, glutathione depletes dramatically in the SN, which causes a selective decrease in mitochondrial complex I activity and a reduced overall mitochondrial function (Jomova, Vondrakova, Lawson, & Valko, 2010). This happens via thiol oxidation of critical residues within the complex itself and causes the aggregation of the presynaptic soluble protein alpha-synuclein, which promotes dopaminergic neuronal cell death (Jomova & Valko, 2011).

The major neuropathological hallmark are Lewy bodies, intracytoplasmic, eosinophilic proteinaceous inclusions which form in the SN and consist mainly of phosphorylated  $\alpha$ -synuclein (Altamura & Muckenthaler, 2009; Oshiro et al., 2011). Excess iron deposition which has been found in dopaminergic neurons within SN, triggers the aggregation of toxic  $\alpha$ -synuclein and causes cellular dysfunction via the generation of hydroxyl radicals by the Fenton reaction (Oshiro

et al., 2011). Studies with pathologic material of PD brains confirm that different molecules as lipids, proteins and DNA undergo oxidative damage (Cacciatore, Baldassarre, Fornasari, Mollica, & Pinnen, 2012; Gaeta & Hider, 2005). As iron is normally stored within ferritin it does not cause oxidative damage, but an inappropriately low level of the protein and an increase of free ferrous iron contributes to the formation of oxidative stress (Altamura & Muckenthaler, 2009).

The pigment neuromelanin is also synthesized in dopaminergic neurons (Altamura & Muckenthaler, 2009), forms stable complexes with iron and might be neuroprotective. When melanin pigments decrease in SN in advanced age, it is important to chelate iron to protect neurons (Oshiro et al., 2011).

### **1.3.1.3. Amyotrophic Lateral Sclerosis (ALS)**

Amyotrophic Lateral Sclerosis is also linked to elevated iron levels in the central nervous system, which causes oxidative stress and inflammations. In ALS patients the most frequently reported hallmark is the gene mutation of the enzyme superoxide dismutase 1 (SOD1), a free radical scavenger which catalyzes the conversion of  $O_2^-$  to  $O_2$  and  $H_2O_2$ . As a consequence, the dysfunctional enzyme leads to an increase in cellular oxidative stress via the imbalance between free radicals and ions. Furthermore, an increased risk for ALS is also associated with the human ataxia type 2 (ATXN2) gene. It is a polyglutamine disease gene and mutated in spinocerebellar ataxia type 2. Some ALS patients show expansion of CAG repeat sequences in the ATXN2 gene (Oshiro et al., 2011).

### **1.3.1.4. Huntington's disease (HD)**

Huntington's Disease is a neurodegenerative genetic disorder (Jomova & Valko, 2011) which is inherited in an autosomal, dominant way (Hersch & Rosas, 2008). It is caused by CAG expansion, a polyglutamine tract near the N-terminus of the huntingtin protein (Hersch & Rosas, 2008), which results in an aberrant protein due to abnormal folding and fibrillary aggregation (Jomova & Valko, 2011). These Huntingtin inclusion bodies are targets of oxidative stress (Jomova & Valko, 2011). HD influences above all muscle coordination or chorea and leads to neurodegeneration (Jomova & Valko, 2011), progressive emotional and motor disturbances and weight loss (Hersch & Rosas, 2008).

### **1.3.1.5. Friedreich's ataxia (FA)**

A hallmark of Friedreich's ataxia is the loss of sensory neurons e.g. of the spinal cord and the dorsal root ganglia (Altamura & Muckenthaler, 2009), which is demonstrated by impaired muscle coordination (ataxia) (Jomova & Valko, 2011), cardiomyopathy and progressive neurological disability (Gille & Reichmann, 2011) and therefore movement disorder (Altamura & Muckenthaler, 2009).

In the majority of cases the disease is caused by a GAA trinucleotide repeat expansion in the first intron of the frataxin (FXN) gene (Gille & Reichmann, 2011) on chromosome 9 that codes for the gene (Jomova & Valko, 2011) and results in lower FXN mRNA expression (Altamura & Muckenthaler, 2009). Frataxin resides in mitochondria where the iron level is elevated in Friedreich's ataxia patients (Altamura & Muckenthaler, 2009; Jomova & Valko, 2011). It functions as an iron chaperone protein responsible for the safe insertion of ferrous iron during the compilation of iron-sulphur clusters in the mitochondrial respiratory chain (Jomova & Valko, 2011). In FA a defect and decrease of the [Fe-S] cluster leads to the accumulation and liberation of mitochondrial iron and therefore oxidative damage (Altamura & Muckenthaler, 2009; Boddaert et al., 2007) through formation of hydroxyl radicals via the Fenton reaction (Jomova & Valko, 2011).

### **1.3.2. Diseases not involving neurodegeneration**

Systemic elevation of body iron leads to haemochromatosis, which is generally marked as a disease with excess iron storage. Consequently the protein serum transferrin is saturated and ferritin levels increase (Beutler, Hoffbrand, & Cook, 2003). A classification into primary and secondary hemochromatosis can be made (Kohgo et al., 2008).

#### **1.3.2.1. Primary or hereditary haemochromatosis (HH)**

Primary or hereditary haemochromatosis is an autosomal recessive iron metabolism disorder with inappropriately high absorption of dietary iron causing iron overload (Gattermann, 2009; Papanikolaou & Pantopoulos, 2005). In the most common genetic disease the abnormal uptake of iron leads to tissue and organ damage derived from free radicals via iron accumulation (Jomova & Valko, 2011; Papanikolaou & Pantopoulos, 2005). HH is a genetically heterogeneous disorder where the suppression of the hepcidin pathway is clearly a common pathogenetic



event. The majority of the cases are attributed to mutations in the HFE gene located on chromosome 6 (Papanikolaou & Pantopoulos, 2005). Hepcidin deficiency or ferroportin resistance to hepcidin lead to increased iron absorption and progressive systemic iron accumulation (Gkouvatsos et al., 2012). This leads to skin hyperpigmentation, fibrosis and cirrhosis of the liver, hypogonadism, arthritis, arthralgia, diabetes mellitus, hepatocellular cancer and cardiac failure (Gkouvatsos et al., 2012; Papanikolaou & Pantopoulos, 2005).

### **1.3.2.2. Secondary hemochromatosis**

Secondary hemochromatosis can arise in many hereditary or acquired disorders (Gattermann, 2009) as a result of chronic blood transfusions in the treatment of various anemias (Papanikolaou & Pantopoulos, 2005). Every milliliter of erythrocytes that is transfused adds about 1 mg of iron to the recipient's organism (Papanikolaou & Pantopoulos, 2005). Each unit of donated blood (400 mL) contains 200 to 250 mg of iron, which corresponds to the total normal intestinal intake over a period of about 6 months. In erythrocytes iron is bound to the haem pigment. During the process of breaking down by the macrophage system, iron is freed and stored in the body (Gattermann, 2009). As the normal daily loss of iron and cell sloughing in the skin and the intestine is only about 1 mg (Papanikolaou & Pantopoulos, 2005), a single unit of erythrocytes is equal to about 200 daily rations of iron (Gattermann, 2009). As humans have no physiological means of excreting excess levels of iron, it necessarily follows that patients with repeated transfusion therapy easily accumulate iron (Kohgo et al., 2008). In addition, in patients with anaemia associated with ineffective erythropoiesis, as for example thalassemia, iron is hyperabsorbed from the gastrointestinal tract (Beutler et al., 2003; Papanikolaou & Pantopoulos, 2005).

## **1.4. Iron Chelators**

Iron overload is treated with selective iron chelation therapy (Papanikolaou & Pantopoulos, 2005). For this reason medicinal chemists have been searching for suitable iron-selective, orally active, nontoxic chelators for over 30 years (Ma, Kong, Abbate, & Hider, 2015) and a large number has been synthesized (Liu et al., 2002; Zhou et al., 2006). Iron chelators, on the one hand, can be used to measure the intracellular iron pool and, on the other to remove excessive iron (Ma, Luo, Camplo, Liu, & Hider, 2005).

Ferric iron possesses six coordination sites, which need to be chelated completely with six donor atoms ligated in an octahedral fashion to the metal centre to prevent the generation of free radicals (Dubey, Sudha, & Parakh, 2007; Liu & Hider, 2002a). Ligands are structurally classified according to the number of donor atoms that each molecule has: when a ligand contains two, three or six donor atoms, it is termed bidentate, tridentate or hexadentate, see Image 1 (Gaeta & Hider, 2005; Hider et al., 2011). When all six donor atoms are incorporated into a single molecular structure (a hexadentate ligand), the thermodynamic stability of the complex is maximized (Liu & Hider, 2002a).

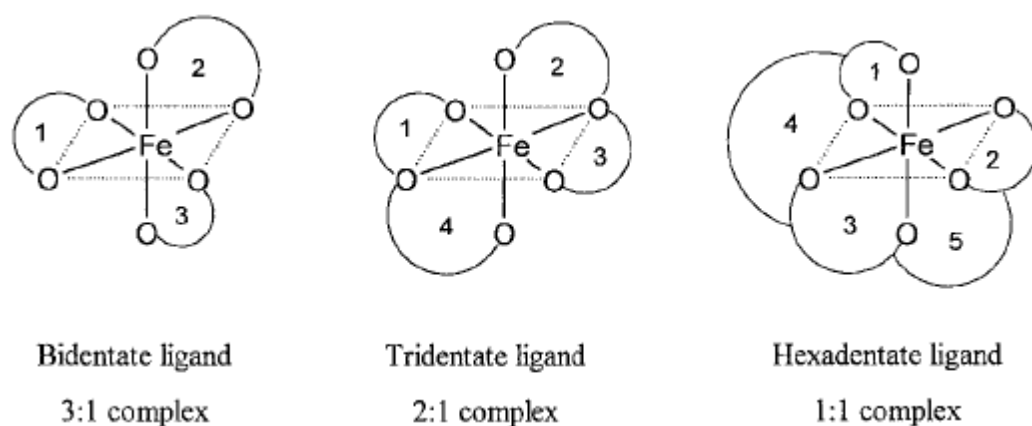


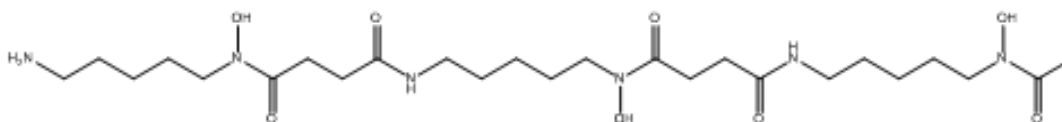
**Image 1** Schematic representation of chelate ring formation in metal-ligand complexes (Liu and Hider 2002)

## 1.5. Design of Iron Chelators

Iron chelators are chemically diverse compounds but they all have in common oxygen, nitrogen or sulfur-donor atoms which coordinate with iron (Gaeta & Hider, 2005; Hatcher, Singh, Torti, & Torti, 2009). They can be designed for the Fe(II) or Fe(III) oxidation state. Fe(II) preferring chelators use nitrogen and sulfur atoms as ligands, but these chelators have the disadvantage of also binding to other bivalent metals as Cu(II) and Zn(II), which are essential for living. Due to this reason the design of a low MW, nontoxic, Fe(II) selective ligand is extremely difficult and might not be possible. Oxygen atoms are used as ligands in Fe(III) selective chelators. Most tribasic cations as Al(III) and Ga(III) are not biologically active and therefore Fe(III) is the main target of the design of iron chelators (Gaeta & Hider, 2005). At present three iron chelators are available for clinical use: Deferoxamine, Deferiprone and Deferasirox. They all reduce elevated levels of iron and prevent organ damage caused by free iron (Kwiatkowski, 2008).

### 1.5.1. Deferrioxamine B (Deferoxamine, DFO, Desferal®)

Desferrioxamine B is a hexadentate chelator (see Formula 1) coordinating all six sites using a single molecule. It forms a more stable complex than ligands, which require more than one molecule (Dubey et al., 2007) .



**Formula 1 Deferrioxamine B (Liu & Hider, 2002a)**

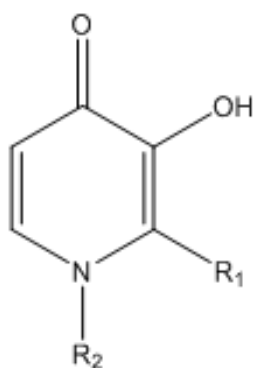
DFO is a Siderophore. Siderophores are typically hexadentate ligands, the coordination sphere of iron (III) is completely occupied by oxygen containing ligands and they utilize catechol, hydroxamate or carboxylate functional groups as ligands. Other examples are enterobactin, deferriferrichrome and ferrioxamine B (Liu & Hider, 2002a). They are low-molecular-weight compounds (500–1500 Da) possessing a very high affinity and selectivity for iron(III) over iron (II). The bioavailability of iron is limited by the very low solubility of Fe (III). Therefore microorganisms, fungi and graminaceous plants produce and release siderophores to scavenge and absorb iron from the environment and form soluble Fe(III) complexes. The iron-siderophore complex is transported to the cytoplasm of the cell where Fe(III) is reduced to Fe(II) (Hider & Kong, 2010).

DFO was discovered accidentally (Hershko, Konijn, & Link, 1998) and is the “gold standard” iron chelator in haematology since 1963 (Dubey et al., 2007). It is safe and effective for transfusional haemosiderosis, but has the major disadvantage of being orally inactive and having a plasma half-life of just some minutes (Neufeld, 2006). Therefore it is administered parenterally, usually as an overnight subcutaneous infusion 5 to 7 nights per week, which hinders optimal compliance (Jang et al., 2013). The iron-DFO complex is charged and therefore does not easily permeate membranes, which is expressed in a low ability to chelate intracellular cardiac and other tissue iron. It is excreted in both urine and stool (Neufeld, 2006). Important side effects that have been observed are local skin reactions at the infusion site, auditory and retinal toxicity, and skeletal changes and growth retardation (Dubey et al., 2007).

As the compliance for the subcutaneously administered DFO is very poor there is a need for a more convenient, oral iron chelator (Cappellini & Pattoneri, 2009). To optimize the compliance the successful design of an orally active, nontoxic, selective iron chelator with a longer half-life has been one of the major goals for medicinal chemists for the past 30 years (Kwiatkowski, 2008; Liu et al., 2002).

For an ideal oral iron chelator the following characteristics must be taken into consideration: Most importantly the metal sensitivity, selectivity and affinity for iron (III), but also the kinetic stability of the iron complex, which should be uncharged to guarantee membrane permeability, a bioavailability and plasma half-life long enough to constantly protect from LPI, it should be non-toxic and have little side effects (Liu & Hider, 2002a; Neufeld, 2006). The free permeability of a compound through the lipid membrane is mainly dependent on three different factors: lipophilicity, molecular size and ionization state (Liu & Hider, 2002a). This is important for the ability of a chelator to remove intracellular cardiac and other tissue iron (Neufeld, 2006).

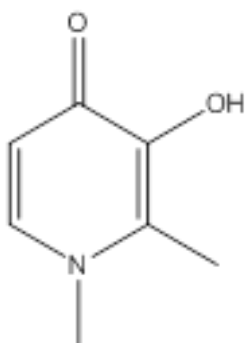
### 1.5.2. Hydroxypyridinones (HPOs)



Formula 2 Hydroxypyridinone

Hydroxypyridinones (see Formula 2) are currently one of the main candidates for the development of orally active iron chelators (Saghaie, Sadeghi, & Nikazma, 2006; Tilbrook & Hider, 1998). They are bidentate ligands where the metal is coordinated by two vicinal oxygen atoms. They are selective for tribasic metal cations. From the three different classes of these ligands, which only differ in the positions of the oxygen substituents, the N-alkyl-3-hydroxypyridin-4-ones possess the highest affinity for  $\text{Fe}^{3+}$  (Liu & Hider, 2002a).

### 1.5.3. Deferiprone (DFP, CP 20, L1, Ferriprox®)



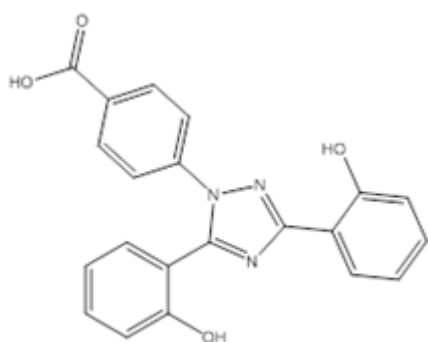
Formula 3 Deferiprone (Liu & Hider, 2002a)

Deferiprone (see Formula 3), the HPO 1,2-dimethyl derivative was synthesized in Prof. Hider's laboratory (Galanello, 2007) at the University of Essex in the United Kingdom in the early 1980s (Cappellini & Pattoneri, 2009). It was the first orally active iron chelator and first used in humans in 1987 (Galanello, 2007).

The small bidentate ligand possesses a clear advantage over hexadentate ligands with respect to oral bioavailability (Hider, 1995; Liu & Hider, 2002b; Tilbrook & Hider, 1998). The low MW, water-soluble compound is rapidly and completely absorbed after oral administration (Galanello, 2007). The drug must be taken three times a day and has a moderate plasma half-life of <2h (Dubey et al., 2007). The required dose of 75 to 100 mg/kg/day is

relatively high. One of the major reasons for the limited efficacy is the extensive metabolism in the liver via glucuronidation of the chelating 3-hydroxyl functionality (Liu & Hider, 2002a). Some side effects such as abdominal discomfort, arthropathy and in rare cases severe agranulocytosis have been observed (Dubey et al., 2007). At low concentrations bidentate chelators like deferiprone show a tendency to dissociate from iron and can in principle generate free radicals (Dubey et al., 2007).

#### 1.5.4. Deferasirox (ICL670, Exjade®)



**Formula 4 Deferasirox (Cappellini & Pattoneri, 2009)**

Deferasirox (see Formula 4) belongs to a new class of oral, tridentate iron chelators— the bishydroxyphenyltriazoles - and was developed by computer modelling (Dubey et al., 2007). The absorption from the gastrointestinal tract is rapid, the peaks are reached after 0.5-1h post dose and the half-life of 8-16h is long; it has therefore the advantage that the dose of 20-30 mg/kg must only be taken once a day. The predominant way of metabolism is

glucuronidation and 84% of drug-induced iron excretion occurs in the faeces (Cappellini & Pattoneri, 2009). The benefit-to-risk profile is favourable as there are only a few adverse effects like transient GI effects and skin rash (Dubey et al., 2007).

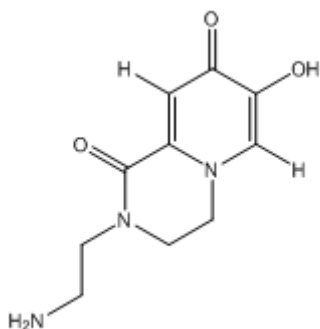
### 1.6. Fluorescence based methods

When a fluorophore absorbs a photon of light, an energetically excited state is formed. Afterwards it returns to the ground state and emits a photon (Gardens, Ha, & Fax, n.d.). The result is deactivation and loss of energy, which is called fluorescence. Other forms of deactivation are non-radioactive loss of energy by emission of a photon and intersystem crossing, which is called phosphorescence.

Fluorescence based methods have been successfully applied to measure intracellular iron as they are highly sensitive, easy in use and relatively non-toxic to cells (Ma, Luo et al. 2005; Ma, Kong et al. 2015). They monitor changes in the cytosolic iron levels in a reproducible manner as both ferric and ferrous iron cause fluorescence quenching of the probes (Ma, Abbate, & Hider, 2015). In iron-specific fluorescent probes the fluorescent and chelating functions are either

covalently linked or the fluorescent part forms part of the chelating moiety (Ma et al., 2005). Hexadentate iron chelators are composed of two moieties, a fluorescent and a chelating part, which are covalently linked. But the introduction of a fluorescent moiety, particularly the larger ones such as fluorescein, seems to dramatically increase the overall size and molecular weight of the molecule and therefore its biological properties and distribution (Ma, Kong, et al., 2015; Ma et al., 2005).

## 2. Overview Statement



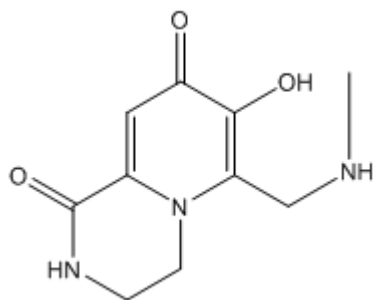
**Formula 5 Structure of the desired iron chelator**

The aim of my project at King's College London was to synthesize a novel bicyclic lactam which is a fluorescent bidentate iron chelator and possesses an amine functional group (see Formula 5). It was fully physicochemically characterized.

Fluorescence based methods have been the most successful for the measurement of intracellular iron as they are highly sensitive, easy in use and relatively non-toxic to cells (Ma, Kong, et al., 2015; Ma et al., 2005). With the novel bicyclic,

fluorescent bidentate iron chelator, the fluorescent moiety merges with the chelating part of the molecule and therefore forms a more compact structure with lower molecular weight. Such molecules could replace traditional fluorescent probes for the quantification of intracellular labile iron pools (Ma, Kong, et al., 2015).

There are some advantages of the new iron chelator when compared to previous synthesized analogues. It is the only one which possesses a primary amine, and this functional group can in future projects be used in order to couple it to a tripodal acid to synthesize a hexadentate chelator or to peptides.



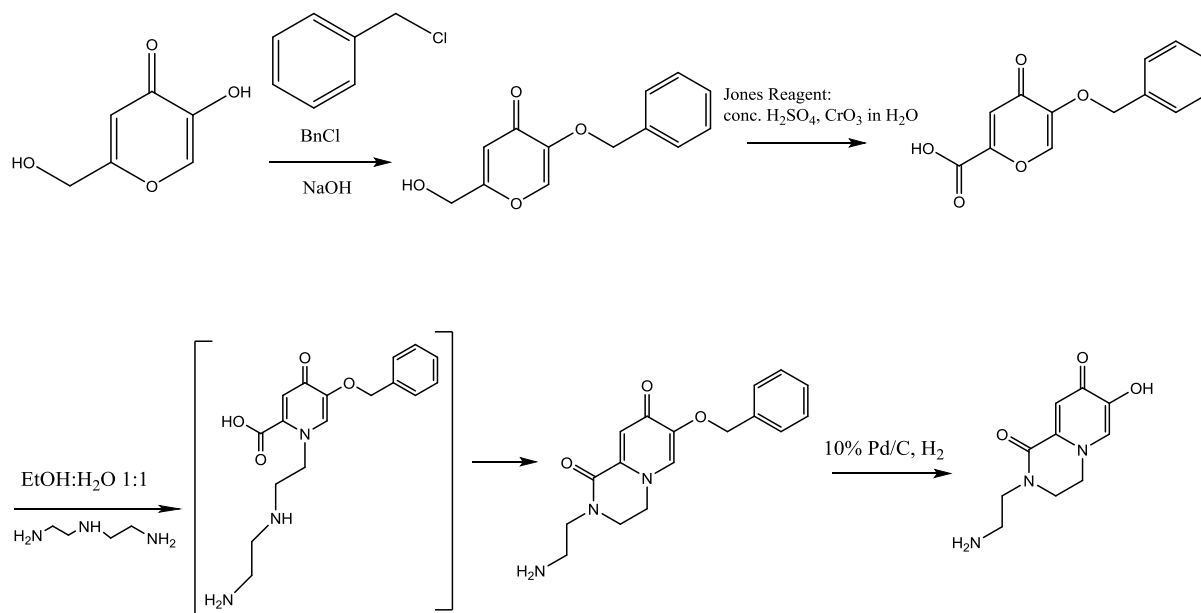
**Formula 6 Structure of compound 4j (Ma, Kong, et al., 2015)**

The bidentate, fluorescent chelator 4j (see Formula 6) (Ma, Kong, et al., 2015) possesses a secondary amine but has the disadvantage that the chelating alcohol functional group must be deprotected in order to make the Mannich reaction work. As soon as a chelator is deprotected it is less convenient to work with as it is of course sensitive to metals in the environment.

Thus the amine of this molecule could be coupled to a tripodal acid via amide formation to form a strong hexadentate ligand with three fluorophore bicyclic parts which chelate iron tightly. This type of hexadentate chelator has not been published yet and brings the advantage that it is fluorescent itself. Up to now all fluorescent hexadentate iron chelators have been composed of two moieties, a fluorescent and a chelating part, which are covalently linked. But the introduction of a fluorescent moiety, particularly the larger ones such as fluorescein, apparently increases the overall size and molecular weight of the molecule dramatically and therefore changes its biological properties and distribution (Ma, Kong, et al., 2015; Ma et al., 2005).

### 3. Synthesis of fluorescent chelators

#### 3.1. Synthetic schemes

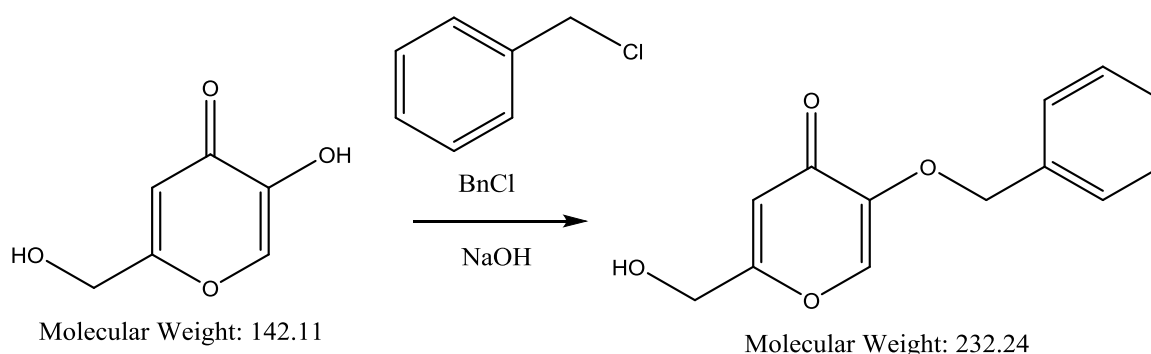


**Scheme 1** Scheme of the synthetic steps from kojic acid to the desired iron chelator

The synthetic scheme of the four step chelator synthesis is briefly described in Scheme 1. The starting material was commercially available kojic acid. It was first benzyl-protected with benzyl chloride and sodium hydroxide in the 5-OH position to 5-benzyloxy-2-hydroxymethyl-4H-pyran-4-one. Afterwards it was oxidized in the 2-OH position to a carboxylic functional group with the powerful oxidant Jones Reagent (a solution of chromium trioxide in concentrated sulfuric acid diluted in water) to obtain 5-(benzyloxy)-4-oxo-4H-pyran-2-carboxylic acid. When the diethylentriamine was added two amine insertion reactions followed: the pyranone was converted to the bicyclic pyrazine 2-(2-aminoethyl)-7-(benzyloxy)-3,4-dihydro-2H-pyrido[1,2-a]pyrazine-1,8-dione via the non-fluorescent transitional state 1-(2-((2-aminoethyl)amino)ethyl)-5-(benzyloxy)-4-oxo-1,4-dihydropyridine-2-carboxylic acid. The final step was then to deprotect the molecule from the benzyl group which seemed to work best via hydrogenation with 10% Pd/C (w/w), in order to obtain the bicyclic, fluorescent, bidentate iron chelator 2-(2-aminoethyl)-7-hydroxy-3,4-dihydro-2H-pyrido[1,2-a]pyrazine-1,8-dione.



### 3.1.1. Synthesis of 5-benzyloxy-2-hydroxymethyl-4H-pyran-4-one (Compound CR 0)



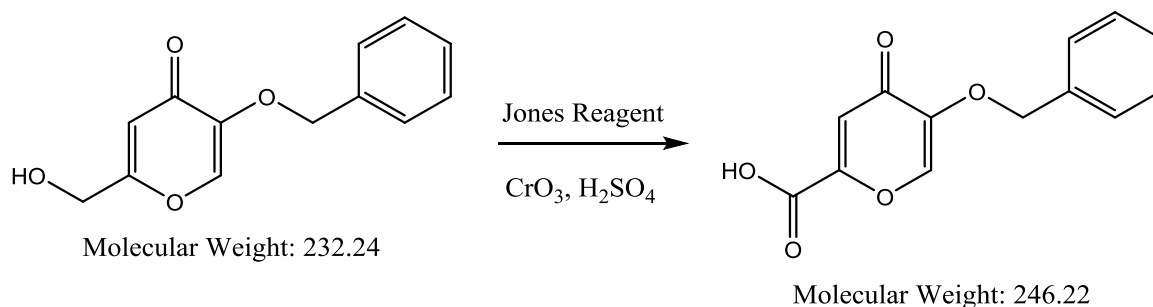
**Scheme 2 Synthesis of 5-benzyloxy-2-hydroxymethyl-4H-pyran-4-one**

The starting material for the preparation of the bicyclic fluorescent iron chelator was commercially available kojic acid (5-hydroxy-2-(hydroxymethyl)-4H-pyran-4-one). The first step was to protect the hydroxy group in the 5-OH position with a benzyl group via the Williamson ether synthesis (see Scheme 2). The starting material was initially treated with sodium hydroxide in order to generate the nucleophilic phenolate: the strong base NaOH first removes the H of the acid in position 5. Then the alkyl halide benzyl chloride was added dropwise and the mixture refluxed overnight. The nucleophilic alkoxide attacks the electrophilic carbon atom of the benzyl chloride which is partially positively charged (delta plus) via an S<sub>N</sub>2 reaction and form the desired benzyl ether. After removal of the solvent, the brown solid was washed with water, followed by MeOH to afford an acceptable yield of a white solid which showed a clear peak at 11.49 in the RP-HPLC (see appendix image 24) and needed no further purification.

The results from the <sup>1</sup>H-NMR clearly proved the presence of the protective benzyl group: the aromatic hydrogen atoms could be found as a multiplet at  $\delta$  7.33-7.44 ppm and the hydrogens of the CH<sub>2</sub>-group appeared as a singlet at a chemical shift of  $\delta$  4.95 ppm. The hydroxymethyl is present with singlets of the hydrogen of the alcohol functional group at a chemical shift of  $\delta$  5.72 ppm and the CH<sub>2</sub>-group at  $\delta$  4.30 ppm. The two hydrogens of the 4-pyrone ring show singlets at chemical shifts of  $\delta$  6.34 and 8.19 ppm. (see appendix image 8).

The detailed synthetic procedure is described in section 3.2.1.

### 3.1.2. Synthesis of 5-(benzyloxy)-4-oxo-4H-pyran-2-carboxylic acid; 3-hydroxy-protected comenic acid (Compound CR 4)



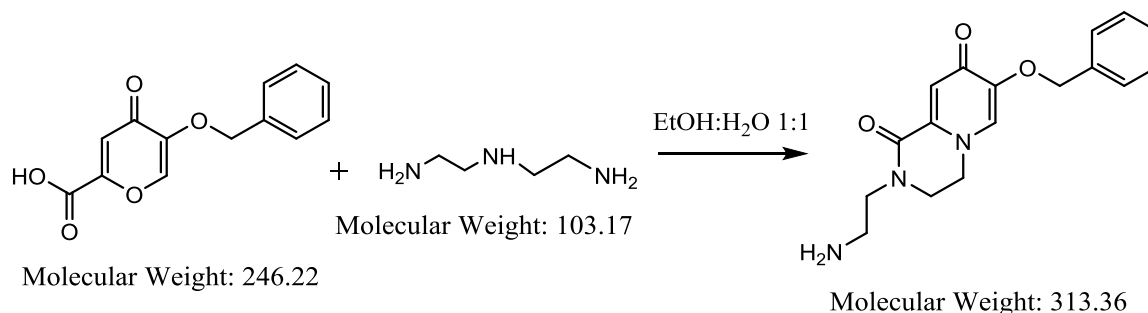
**Scheme 3 Synthesis of 5-(benzyloxy)-4-oxo-4H-pyran-2-carboxylic acid**

The second step was the oxidation reaction from the primary alcohol functional group to the carboxylic acid (see Scheme 3). For the oxidation, the previously prepared benzyl-protected kojic acid 5-benzyloxy-2-hydroxymethyl-4H-pyran-4-one was treated with Jones reagent, which is a solution of chromium trioxide in diluted concentrated sulfuric acid. At the outset of the reaction it is important to cool the flask to 0°C with an ice bath as it is quite exothermic. Water and acetone were used as solvents. The powerful oxidant chromium (VI) is able to convert the alcohol function via an aldehyde to an acid. Due to the oxidation of the alcohol group to the acid, the orange Jones reagent with Cr(VI) was reduced to the green Cr(III). After removal of the inorganic Cr(III) via filtration the filtrate was evaporated to dryness, washed with acetone and recrystallized with MeOH to afford the product (5-(benzyloxy)-4-oxo-4H-pyran-2-carboxylic acid or 3-hydroxy-protected comenic acid) as pure white needles. During the reaction, the compound was checked several times via HPLC until there was only a single peak visible at 10.77, which determined the higher polarity and the purity of the compound (see appendix image 25).

The results from the <sup>1</sup>H-NMR in deuterated DMSO proved that the oxidation from the alcohol to the acid functional group worked: the two singlets from the hydroxymethyl at δ 4.30 ppm (CH<sub>2</sub>) and δ 5.72 ppm (OH) disappeared. It showed that the benzyl-protective group was still present (singlet at a chemical shift of δ 7.42 ppm (5H) and singlet at δ 4.98 ppm (2H)), and the hydrogens in the 4-pyrone appeared as singlets at δ 6.95 ppm and δ 8.35 ppm (see appendix image 9).

The detailed synthetic procedure is described in section 3.2.2.

### 3.1.3. Synthesis of 2-(2-aminoethyl)-7-(benzyloxy)-3,4-dihydro-2H-pyrido[1,2-a]pyrazine-1,8-dione (Compound CR 6)



**Scheme 4 Synthesis of 2-(2-aminoethyl)-7-(benzyloxy)-3,4-dihydro-2H-pyrido[1,2-a]pyrazine-1,8-dione**

After the benzylation and oxidation of the kojic acid, the third step was to synthesize the bicyclic fluorescent molecule via two amine insertion reactions (see Scheme 4). The conversion of the pyranone via the pyridinone to the pyrazine works via the following scheme:

The 3-hydroxy-protected comenic acid was suspended in a mixed solution of EtOH and water. When diethylenetriamine was added, the mixture turned yellow and the reaction mixture was stirred with reflux at 200°C overnight. Initially one of the primary, nucleophilic amines of the diethylenetriamine targets the oxygen of the 4-pyranone of the 5-(benzyloxy)-4-oxo-4H-pyran-2-carboxylic acid via nucleophilic attack, the ring opens, closes again, eliminates one molecule of water and forms pyridinone as the non-fluorescent transitional state 1-(2-((2-aminoethyl)amino)ethyl)-5-(benzyloxy)-4-oxo-1,4-dihydropyridine-2-carboxylic acid (see Scheme 1). The heating led to an intra-molecular condensation to produce the bicyclic lactam. The secondary, nucleophilic amine reacts with the acid function and generates the pyrazine and the second ring via elimination of another molecule of water. The next day the light orange mixture was evaporated to dryness and the yellow crude solid was recrystallized by dissolving it in a minimal MeOH and crushing it with excess of cooled ether to obtain a yellow solid. The analysis via RP-HPLC with a peak at 9.09 mins showed that the compound was getting more hydrophilic due to the amine functional group (see characterization of CR 19 Figure 7).

The  $m/z$  of 314.2  $[M+H]^+$  (see appendix image 1) from the ESI-MS corresponds with the calculated MW of 313.36 (see Scheme 4).

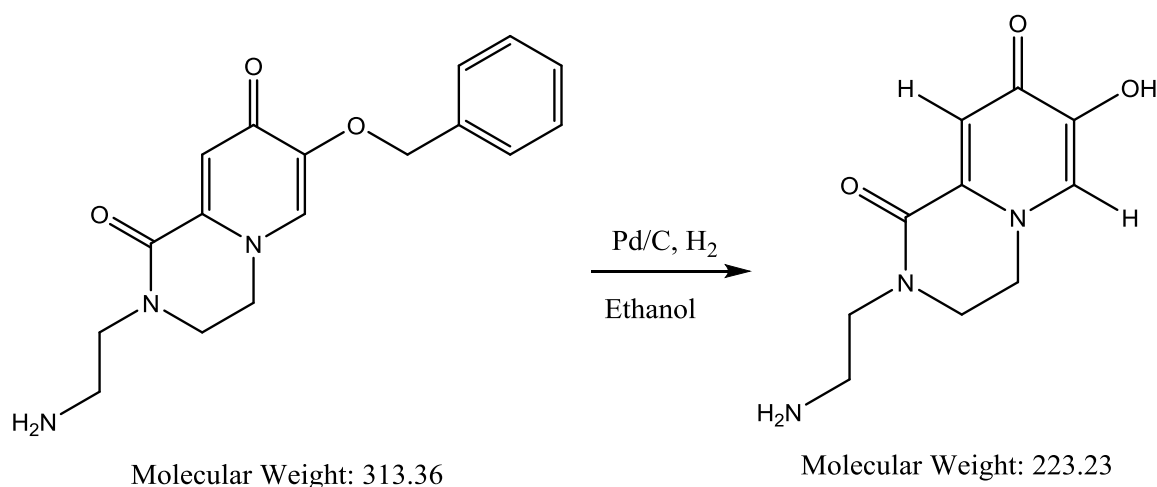
The analysis via  $^1\text{H-NMR}$  in deuterated DMSO proved the presence of the newly inserted alkane groups: the carbons of the chain appear at  $\delta$  2.72-2.75 ppm (t, 2H) and  $\delta$  3.43-3.49 ppm (t, 2H),

the primary carbons in the piperazine ring at  $\delta$  3.73-3.76 ppm (t, 2H) and  $\delta$  4.16-4.19 ppm and the primary amine at  $\delta$  2.50-2.51 ppm (t, 2H). The benzyl-protective group was still present with a multiplet at a chemical shift of  $\delta$  7.33-7.45 ppm (m, 5H) and a singlet at  $\delta$  5.00 ppm (2H), the hydrogens in the pyridine ring show peaks at single peaks at  $\delta$  6.77 (s, 1H) and 7.72 ppm (s, 1H) (see appendix image 10).

The  $^{13}\text{C}$ -NMR and  $^{13}\text{C}$ -NMR DEPT mode verified that the desired structure was synthesized: In the  $^{13}\text{C}$ -NMR the carbonyl-C shows a peak at the chemical shift of 171.10 ppm, the amide at 157.55 ppm and the other two quaternary carbons in the pyridine ring at 149.18 and 136.60 ppm. They are all absent in the DEPT mode indicating that they are quaternary carbons. The aromatic carbons from the benzyl were obtained at 128.01-128.37 ppm and the two carbons in the pyridine ring show peaks at 125.54 and 115.91 ppm. They all remain positive in the DEPT mode proving that they are tertiary carbons. The carbinol C at 70.42 ppm and the shifts of the other aliphatic carbons at 50.07, 47.94, 44.58 and 38.82 ppm point downwards in the DEPT mode which declares that they are secondary carbons (see appendix image 11 and 12).

The detailed synthetic procedure is described in section 3.2.3.

### 3.1.4. Synthesis of 2-(2-aminoethyl)-7-hydroxy-3,4-dihydro-2H-pyrido[1,2-a]pyrazine-1,8-dione (Compound CR 19)



**Scheme 5 Synthesis of 2-(2-aminoethyl)-7-hydroxy-3,4-dihydro-2H-pyrido[1,2-a]pyrazine-1,8-dione**

The final step was the O-debenzylation of the protected fluorescent, bicyclic molecule to obtain the bidentate chelator (see Scheme 5). The deprotection of the benzyl group was attempted in different ways: With BCl<sub>3</sub> in DCM and hydrogenation with palladium on carbon (Pd/C) in different concentrations of Pd (5 and 10%) and different solvents (EtOH and MeOH). The analysis via <sup>1</sup>H and <sup>13</sup>C-NMR, HPLC and ESI-MS showed that it worked best when the protected compound was dissolved in methanol and hydrogenated with 10% palladium on carbon overnight.

First the benzyloxy protected compound 2-(2-aminoethyl)-7-(benzyloxy)-3,4-dihydro-2H-pyrido[1,2-a]pyrazine-1,8-dione was dissolved in methanol, and then a catalytic amount of Pd(0) was added. The Pd is linked between the ether group and the carbon atom via oxidative addition and gets oxidized to Pd(II). The H<sub>2</sub> which is lead into the reaction flask in excess coordinates to the Pd(II). The desired bicyclic iron chelator with the alcohol functional group is eliminated via deprotonation and the Pd(II) linked to the toluene is cleaved so one equivalent of toluene is eliminated as a by-product. The catalysts were removed via filtration; the filtrate was acidified to pH 1 with conc. HCl, evaporated to dryness and recrystallized by dissolving the crude residue in minimal MeOH and crushing it with excess of cold ether to obtain a yellow solid.

After the hydrogenation with 10% Pd/C (w/w) the desired structure could be confirmed via <sup>1</sup>H and <sup>13</sup>C-NMR in deuterated DMSO. The characteristic shifts of the aromatic hydrogens at δ 7.45-

7.33 ppm (m, 5H) and the CH<sub>2</sub> at  $\delta$  5.02-4.98 ppm (t, 2H) in the <sup>1</sup>H-NMR and at 128.01-128.37 and 70.42 ppm in the <sup>13</sup>C-NMR of the benzyl-protecting group disappeared (see characterization of CR 19 Figure 3, Figure 5 and Figure 6).

The analysis via <sup>1</sup>H-NMR and <sup>13</sup>C-NMR after the treatment with BCl<sub>3</sub> showed that the benzyl had not been removed; the characteristic shifts at 5.27 and 5.28 ppm (d, 2H) and 7.38-7.53 ppm (m, 5H) and 71.72 and 128.36-129.25 ppm were still visible in the spectra (see appendix image 13 and 14).

The analysis via <sup>1</sup>H-NMR after the attempted deprotection with 5% Pd/C (w/w) showed that this method wasn't efficient enough either, there still remained a tiny signal around 7.40 (see appendix image 15).

The m/z of 224.1030 [M+H]<sup>+</sup> in the HRMS corresponds almost perfectly with the calculated m/z of 224.1035 [M+H]<sup>+</sup> (see characterization of CR 19 Figure 1).

In the RP-HPLC analysis the peak of the protected molecule disappeared and a single peak at 1.73 min appeared which is supposed to derive from the compound (see characterization of CR 19 Figure 8).

The detailed synthetic procedure is described in section 3.2.4.

The compound will be characterized in section 4.

### **3.1.5. Synthetic schemes of the attempts of forming the hexadentate, fluorescent iron chelator**

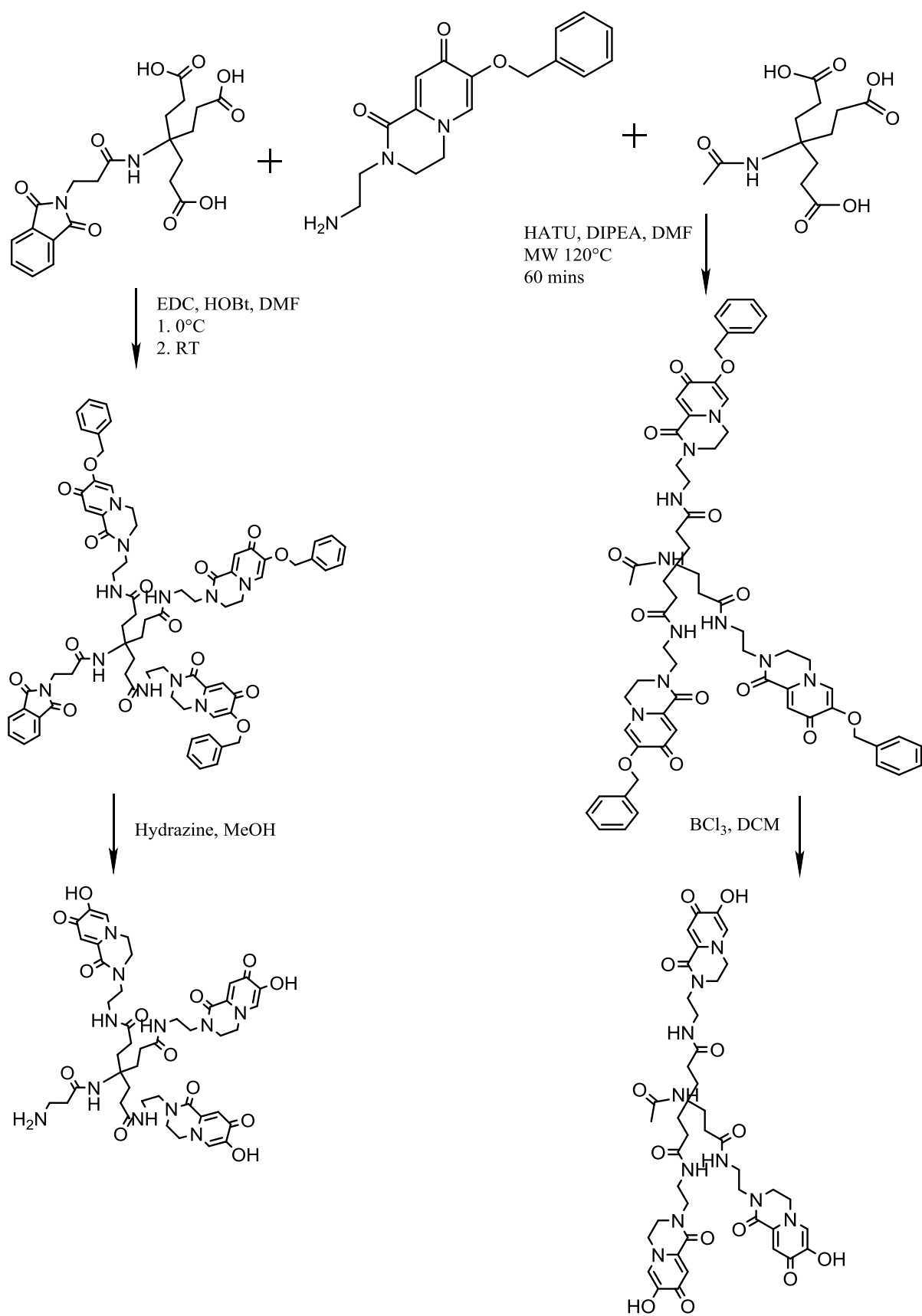
Several hexadentate siderophore analogues have been constructed by derivatizing bidentate HPOs and attaching them to suitable frameworks (Liu & Hider, 2002a). The synthesized bidentate iron chelator possesses a HPO component and is fluorescent due to the second ring. Compared to other similarly synthesized chelators it has the advantage of a primary amine functional group which allows us to couple it to carboxylic acids via amide formation.

The bicyclic fluorescent chelator was coupled with different coupling reagents to two different tripodal carboxylic acids (see Scheme 6) in order to generate a very strong hexadentate chelator, which is fluorescent. The optimum length of 3 carbon atoms between the carboxylic acid group and the nitrogen atom had been established in previous experiments.

The experiments were carried out with different coupling reagents, with 3 equivalents of EDC, where 3 equivalents of HOBt were added or 4 equivalents of the catalyst DIPEA with 4 equivalents of HATU. The amine was always added in 1:2 excess compared to the acid which was tripodal, yielding in a 1:6 ration in total. On the one hand it was carried out at room temperature and left to stir for 2 days and on the other hand in a microwave reactor.

All conditions produced some of the desired product, but the method with EDC seemed to work best. The workup of the sticky DIPEA/HATU product was inconvenient.

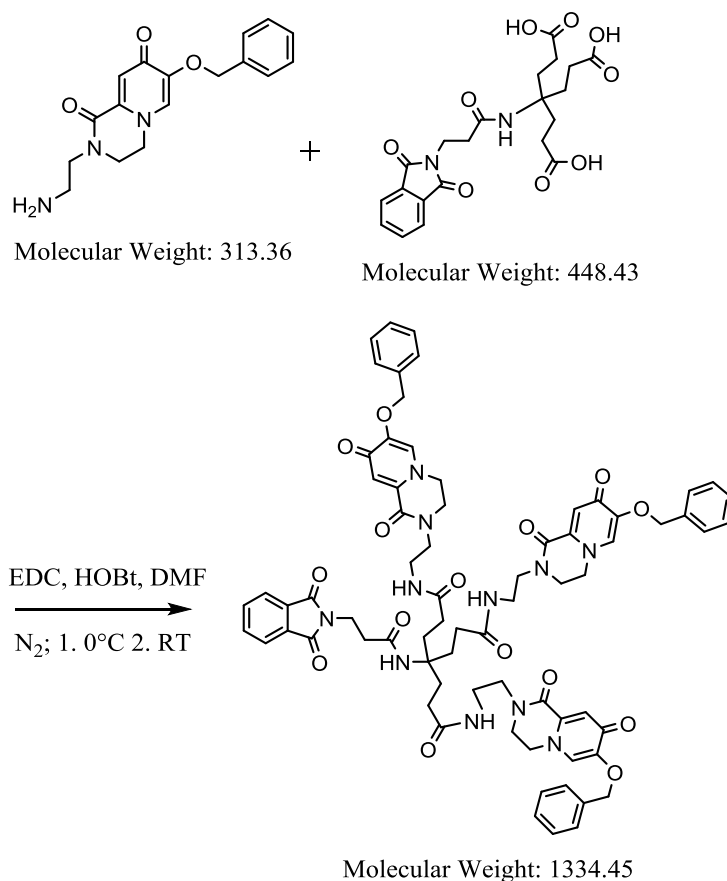
The cleavage of the protecting groups was difficult: it was attempted with hydrazine in MeOH for the compound which was protected with the phthalimide and benzyl groups and  $\text{BCl}_3$  in DCM for the compound which was only benzyl-protected.



Scheme 6 Scheme of the synthetic steps to form the hexadentate chelators



**3.1.5.1. Attempted synthesis of N1,N7-bis(2-(7-(benzyloxy)-1,8-dioxo-1,3,4,8-tetrahydro-2H-pyrido[1,2-a]pyrazin-2-yl)ethyl)-4-(3-((2-(7-(benzyloxy)-1,8-dioxo-1,3,4,8-tetrahydro-2H-pyrido[1,2-a]pyrazin-2-yl)ethyl)amino)-3-oxopropyl)-4-(3-(1,3-dioxoisindolin-2-yl)propanamido)heptanediamide (Compound CR 8)**



**Scheme 7 Attempted synthesis of N1,N7-bis(2-(7-(benzyloxy)-1,8-dioxo-1,3,4,8-tetrahydro-2H-pyrido[1,2-a]pyrazin-2-yl)ethyl)-4-(3-((2-(7-(benzyloxy)-1,8-dioxo-1,3,4,8-tetrahydro-2H-pyrido[1,2-a]pyrazin-2-yl)ethyl)amino)-3-oxopropyl)-4-(3-(1,3-dioxoisindolin-2-yl)propanamido)heptanediamide**

The previously prepared phthalimid protected triacid 4-(2-carboxyethyl)-4-(3-(1,3-dioxoisindolin-2-yl)propanamido)heptanedioic acid, EDC and HOBt were dissolved in dry DMF (see Scheme 7) and minimal DMSO was added as a solubilizer. After cooling the flask to 0°C it was flushed with nitrogen to obtain an oxygen free environment.

The carboxyl activating reagent EDC deprotonates the acid and one of its nitrogen atoms gets protonated itself. The free electron pair of the acid targets the carbon atom of the EDC. The OH of the HOBt targets the formed ether and eliminates the urea by-product.

The amine was added after 2h and left to stir at room temperature for two days (see Scheme 7). In this reaction step the amide is being formed: the nucleophilic, primary amine 2-(2-aminoethyl)-7-(benzyloxy)-3,4-dihydro-2H-pyrido[1,2-a]pyrazine-1,8-dione targets the three HOBt-activated acids and forms the amide bonds by eliminating three molecules of HOBt.

The analysis via RP-HPLC showed a peak at 16.14 min, but as the amine was added in excess, there was still an amount of the educt left (9.06 min) (see appendix image 26).

The purification of the product was attempted twice:

For the liquid liquid extraction the product was diluted with water and extracted with chloroform. The chloroform phase was first washed with a 5% NaHCO<sub>3</sub> solution and then with brine. The organic extracts were dried over anhydrous sodiumsulfate, filtered and evaporated under reduced pressure to a very low yield of light orange crystals. The compound was also purified via preparative HPLC, which showed a peak at 16.09 mins in the RP-HPLC (see appendix image 27).

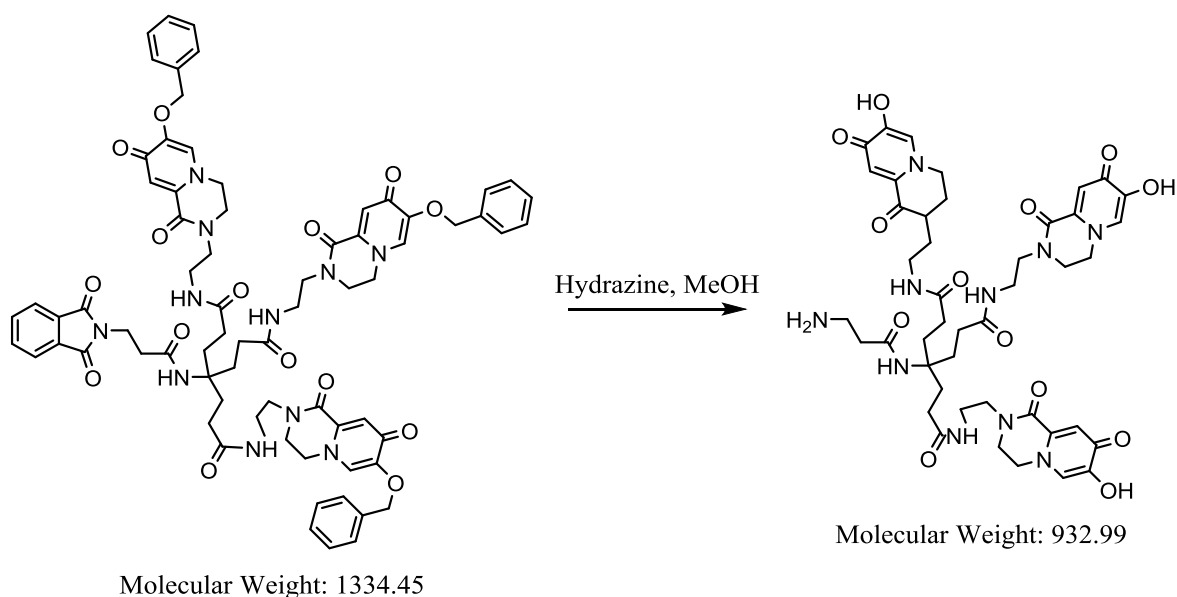
The analysis via ESI-MS proved the presence of the product with m/z: 1334.1, 668.3 [M+2H]<sup>2+</sup> (see appendix image 2) which correspond with the calculated value of 1334.45 (see Scheme 7).

The results of the <sup>1</sup>H-NMR in deuterated DMSO showed the alkane hydrogens at 1.66-1.70 (2H, t), 2.51-2.52 (2H, t), 2.73-2.80 (2H, t), 2.99-3.04 (2H, t), 3.04 (s, 2H), 3.27 (s, 2H), 3.50 (s, 2H), 3.71-3.80 (t, 2H) and 4.21-4.26 ppm (t, 2H). The characteristic shifts of the benzyl-protecting group are present with a singlet of the CH<sub>2</sub> at 5.00 ppm (s, 2H) and a multiplet of the aromatic hydrogens at 7.73-7.81 ppm (m, 5H). The shifts of the four aromatic hydrogens of the phthalimide were obtained at 7.33-7.48 ppm (m, 4H), the two hydrogens of the pyridine ring show shifts at 6.79-6.80 (d, 1H) and 7.20-7.23 ppm (t, 1H) (see appendix image 17).

In the <sup>13</sup>C-NMR the shifts of the quaternary carbons at 136.48, 142.90, 149.25, 158.28, 158.43, 162.31, 167.70, 171.00 and 172.42 ppm disappear in the DEPT mode, the benzyle protecting group is present with the characteristic shifts of the multiplet of the benzene ring at 127.85-128.37 and of the CH<sub>2</sub> at 70.42 ppm, which points down in the DEPT mode and proves that it is a secondary carbon. The aliphatic carbons are present at 25.89, 34.33, 36.56, 36.71, 42.72, 43.42, 44.26 and 54.97 ppm and are negative in the DEPT mode which determines they are secondary. The two tertiary carbons in the pyridine ring were obtained at 110.61 and 118.34 ppm, and the aromatic carbons in the phthalimide at 122.94-123.05 ppm (see appendix image 18 and 19).

The detailed synthetic procedure is described in section 3.2.5.1.

### 3.1.5.2. Attempted synthesis of 4-(3-aminopropanamido)-N1,N7-bis(2-(7-(benzyloxy)-1,8-dioxo-1,3,4,8-tetrahydro-2H-pyrido[1,2-a]pyrazin-2-yl)ethyl)-4-(3-((2-(7-(benzyloxy)-1,8-dioxo-1,3,4,8-tetrahydro-2H-pyrido[1,2-a]pyrazin-2-yl)ethyl)amino)-3-oxopropyl)heptanediamide (Compound CR 11)



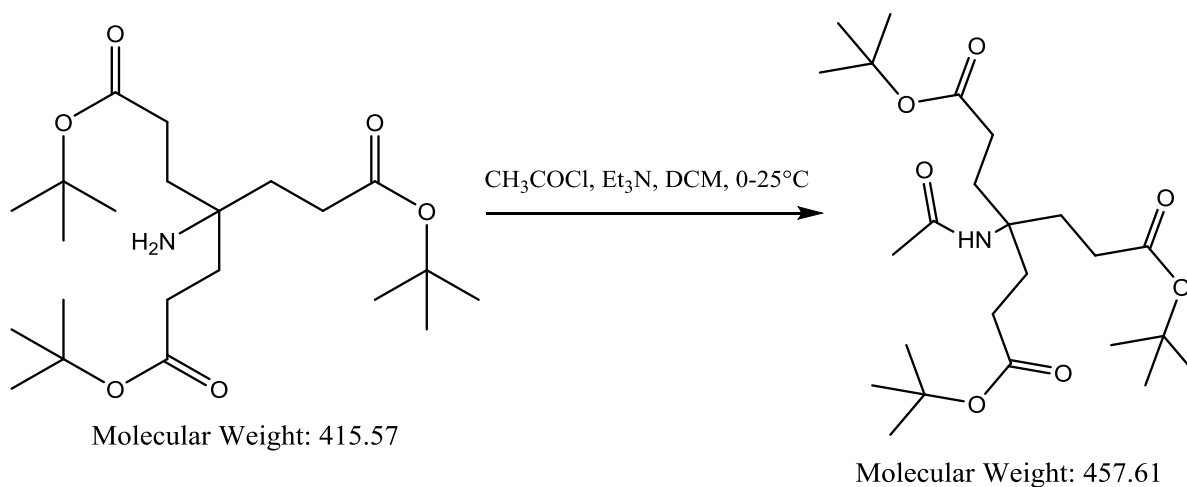
**Scheme 8 Attempted Synthesis of 4-(3-aminopropanamido)-N1,N7-bis(2-(7-(benzyloxy)-1,8-dioxo-1,3,4,8-tetrahydro-2H-pyrido[1,2-a]pyrazin-2-yl)ethyl)-4-(3-((2-(7-(benzyloxy)-1,8-dioxo-1,3,4,8-tetrahydro-2H-pyrido[1,2-a]pyrazin-2-yl)ethyl)amino)-3-oxopropyl)heptanediamide**

The next step was to deprotect the primary amine from the phthalimide and the benzyl groups (see Scheme 8). This was performed with hydrazine, which cleaves N-alkylated phthalimide derivatives. Methanol was used as a solvent as it dissolved the compound better than ethanol. Hydrazine was added to the solution and the mixture was heated to reflux overnight. In the morning it was cooled to 0°C in an ice bath, the product was centrifuged and the supernatant evaporated to a brown solid which needed purification via preparative HPLC using a prep C18 column and an acetonitrile/water gradient.

The product could not be characterized via NMR.

The detailed synthetic procedure is described in section 3.2.5.2.

### 3.1.5.3. Synthesis of di-tert-butyl 4-acetamido-4-(3-(tert-butoxy)-3-oxopropyl)heptanedioate (Compound CR 14)



**Scheme 9 Synthesis of di-tert-butyl 4-acetamido-4-(3-(tert-butoxy)-3-oxopropyl)heptanedioate**

The previously prepared tripodal-amino ester was dissolved in DCM, to this solution triethylenamine was added. The solution was cooled to 0°C in an ice bath and acetyl chloride was quickly added dropwise (see Scheme 9). It was stirred for 4h and slowly allowed to warm to room temperature.

First the positively charged carbon – with a delta plus – of the acetyl chloride gets coupled to the amine via nucleophilic attack as the nitrogen atom possesses a free electron pair. The double bond formation of the oxygen kicks the chloride out and produces HCl with the proton of the amine, which neutralizes to a salt with the triethylamine.

Afterwards the workup followed. The solution was poured into a separating funnel, washed two times with 5% aqueous HCl and once with brine. It was dried over sodiumsulfate and filtrated. Then the solvents were removed under reduced pressure. The crude residue was purified by CC with EtOAc:Hexane 1:1 as eluent. The fractions were checked via TLC with the same mobile phase. The desired acetamide fractions were detected by dunking the plates in a solution of permanganate and heating them to show the different R<sub>f</sub> values of the amine and the acetamide as light spots. The tripodal-acetyl ester fractions were evaporated to dryness to obtain a white solid.

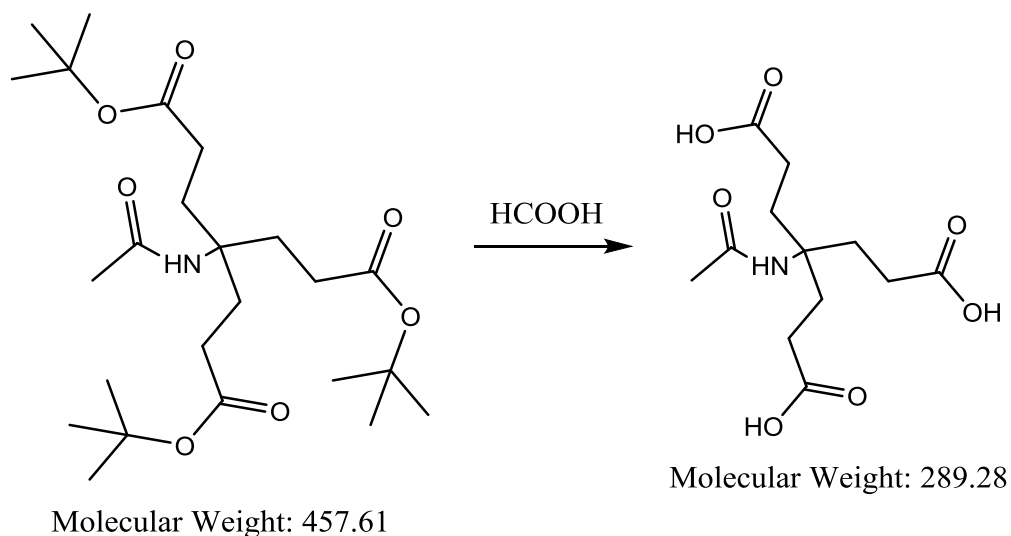
The ESI-MS analysis showed the desired product with an  $m/z$  of 458.4  $[M+H]^+$  and 481.3  $[M+Na]^+$  (see appendix image 3) which correspond with the calculated MW (see

Scheme 9).

The  $^1\text{H}$ -NMR in deuterated DMSO proved the presence of the tertial butyl protecting group at  $\delta$  1.39 ppm (s, 3H). The acetamide is present with its bond to the carbon atom at chemical shifts of  $\delta$  1.75-1.78 ppm (t, 3H) and a small shift at  $\delta$  7.20 ppm (s, 1H) deriving from the bond to the nitrogen. The alkane chain was confirmed with chemical shifts at  $\delta$  2.07-2.11 (t, 2H) and 2.50-2.52 ppm (t, 2H) (see appendix image 20).

The detailed synthetic procedure is described in section 3.2.5.3.

### 3.1.5.4. Synthesis of 4-acetamido-4-(2-carboxyethyl)heptanedioic acid (Compound CR 15)



**Scheme 10** Synthesis of 4-acetamido-4-(2-carboxyethyl)heptanedioic acid

The next step was to deprotect the synthesized ester from the acid-labile protecting group tertiary butyl with formic acid to form the tripodal-acetyl acid (see Scheme 10).

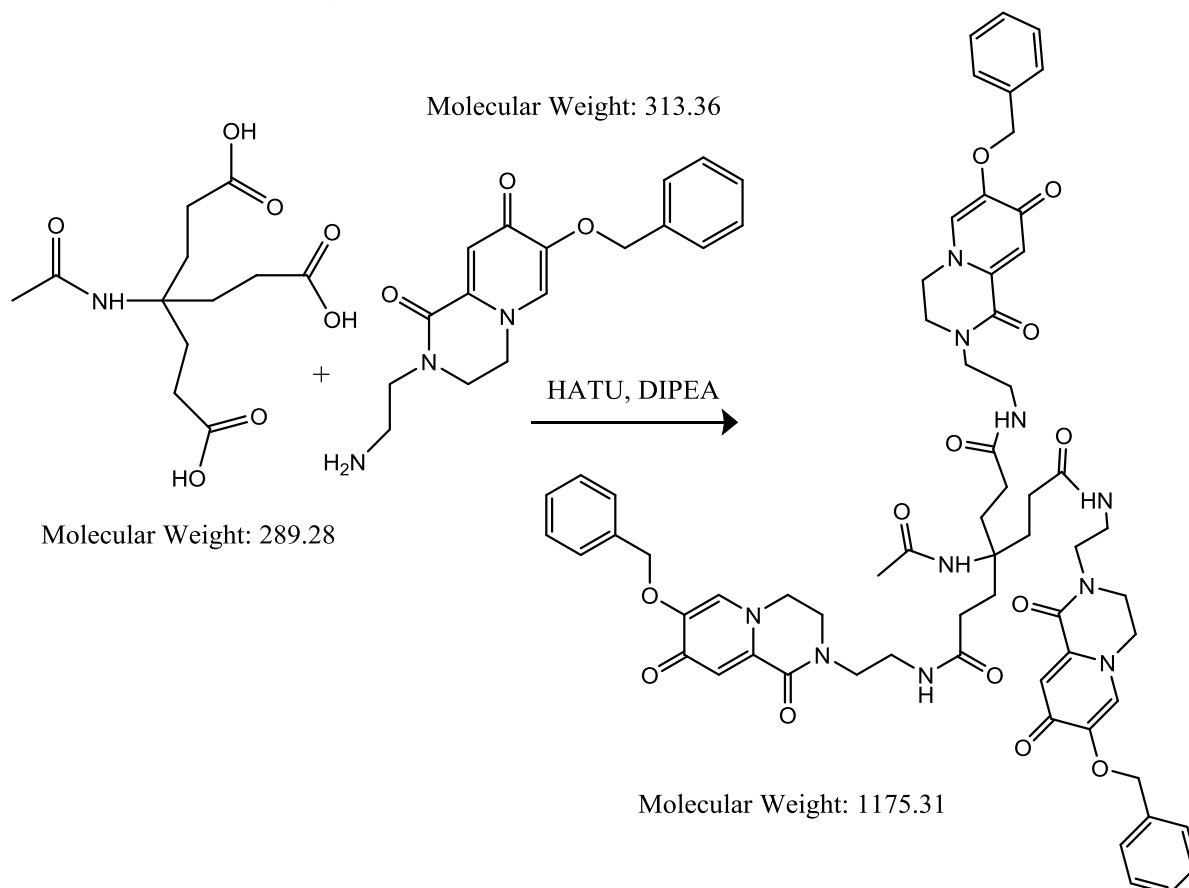
The protected tripodal acetyl ester was dissolved in formic acid (96%) and left to stir at room temperature overnight. The oxygen next to the butyl group gets protonated and eliminates the tertiary butyl cations. To get rid of the formic acid, azeotropic distillation with toluene was applied. The crude residue, a white oil, was recrystallized by dissolving it in minimal EtOH and crushing it with excess of cold hexane. It was cooled in the fridge overnight to obtain an acceptable yield of the product as a white solid.

The value of  $m/z$  290.2  $[M+H]^+$ , via ESI-MS obtained (see appendix image 4) corresponds with the calculated MW (see Scheme 10).

The analysis via  $^1\text{H-NMR}$  in deuterated water proved that the compound was deprotected from the tertial butyl groups as the shifts at  $\delta$  1.39 ppm (s, 3H) disappeared. The characteristic chemical shifts of the alkane chain were obtained at  $\delta$  1.86-1.90 (t, 2H) and 2.21-2.25 ppm (t, 2H). The acetamide group is still present with the tiny shift at 7.30 (s, 1H), which derives from the bond to the nitrogen atom and the shift at  $\delta$  1.82 ppm (s, 3H) of the bond to the carbon (see appendix image 21).

The detailed synthetic procedure is described in section 3.2.5.4.

**3.1.5.5. Attempted synthesis of 4-acetamido-N1,N7-bis(2-(7-(benzyloxy)-1,8-dioxo-1,3,4,8-tetrahydro-2H-pyrido[1,2-a]pyrazin-2-yl)ethyl)-4-(3-((2-(7-(benzyloxy)-1,8-dioxo-1,3,4,8-tetrahydro-2H-pyrido[1,2-a]pyrazin-2-yl)ethyl)amino)-3-oxopropyl)heptanediamide (Compound CR 16)**



**Scheme 11 Attempted synthesis of 4-acetamido-N1,N7-bis(2-(7-(benzyloxy)-1,8-dioxo-1,3,4,8-tetrahydro-2H-pyrido[1,2-a]pyrazin-2-yl)ethyl)-4-(3-((2-(7-(benzyloxy)-1,8-dioxo-1,3,4,8-tetrahydro-2H-pyrido[1,2-a]pyrazin-2-yl)ethyl)amino)-3-oxopropyl)heptanediamide**

As a next step, the amide formation between the newly synthesized tripodal carboxylic acid and the amine was carried out in a microwave reactor (see Scheme 11). With this method the reaction time is cut down to a minimum, which has mainly two reasons: Due to the microwaves the compounds vibrate and via the higher temperature the end group is more easily accessible.

HATU, DIPEA and the tripodal-acetyl acid were dissolved in a minimal amount of dry DMF, in the end the amine was added and the mixture turned yellow. This mixture was heated in the microwave reactor at 120°C for 30 minutes. The reaction mechanism is being carried out in two

different reaction steps. First the carboxylic acids react with the HATU to form the OAt-active esters, then the nucleophilic amine forms the acylated product with the activated ester.

The progress of the reaction was checked via HRMS in between which showed the presence of the amine at  $m/z$ : 314.1517  $[M+H]^+$  and the one and two armed product at  $m/z$ : 392.5133  $[M+2H]^{2+}$  and  $m/z$ : 440.6990  $[M+2H]^{2+}$  (see appendix image 6). Therefore it was heated again under the same conditions. In the analysis via HRMS it seemed as if the amine and one and two armed product had disappeared and it showed the presence of the product at  $m/z$ : 1175.5218  $[M+H]^+$ , the double charged at 588.2657  $[M+2H]^{2+}$  and the quaternary charged at 295.2889  $[M+4H]^{4+}$ . The peak at 342.1478 derives from an impurity of the column (see appendix image 7). After the coupling reaction in the microwave it was a homogenous, red solution, which was evaporated yielding a dark-red oil that needed purification.

The separation was attempted via preparative TLC with MeOH:CHCl<sub>3</sub> 1:1 with 1% of AA as an eluent, where the band at  $R_f$ =0.4 was scratched and extracted. In the ESI-MS analysis it showed the presence of the desired product at  $m/z$  1175.1  $[M+H]^+$  and the double charged one at 588.6  $[M+2H]^{2+}$  (see appendix image 5). Therefore an attempt of purification via CC followed. The same mobile phase was used and the fractions were checked via TLC which absorbed fluorescence under the UV-lamp at a wavelength of 254nm. There was evidence that the separation worked as the yellowish coloured fractions had the same  $R_f$  values in the TLC. They were evaporated to dryness, but the analysis via ESI-MS showed that after the separation via CC the product was somehow lost.

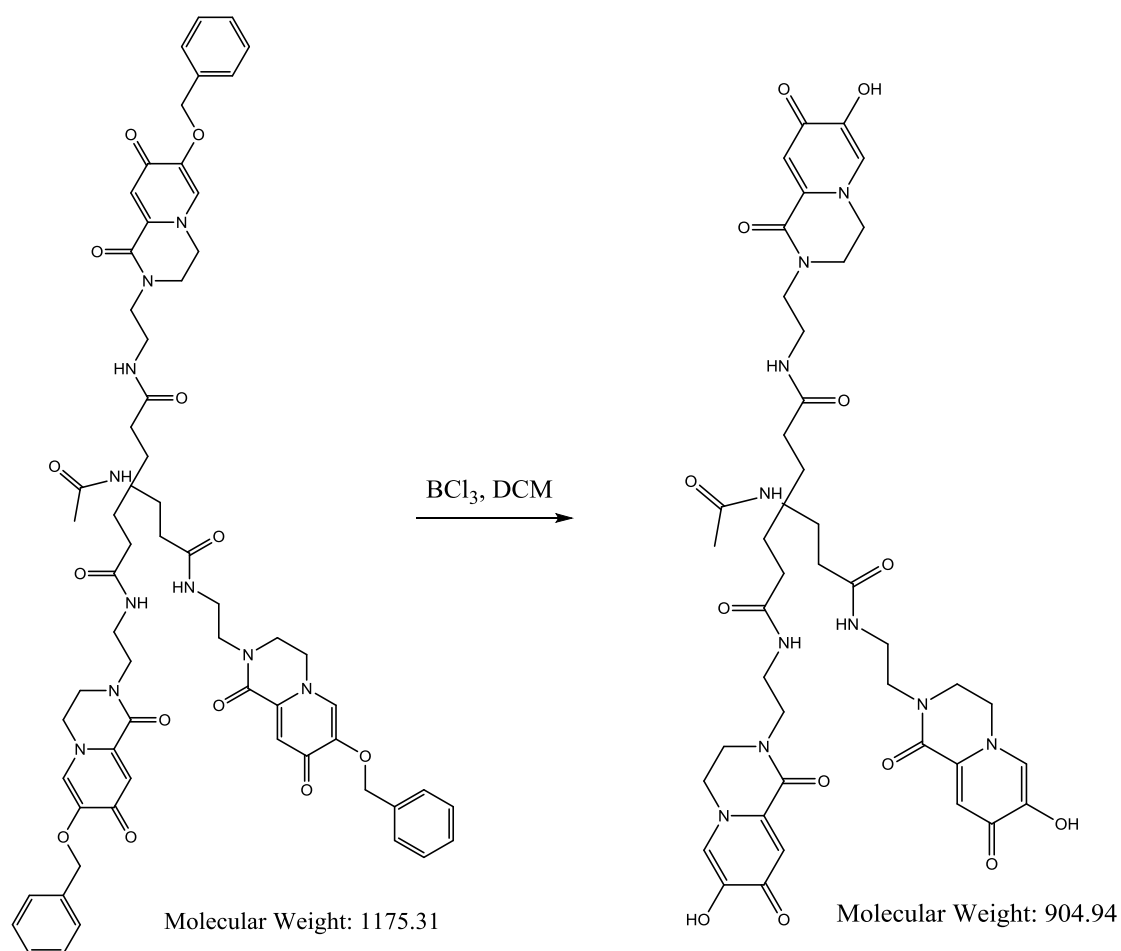
In the next trial it was purified via preparative HPLC using a prep C18 column and an acetonitrile/water gradient. The two-armed product could be collected, was injected into the RP-HPLC and showed a clear peak at 15.91 mins (see appendix image 28) which suggests that in all previous attempts mainly the two-armed product was formed as the peaks of the products were always around this retention time.

The <sup>1</sup>H-NMR in deuterated DMSO proved the presence of the CH<sub>2</sub> groups at 1.72-1.79 (d, 2H), 1.95 (s, 2H), 1.97 (s, 2H), 3.35-3.55 (t, 2H), 2.58-3.75 (t, 2H), 3.80-3.87 (t, 2H), 4.31-4.38 (t, 2H) and 4.44-4.50 ppm (t, 2H), the characteristic shifts of the benzyl-protecting group were present with the CH<sub>2</sub> group at 5.10 ppm (s, 2H) and the aromatic hydrogens at 7.14-7.46 ppm (m, 5H). The singlets of the pyridine ring were shown at 6.78 (s, 1H) and 7.30 ppm (s, 1H) and the shifts of the hydrogens of the secondary amides were obtained at 7.98 (s, 1H), 8.06 (s, 1H) and 8.15 ppm (s, 1H) (see appendix image 22).

The detailed synthetic procedure is described in section 3.2.5.5.



**3.1.5.6. Attempted synthesis of 4-acetamido-N1,N7-bis(2-(7-hydroxy-1,8-dioxo-1,3,4,8-tetrahydro-2H-pyrido[1,2-a]pyrazin-2-yl)ethyl)-4-(3-((2-(7-hydroxy-1,8-dioxo-1,3,4,8-tetrahydro-2H-pyrido[1,2-a]pyrazin-2-yl)ethyl)amino)-3-oxopropyl)heptanediamide (CR 17)**



**Scheme 12 Attempted synthesis of 4-acetamido-N1,N7-bis(2-(7-hydroxy-1,8-dioxo-1,3,4,8-tetrahydro-2H-pyrido[1,2-a]pyrazin-2-yl)ethyl)-4-(3-((2-(7-hydroxy-1,8-dioxo-1,3,4,8-tetrahydro-2H-pyrido[1,2-a]pyrazin-2-yl)ethyl)amino)-3-oxopropyl)heptanediamide**

In order to generate the hexadentate chelator (see Scheme 12) the previously prepared benzyl-protected 4-acetamido-N1,N7-bis(2-(7-(benzyloxy)-1,8-dioxo-1,3,4,8-tetrahydro-2H-pyrido[1,2-a]pyrazin-2-yl)ethyl)-4-(3-((2-(7-(benzyloxy)-1,8-dioxo-1,3,4,8-tetrahydro-2H-pyrido[1,2-a]pyrazin-2-yl)ethyl)amino)-3-oxopropyl)heptanediamide was suspended in DCM and flushed with N<sub>2</sub>. After the flask was cooled to 0°C, BCl<sub>3</sub> in DCM was slowly added and the reaction mixture was allowed to stir at room temperature for 5 h. BCl<sub>3</sub> is a strong Lewis acid, it forms an

adduct with the ether and then cleaves the bond between the carbon and the oxygen to get rid of the protecting group as toluene. The excess of  $\text{BCl}_3$  was eliminated at the end of the reaction by the addition of MeOH and left to stir for another 0.5 h. The solvents were removed under reduced pressure and the crude residue was purified via recrystallization by dissolving it in minimal MeOH and crushing it with excess of cold Acetone.

The result of the  $^1\text{H}$ -NMR (see appendix image 23) was not completely clear. It proved that the debenzylation was almost complete, but a tiny shift of the multiplet around 7.32 ppm was still present. It seemed as if the product was destroyed as only one of the C-H bonds in the pyridine ring was visible, the chromatogram showed only one of the characteristic shifts of the secondary amides (at 8.04 ppm) and some of the  $\text{CH}_2$  shifts were missing.

The detailed synthetic procedure is described in section 3.2.5.6.

## 3.2. Synthetic Details

### 3.2.1. Synthesis of 5-Benzyloxy-2-hydroxymethyl-4H-pyran-4-one (Compound CR 0)

To a solution of kojic acid (35.5g, 0.25 Mol) in MeOH (250 mL) was added sodium hydroxide (11 g, 0.275 Mol) dissolved in water (25 mL). Benzylchloride (35 g, 0.277 Mol) was added dropwise over 10 mins and the resulting brown mixture was refluxed overnight. The solvent was removed by rotary evaporation, and the residue, a brown solid was washed with water, followed by MeOH to afford a pure white solid, which showed a clear peak at 11.49 mins in the RP-HPLC (see appendix image 24) (Ma, Kong, et al., 2015) (Yield: 32.05 g, 55 %).

<sup>1</sup>H-NMR (DMSO-d<sub>6</sub>) 4.30 (s, 2H), 4.95 (s, 2H), 5.72 (s, 1H), 6.34 (s, 1H), 7.33-7.44 (m, 5H), 8.19 (s, 1H) (see appendix image 8)

### 3.2.2. Synthesis of 5-(benzyloxy)-4-oxo-4H-pyran-2-carboxylic acid; 3-hydroxy-protected comenic acid (Compound CR 4)

The previously prepared 5-Benzyloxy-2-hydroxymethyl-4H-pyran-4-one (5.9770 g, 25.736 mMol) was suspended in Acetone (300 mL), the flask cooled in an ice bath to 0°C, and then 20 mL of Jones reagent were added dropwise over 10 mins. In order to produce the Jones reagent 26.72 g of chromic trioxide were dissolved in water to 77 mL and then 23 mL of concentrated sulfuric acid were added to a total volume of 100 mL. The reaction was stirred for one day at room temperature until the RP-HPLC showed only one peak at 10.77 mins (see appendix image 25). Afterwards the inorganic material was removed by filtration and the filtrate evaporated to dryness. The crude product was washed with Acetone to get rid of the rest of the green Cr(III) and recrystallized from methanol to afford the compound as pure white needles (Yield 3.01 g, 48 %) (Ma, Kong, et al., 2015).

<sup>1</sup>H-NMR (DMSO-d<sub>6</sub>) 4.98 (s, 2H), 6.95 (s, 1H), 7.42 (s, 5H), 8.35 (s, 1H) (see appendix image 9)

### 3.2.3. Synthesis of 2-(2-aminoethyl)-7-(benzyloxy)-3,4-dihydro-2H-pyrido[1,2-a]pyrazine-1,8-dione (Compound CR 6)

The beforehand synthesized 3-hydroxy-protected comenic acid (3.0076 g, 12.2256 mMol, 1 eq) was suspended in a mixed solution of EtOH and water (1:1, 92 mL). When the diethylenetriamine (1154  $\mu$ L, 18.338 mMol, 1.5 eq) was added, the mixture turned yellow. The reaction mixture was stirred with reflux at 200°C overnight, turning light orange. After removal of the solvents by rotary evaporation, the yellow crude solid was recrystallized by dissolving it in minimal MeOH and crushing it with excess of cooled ether to obtain the fluorescent product as a yellow solid which showed a peak at 9.09 mins in the RP-HPLC (see characterization of CR 19 Figure 7) (Yield 2.78 g, 73%) (Ma, Kong, et al., 2015).

MS m/z: 314.2 [M+H]<sup>+</sup> (see appendix image 1)

<sup>1</sup>H-NMR (DMSO-d<sub>6</sub>) 2.50-2.51 (t, 2H), 2.72-2.75 (t, 2H), 3.43-3.49 (t, 2H), 3.73-3.76 (t, 2H), 4.16-4.19 (t, 2H), 4.98-5.02 (t, 2H), 6.77 (s, 1H), 7.33-7.45 (m, 5H), 7.72 (s, 1H) (see appendix image 10)

<sup>13</sup>C-NMR (DMSO-d<sub>6</sub>) 171.10, 157.55, 149.18, 136.60, 128.37-128.01, 115.91, 70.42, 50.07, 47.94, 44.58, 38.82 (see appendix image 11)

<sup>13</sup>C-NMR DEPT (DMSO-d<sub>6</sub>) 128.01-128.37, 125.54, 115.90, 70.42, 50.07, 47.94, 44.56, 39.36 (see appendix image 12)

### 3.2.4. Synthesis of 2-(2-aminoethyl)-7-hydroxy-3,4-dihydro-2H-pyrido[1,2-a]pyrazine-1,8-dione (Compound CR 19)

Afterwards the bicyclic, fluorescent compound was treated in different ways to get rid of the benzyl-protecting group. After several attempts it was then always dissolved in methanol and removed by 10% palladium-catalysed hydrogenation to afford the desired bicyclic, fluorescent, bidentate iron chelator, which is described in the following.

The compound 2-(2-aminoethyl)-7-(benzyloxy)-3,4-dihydro-2H-pyrido[1,2-a]pyrazine-1,8-dione (510.8 mg, 1.6 mMol) was dissolved in MeOH (35 mL) and subjected to hydrogenolysis in presence of an catalytic amount of about 50 mg 10% Pd/C (w/w) catalyst overnight. The catalysts were removed by filtration, the filtrate acidified to pH 1 with concentrated HCl, evaporated to dryness and recrystallized by dissolving it in minimal MeOH and crushing it with excess of cooled ether to obtain the fluorescent chelator as a yellow solid (Yield: 0.3693 g, 45%).

m/z: 224.1030 [M+H]<sup>+</sup> (see characterization of CR 19 Figure 1)

<sup>1</sup>H-NMR (DMSO-d<sub>6</sub>) 2.50-2.51 (t, 2H), 3.06-3.08 (t, 2H), 3.75-3.78 (t, 2H), 3.93-3.95 (t, 2H), 4.72-4.74 (t, 2H), 7.93 (s, 1H), 8.31 (s, 2H), 8.40 (s, 1H) (see characterization of CR 19 Figure 3)

<sup>13</sup>C-NMR (DMSO-d<sub>6</sub>) 160.54, 156.73, 146.79, 135.52, 130.34, 112.54, 50.88, 44.67, 43.67, 36.45 (see characterization of CR 19 Figure 5)

<sup>13</sup>C-NMR DEPT (DMSO-d<sub>6</sub>) 130.34, 112.54, 50.88, 44.67, 43.67, 36.45 (see characterization of CR 19 Figure 6)

Other attempts to deprotect the compound from the benzyl-protecting group:

Reaction with BCl<sub>3</sub>:

0.5g (1.6 mMol) of 2-(2-aminoethyl)-7-(benzyloxy)-3,4-dihydro-2H-pyrido[1,2-a]pyrazine-1,8-dione were suspended in 30 mL of DCM, the flask was cooled to 0°C and flushed with nitrogen. Then the strong acid BCl<sub>3</sub> (1M in DCM, 8 mL) was slowly added, which gave a yellow suspension, and the reaction mixture was allowed to stir at room temperature for 5 h. The excess of borontrichloride was eliminated at the end of the reaction by the addition of 10 mL MeOH and left to stir for another 0.5 h. The solvents were removed under reduced pressure, yielding a light yellow solid, which was purified by recrystallization from minimal MeOH and excess of cooled diethylether to obtain a yellow solid (537.5 mg, 150 %) (Ma, Luo, Quinn, Liu, & Hider, 2004). As the high amount of the calculated yield already hypothesised, the analysis via NMR (see

appendix image 14) showed that the cleavage with the strong acid  $\text{BCl}_3$  did not remove the benzyl. One of the problems might have been that the protected lactam was not soluble in DCM.

Reaction with 5 % Pd/C (w/w) catalyst in EtOH:

0.5g (1.6 mMol) of the protected lactam were dissolved in 20 mL EtOH and subjected to hydrogenolysis in presence of a catalytic amount of about 100 mg 5% Pd/C (w/w) catalyst overnight. The catalysts were removed by filtration, the filtrate was acidified to pH 1 with concentrated HCl and evaporated to dryness (Ma, Kong, et al., 2015). The light-yellow crude was recrystallized by dissolving it in MeOH and afterwards crushing it with cold acetone. The analysis via NMR (see appendix image 15) showed that the hydrogenation with 5% palladium on carbon was not efficient enough either.

### 3.2.5. Synthetic details of the attempts of forming the hexadentate, fluorescent iron chelator

#### 3.2.5.1. Attempted synthesis of N1,N7-bis(2-(7-(benzyloxy)-1,8-dioxo-1,3,4,8-tetrahydro-2H-pyrido[1,2-a]pyrazin-2-yl)ethyl)-4-(3-((2-(7-(benzyloxy)-1,8-dioxo-1,3,4,8-tetrahydro-2H-pyrido[1,2-a]pyrazin-2-yl)ethyl)amino)-3-oxopropyl)-4-(3-(1,3-dioxoisindolin-2-yl)propanamido)heptanediamide (Compound CR 8)

A mixture of the previously prepared triacid 4-(2-carboxyethyl)-4-(3-(1,3-dioxoisindolin-2-yl)propanamido)heptanedioic acid (502.9 mg, 1.116 mMol), EDC (641.81 mg, 3.348 mMol) and HOBt (512.69 mg, 3.348 mMol) was dissolved in dry DMF (8 mL) and 0.2 mL of DMSO were added to increase the solubility. The compounds were added under nitrogen and stirred in a flask cooled to 0°C. After 2 h the amine 2-(2-aminoethyl)-7-(benzyloxy)-3,4-dihydro-2H-pyrido[1,2-a]pyrazine-1,8-dione (2.098 g, 6.696 mMol) was added and left to stir for 2 days at room temperature. The RP-HPLC showed a peak at 16.14 mins, but there was still an amount of amine left (9.06 mins) (see appendix image 26).

Two different trials of purifying the product were carried out:

As the amine was soluble in water, the idea was to get rid of it via liquid liquid extraction. The product was diluted with water (12 mL) and extracted three times with chloroform (20 mL), which seemed to work better than DCM. The chloroform phase was first washed with 5% NaHCO<sub>3</sub> solution and then with brine. The organic extracts were dried over anhydrous sodiumsulfate, filtered and evaporated under reduced pressure to light orange crystals (yield 80.10 mg, 5%).

The compound was also purified via preparative HPLC, which showed a peak at in the RP-HPLC (see appendix image 27).

m/z: 1334.1, 668.3 [M+2H]<sup>2+</sup> (see appendix image 2)

<sup>1</sup>H-NMR (DMSO-d<sub>6</sub>) 1.66-1.70 (2H, t), 2.51-2.52 (2H, t), 2.73-2.80 (2H, t), 2.99-3.04 (2H, t), 3.04 (s, 2H), 3.27 (s, 2H), 3.50 (s, 2H), 3.71-3.80 (t, 2H), 4.21-4.26 (t, 2H), 5.00 (s, 2H), 6.79-6.80 (d, 1H), 7.20-7.23 (t, 1H), 7.33-7.48 (m, 4H), 7.73-7.81 (m, 5H) (see appendix image 17)

<sup>1</sup>C-NMR (DMSO-d<sub>6</sub>) 25.89, 34.33, 36.56, 36.71, 42.72, 43.42, 44.26, 54.97, 70.42, 110.61, 118.34, 122.94, 123.05, 127.85-128.37, 136.48, 142.90, 149.25, 158.28, 158.43, 162.31, 167.70, 171.00, 172.42 (see appendix image 18)

**3.2.5.2. Attempted synthesis of 4-(3-aminopropanamido)-N1,N7-bis(2-(7-(benzyloxy)-1,8-dioxo-1,3,4,8-tetrahydro-2H-pyrido[1,2-a]pyrazin-2-yl)ethyl)-4-(3-((2-(7-(benzyloxy)-1,8-dioxo-1,3,4,8-tetrahydro-2H-pyrido[1,2-a]pyrazin-2-yl)ethyl)amino)-3-oxopropyl)heptanediamide (Compound CR 11)**

To a solution of N1,N7-bis(2-(7-(benzyloxy)-1,8-dioxo-1,3,4,8-tetrahydro-2H-pyrido[1,2-a]pyrazin-2-yl)ethyl)-4-(3-((2-(7-(benzyloxy)-1,8-dioxo-1,3,4,8-tetrahydro-2H-pyrido[1,2-a]pyrazin-2-yl)ethyl)amino)-3-oxopropyl)-4-(3-(1,3-dioxoisindolin-2-yl)propanamido)heptanediamide (207.6 mg, 0.16 mMol) in ethanol (2 mL) was added 5.5 % aqueous Hydrazine (0.16 mL). After being refluxed overnight, the reaction mixture was cooled to 0°C. In the first trial it was then acidified to pH 1 with concentrated HCl and filtered. The filtrate was concentrated in vacuo, and the residue was dissolved in distilled water, adjusted to pH 12 with 10 M NaOH. This led to a change of the colour to dark orange. Afterwards the compound was extracted with chloroform (4 times 20 mL) and the combined organic extracts were dried over Na<sub>2</sub>SO<sub>4</sub> under reduced pressure to furnish the product as a brown solid (Zhou et al., 2006).

In the next trial the protected hexadentate chelator (0.25235 g, 0.189 mMol) was dissolved in methanol (4 mL), in which the compound seemed to be better soluble. To the solution 5.5 % aqueous Hydrazine (0.2 mL) was added. This time the workup was stopped before the acid/base extraction. The product was centrifuged after being cooled to 0°C and the supernatant evaporated to a brown solid (yield: 0.1788 g, 101 %), which was purified via preparative HPLC using a prep C18 column and an acetonitrile/water gradient.

The product could not be characterized via NMR.



### 3.2.5.3. Synthesis of di-tert-butyl 4-acetamido-4-(3-(tert-butoxy)-3-oxopropyl)heptanedioate (Compound CR 14)

6 g (14.4578 mMol, 1 eq) of a previously prepared tripodal-amino ester (di-tert-butyl 4-amino-4-(3-(tert-butoxy)-3-oxopropyl)heptanedioate) were dissolved in 30 mL DCM and triethylamine (1.75 g, 17.349 mMol, 1.2 eq) was added. The mixture was cooled to 0°C with an ice bath and acetyl chloride (1.36 g, 17.349 mMol, 1.2 eq) was added dropwise. The solution was stirred for further 4 h and allowed to warm slowly to room temperature. Afterwards it was poured into a separating funnel and washed 2 times with 90 mL HCl (5% aqueous) and once with 90 mL brine. The solution was dried over sodiumsulfate and filtrate. Then the solvents were removed in vacuo. The crude residue was dissolved in minimal EtOAc and purified by column chromatography with EtOAc:Hexane (1:1) as mobile phase. Then the different fractions were checked by TLC with the starting material amine as a reference and the newly synthesized amide. The different R<sub>f</sub> values were detected by dunking the TLC plates in a solution of permanganate and heating them. The amide fractions were evaporated to dryness to yield the tripodal-acetyl ester di-tert-butyl 4-acetamido-4-(3-(tert-butoxy)-3-oxopropyl)heptanedioate as a white solid (yield: 4.28 g, 69 %) (Berry, Ma et al. 2011).

m/z: 458.4 [M+H]<sup>+</sup>, 481.3 [M+Na]<sup>+</sup> (see appendix image 3)

<sup>1</sup>H-NMR (DMSO-d<sub>6</sub>) 1.39 (s, 3H), 1.75-1.78 (t, 3H), 2.07-2.11 (t, 2H), 2.50-2.52 (t, 2H), 7.20 (s, 1H) (see appendix image 20)

#### 3.2.5.4. Synthesis of 4-acetylamido-4-(2-carboxyethyl)heptanedioic acid (Compound CR 15)

4.2842g (9.37 mMol) of tripodal-acetyl ester di-tert-butyl 4-acetamido-4-(3-(tert-butoxy)-3-oxopropyl)heptanedioate was dissolved in 57 mL of formic acid (96 %) and left to stir at room temperature overnight. Then the formic acid was removed by azeotropic distillation with 5 times 60 mL portions of toluene. The crude residue, a white oil, was recrystallized by dissolving it in minimal EtOH and crushing it with cold hexane and cooled overnight in the fridge to get an acceptable yield of a pure tripodal-acetyl acid 4-acetamido-4-(2-carboxyethyl)heptanedioic acid as a white solid (yield: 1.5136 g, 56 %) (Berry et al., 2011).

m/z 290.2 [M+H]<sup>+</sup> (see appendix image 4)

<sup>1</sup>H-NMR (D<sub>2</sub>O-d<sub>6</sub>) 1.82 ppm (s, 3H), 1.86-1.90 (t, 2H), 2.21-2.25 (t, 2H), 7.30 (s, 1H) (see appendix image 21)

#### 3.2.5.5. Attempted synthesis of 4-acetamido-N1,N7-bis(2-(7-(benzyloxy)-1,8-dioxo-1,3,4,8-tetrahydro-2H-pyrido[1,2-a]pyrazin-2-yl)ethyl)-4-(3-((2-(7-(benzyloxy)-1,8-dioxo-1,3,4,8-tetrahydro-2H-pyrido[1,2-a]pyrazin-2-yl)ethyl)amino)-3-oxopropyl)heptanediamide (Compound CR 16)

HATU (805.6 mg, 2.12 mMol, 4 eq), DIPEA (273.99 mg, 2.12 mMol, 4 eq) and the previously prepared tripodal-acetyl acid (144.64 mg, 0.5 mMol, 1 eq) were added into a microwave vial and dissolved in 5 mL DMF. When the amine (664.32 mg, 2.12 mMol, 4 eq) was added in the end, the mixture turned yellow. The mixture was heated in a microwave reactor, twice for 30 mins at 120°C until the amine at m/z: 314.1517 [M+H]<sup>+</sup> seemed to be gone which was checked via HRMS in between. It also looked as if the one and the two armed product at m/z: 392.5133 [M+2H]<sup>2+</sup> and m/z: 440.6990 [M+2H]<sup>2+</sup> (see appendix image 6) disappeared.

m/z: 1175.5218 [M+H]<sup>+</sup>, 588.2657 [M+2H]<sup>2+</sup>, 295.2889 [M+4H]<sup>4+</sup> (see appendix image 7).

<sup>1</sup>H-NMR 1.72-1.79 (d, 2H), 1.95 (s, 2H), 1.97 (s, 2H), 3.35-3.55 (t, 2H), 2.58-3.75 (t, 2H), 3.80-3.87 (t, 2H), 4.31-4.38 (t, 2H), 4.44-4.50 (t, 2H), 5.10 (s, 2H), 6.78 (s, 1H), 7.30 (s, 1H), 7.14-7.46 (m, 5H), 7.98 (s, 1H), 8.06 (s, 1H), 8.15 (s, 1H) (see appendix image 22)

### 3.2.5.6. Attempted synthesis of 4-acetamido-N1,N7-bis(2-(7-hydroxy-1,8-dioxo-1,3,4,8-tetrahydro-2H-pyrido[1,2-a]pyrazin-2-yl)ethyl)-4-(3-((2-(7-hydroxy-1,8-dioxo-1,3,4,8-tetrahydro-2H-pyrido[1,2-a]pyrazin-2-yl)ethyl)amino)-3-oxopropyl)heptanediamide (CR 17)

For the debenzylation the protected compound 4-acetamido-N1,N7-bis(2-(7-(benzyloxy)-1,8-dioxo-1,3,4,8-tetrahydro-2H-pyrido[1,2-a]pyrazin-2-yl)ethyl)-4-(3-((2-(7-(benzyloxy)-1,8-dioxo-1,3,4,8-tetrahydro-2H-pyrido[1,2-a]pyrazin-2-yl)ethyl)amino)-3-oxopropyl)heptanediamide (382.9 mg, 0.3258 mMol) was suspended in DCM (10 mL) and flushed with nitrogen. After the flask was cooled to 0°C, the strong Lewis acid BCl<sub>3</sub> (1 M in DCM, 5.5 mL) was slowly added with a syringe through a septum and the reaction mixture was allowed to stir at room temperature for 5h. To get rid of the excess of BCl<sub>3</sub>, MeOH (15 mL) was added at the end of the reaction and left to stir for another 0.5 h. After the removal of the solvents under reduced pressure, the residues were purified by recrystallization by dissolving it in minimal MeOH and crushing it with excess of cooled Acetone to obtain a red solid (Ma et al., 2004).

The result of the <sup>1</sup>H-NMR was not completely clear and it was supposed that the product was destroyed. One of the reasons could be that the strong acid BCl<sub>3</sub> was too harsh.

<sup>1</sup>H-NMR 1.03-1.06 (t, 2H), 1.78 (s, 2H), 2.75 (s, 2H), 2.42-3.46 (t, 2H), 3.79-3.82 (t, 2H), 3.87-3.90 (t, 2H), 7.32 (s, 5H), 7.65 (s, 1H), 8.04 (s, 1H) (see appendix image 23)

#### 4. Characterization of 2-(2-aminoethyl)-7-hydroxy-3,4-dihydro-2H-pyrido[1,2-a]pyrazine-1,8-dione (Compound CR 19)

Table 1 shows a summary of the physicochemical properties of the synthesized compound 2-(2-aminoethyl)-7-hydroxy-3,4-dihydro-2H-pyrido[1,2-a]pyrazine-1,8-dione compared to the similarly synthesized and characterized analogues 4i (6-((dimethylamino)methyl)-7-hydroxy-3,4-dihydro-2H-pyrido[1,2-a]pyrazine-1,8-dione) and 4j (7-hydroxy-6-((methylamino)methyl)-3,4-dihydro-2H-pyrido[1,2-a]pyrazine-1,8-dione) (Ma, Kong, et al., 2015).

As you can see, the results of the molecular weight (MW), maximum absorption wavelength (abs), maximum emission wavelength (em) and fluorescence quantum yield ( $\phi_F$ ) correspond with the previously obtained ones. The molar extinction coefficient  $\epsilon$  and the  $pFe^{3+}$  value are slightly lower and the ClogP and all  $pK_a$  values are somewhat higher.

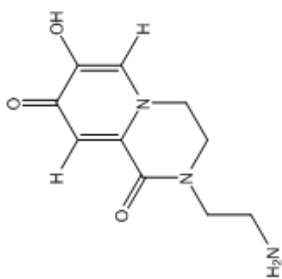
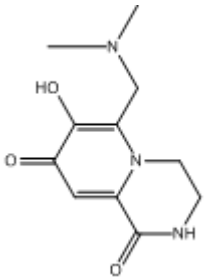
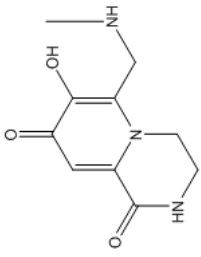
Compound	Structure	MW	abs (nm)	em (nm)	$\epsilon$ ( $M^{-1}cm^{-1}$ ) at 320 or 225 nm	$\phi_F$	Clog P	pK <sub>a</sub>	pFe <sup>3+</sup>
CR 19		223	320	469	2667.1	0.16	-1.29	2.34, 7.45, 10.43	18.46
4i		237	325	470	3500	0.12	-2.77	1.82, 6.36, 8.71	21.4
4j		223	325	470	ND	ND	-3.23	1.41, 6.62, 9.32	20.4

Table 1 Table of the characterization of the synthesized bidentate chelator CR 19

## 4.1. Basic physicochemical properties

Calculated c-log P = -1.29

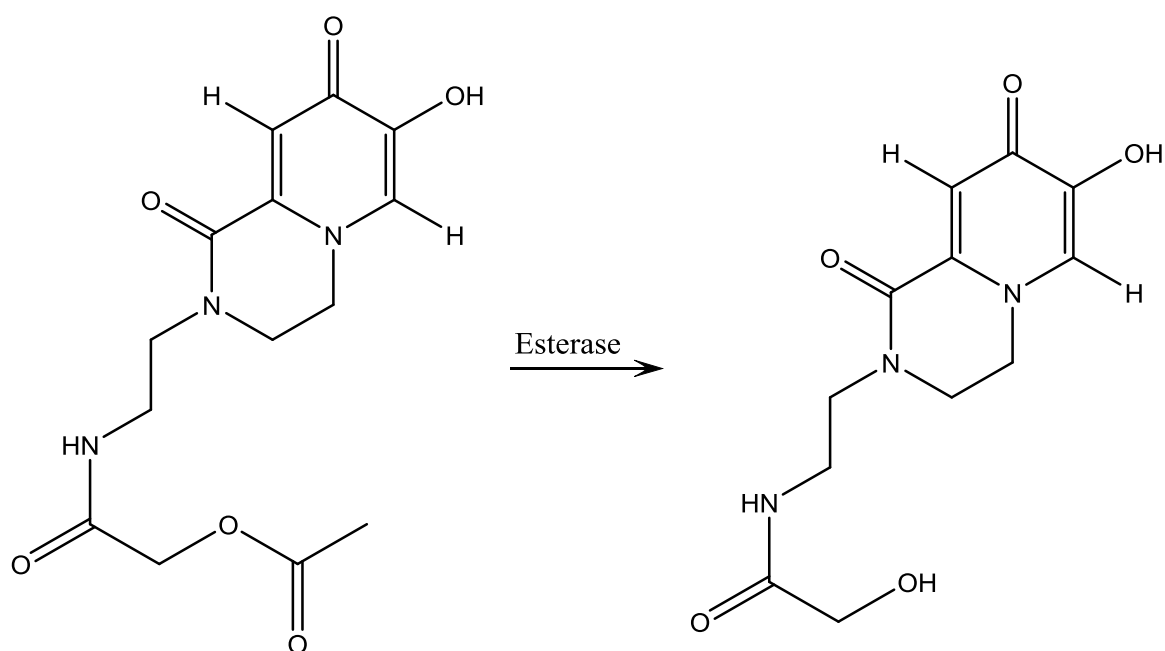
With a clogP of -1.29, which means that the compound is too hydrophilic, the fluorescent bidentate chelator will never permeate membranes.

Even when the amide group is coupled to esters (see Formula 7) which would be catalyzed by esterases in the body, it is still too hydrophilic to permeate membranes.

But the hydrophilic amine group of the compound has the advantage of giving us the possibility to couple it to carboxylic groups via amide formation.

mi-log P = -2.16

c-logD 7.4 = -2.84



**Formula 7** The chelator after esterification

clogP = - 1.85

milogP = - 1.78

clogD 7.4 = -1.85

clogP = -2.29

milogP = -2.49

clogD 7.4 = -2.29

## 4.2. High Resolution Mass Spectrometry (HRMS)

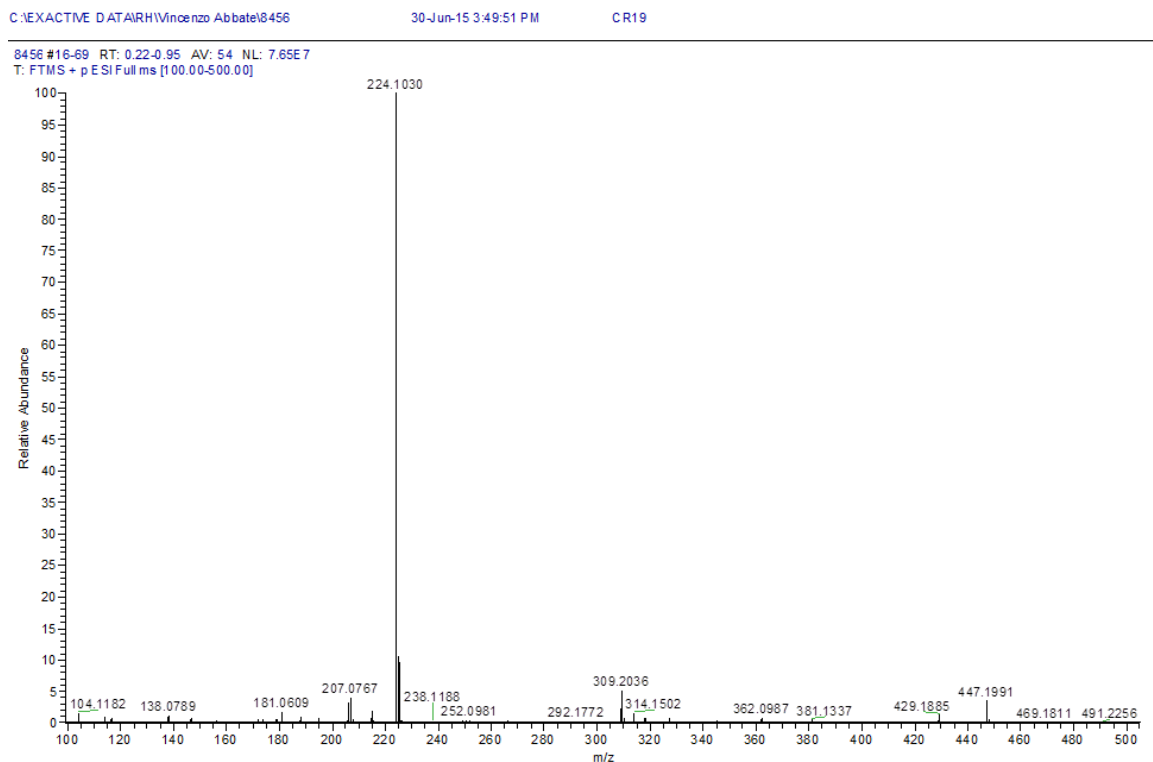


Figure 1 HRMS of 2-(2-aminoethyl)-7-hydroxy-3,4-dihydro-2H-pyrido[1,2-a]pyrazine-1,8-dione

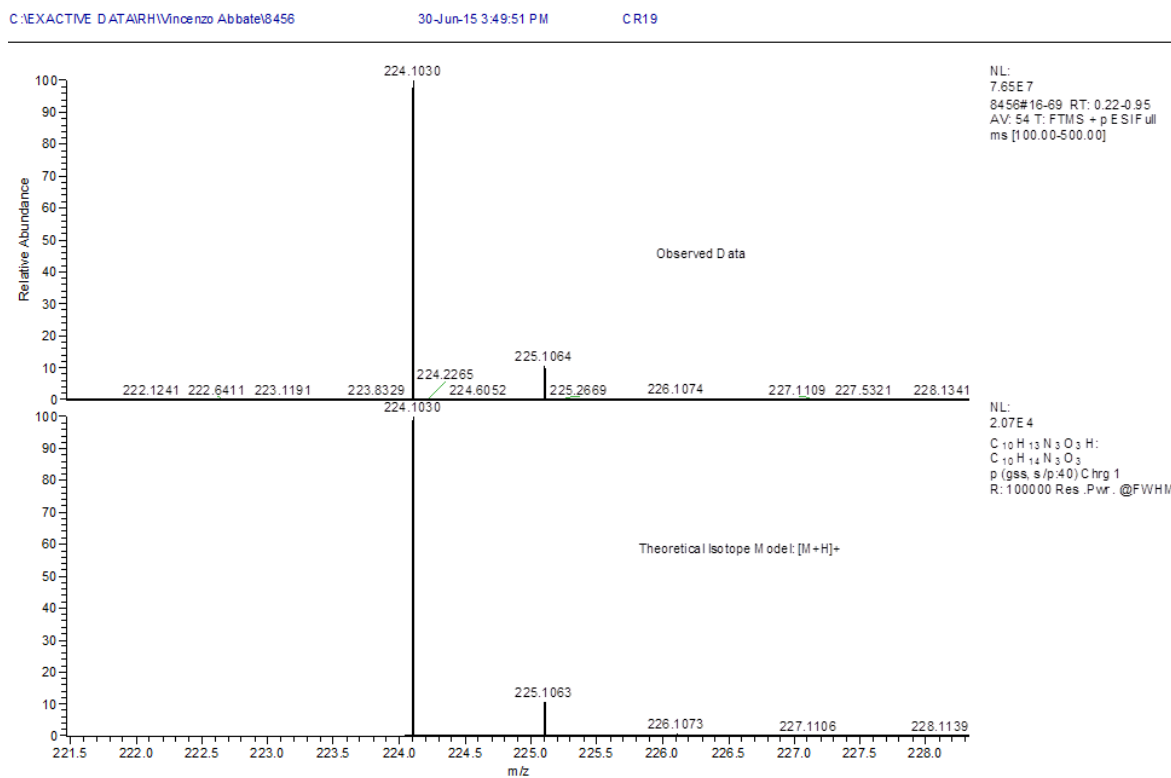


Figure 2 HRMS of the isotopes of 2-(2-aminoethyl)-7-hydroxy-3,4-dihydro-2H-pyrido[1,2-a]pyrazine-1,8-dione

The m/z of 224.1030  $[M+H]^+$  (see Figure 1 and Figure 2) corresponds almost perfectly with the via Chem Bio Draw Ultra 14.0 calculated m/z for  $[M+H]^+$  which is 224.1035. The single peak shows that quality of the product is very pure.



## 4.3. Nuclear Magnetic Resonance (NMR)

### 4.3.1. $^1\text{H}$ -NMR

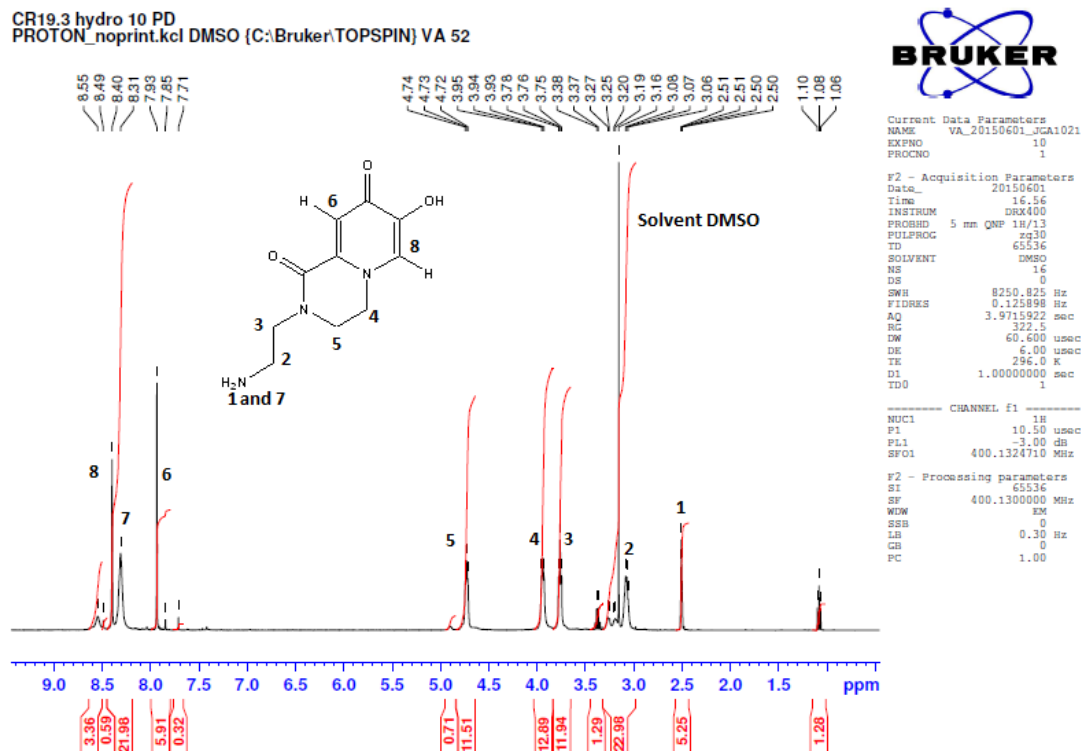
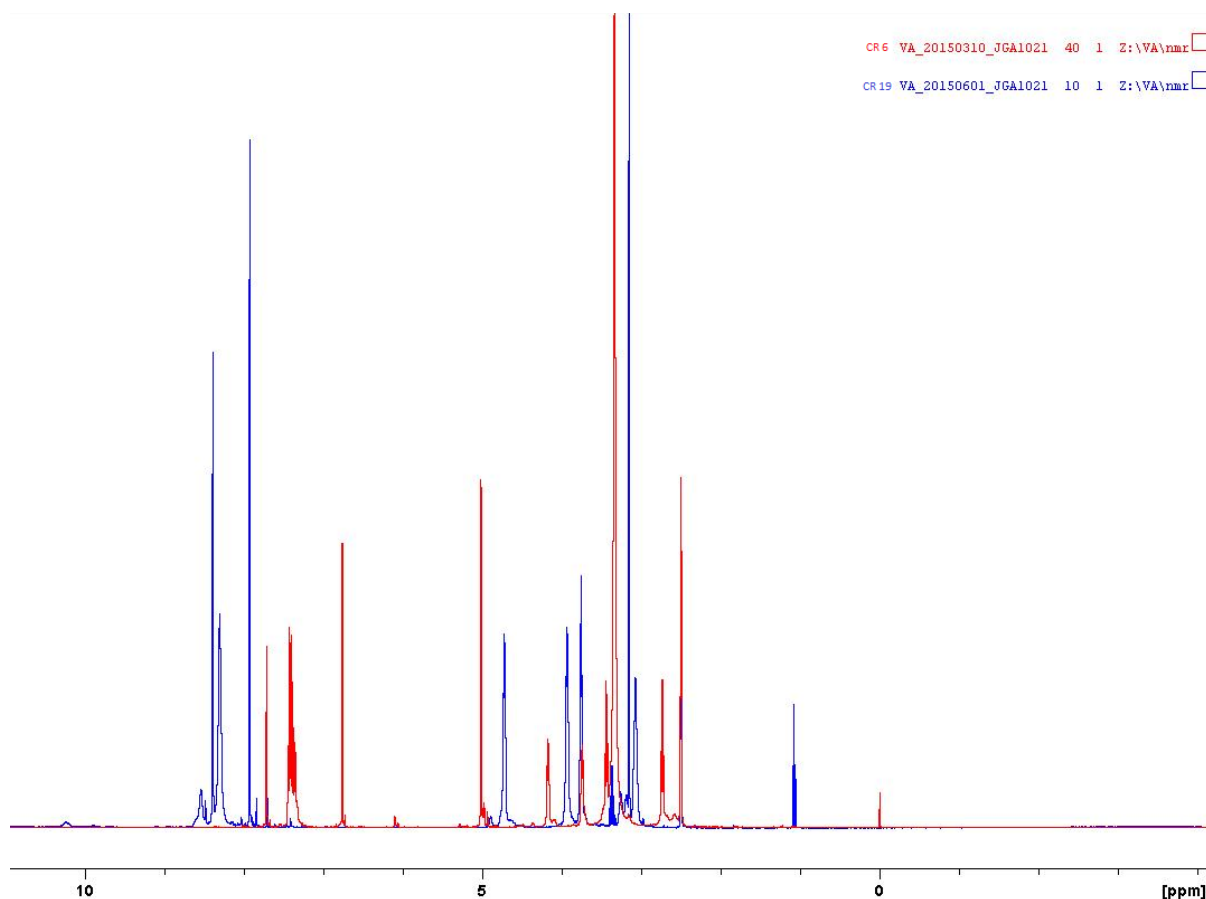


Figure 3  $^1\text{H}$ -NMR of 2-(2-aminoethyl)-7-hydroxy-3,4-dihydro-2H-pyrido[1,2-a]pyrazine-1,8-dione

The  $^1\text{H}$ -NMR in  $\text{DMSO}-d_6$  shows the presence of the primary amine at the chemical shifts of  $\delta$  2.50-2.51 ppm (t, 2H) and 8.31 ppm (s, 2H), the alkanes of the chain at  $\delta$  3.06-3.08 (t, 2H) and 3.75-3.78 ppm (t, 2H), and the hydrogens in the piperazine ring at  $\delta$  3.93-3.95 (t, 2H) and 4.72-4.74 ppm (t, 2H). The two hydrogens of the pyridine ring appear at  $\delta$  7.93 (s, 1H) and 8.40 ppm (s, 1H) (see Figure 3).



**Figure 4** overlap of the  $^1\text{H}$ -NMRs of the benzyl-protected CR 6 and the bidentate chelator CR 19

The overlap (see Figure 4) of the benzyl-protected (in red) and the with 10% PD/C (w/w) hydrogenated (in blue) compound clearly shows that the characteristic shifts of the aromatic hydrogens at  $\delta$  7.45-7.33 ppm (m, 5H) and the  $\text{CH}_2$  at  $\delta$  5.02-4.98 ppm (t, 2H) of the benzyl-protecting group disappeared.

### 4.3.2. $^{13}\text{C}$ -NMR

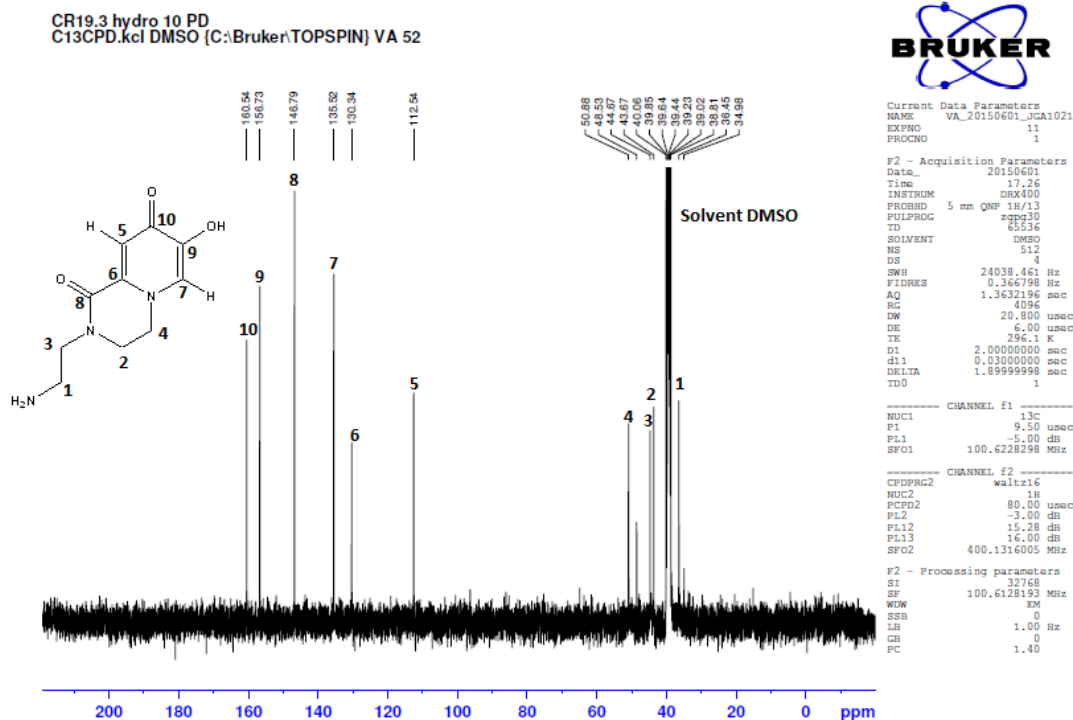


Figure 5  $^{13}\text{C}$ -NMR CR, 19 2-(2-aminoethyl)-7-hydroxy-3,4-dihydro-2H-pyrido[1,2-a]pyrazine-1,8-dione

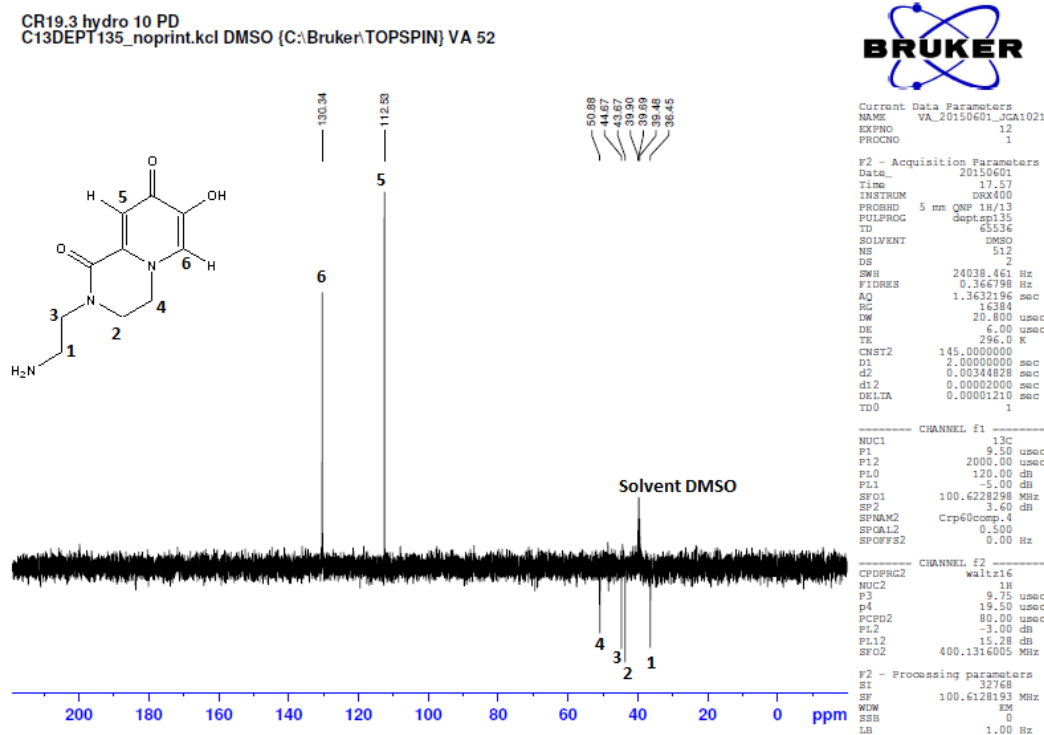


Figure 6  $^{13}\text{C}$ -NMR DEPT of 2-(2-aminoethyl)-7-hydroxy-3,4-dihydro-2H-pyrido[1,2-a]pyrazine-1,8-dione

The analysis via  $^{13}\text{C}$ -NMR and  $^{13}\text{C}$ -NMR DEPT mode proofed that the desired structure was synthesized: In the  $^{13}\text{C}$ -NMR the carbonyl-C shows a peak at the chemical shift of 160.54 ppm, the amide at 156.73 ppm and the other two quaternary carbons in the pyridine ring at 146.79 and 135.52 ppm. They are all absent in the DEPT mode, indicating that they are quaternary carbons. Compared to the benzyl-protected compound the aromatic carbons at 128.01-128.37 ppm and the chemical shift of the carbinol C at 70.42 ppm disappear in the spectrum, showing that the hydrogenation with 10% Pd/C (w/w) was successful. The chemical shifts of the carbons of the pyridine ring at 130.34 and 112.54 ppm remain positive in the DEPT mode which proves that they are tertiary. The shifts at 50.88, 44.67, 43.67 and 36.45 ppm point downwards in the DEPT mode which declares that they are secondary carbons (see image Figure 5 and Figure 6).

#### 4.4. High Performance Liquid Chromatography (HPLC)

The analysis via RP-HPLC showed that after the hydrogenation with 10 % Pd/C (w/w) the peak at 9.09 mins (see Figure 7) disappeared, which determines the polarity and purity of the chelator. A new single peak at 1.73 mins (see Figure 8) appeared, it could derive from the chelator 2-(2-aminoethyl)-7-hydroxy-3,4-dihydro-2H-pyrido[1,2-a]pyrazine-1,8-dione or from solvents.

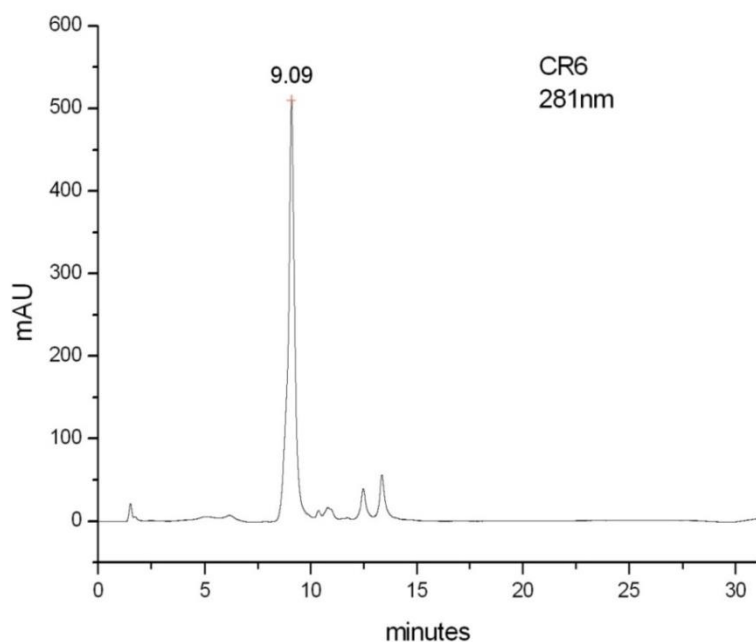


Figure 7 HPLC of CR 6, 2-(2-aminoethyl)-7-(benzyloxy)-3,4-dihydro-2H-pyrido[1,2-a]pyrazine-1,8-dione

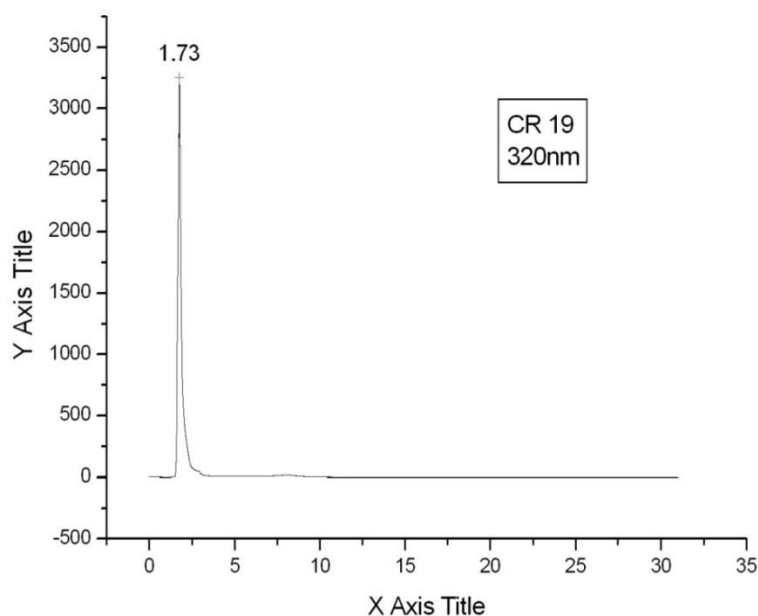


Figure 8 HPLC of CR 19, 2-(2-aminoethyl)-7-hydroxy-3,4-dihydro-2H-pyrido[1,2-a]pyrazine-1,8-dione

## 4.5. UV/Vis spectroscopy

### 4.5.1. UV/Vis spectrum

The UV/Vis spectrum of the bicyclic iron chelator (see Figure 9) was performed in MOPS buffer (0.1 molar, at the physiological pH 7.4) at room temperature.

The buffer was prepared as follows: 5.25g MOPS were dissolved in ultra-high pure water, adjusted to pH 7.4 with increasing concentrations of KOH and once it was buffered, the volumetric flask was filled up to 0.25 L with ultra-high pure water.

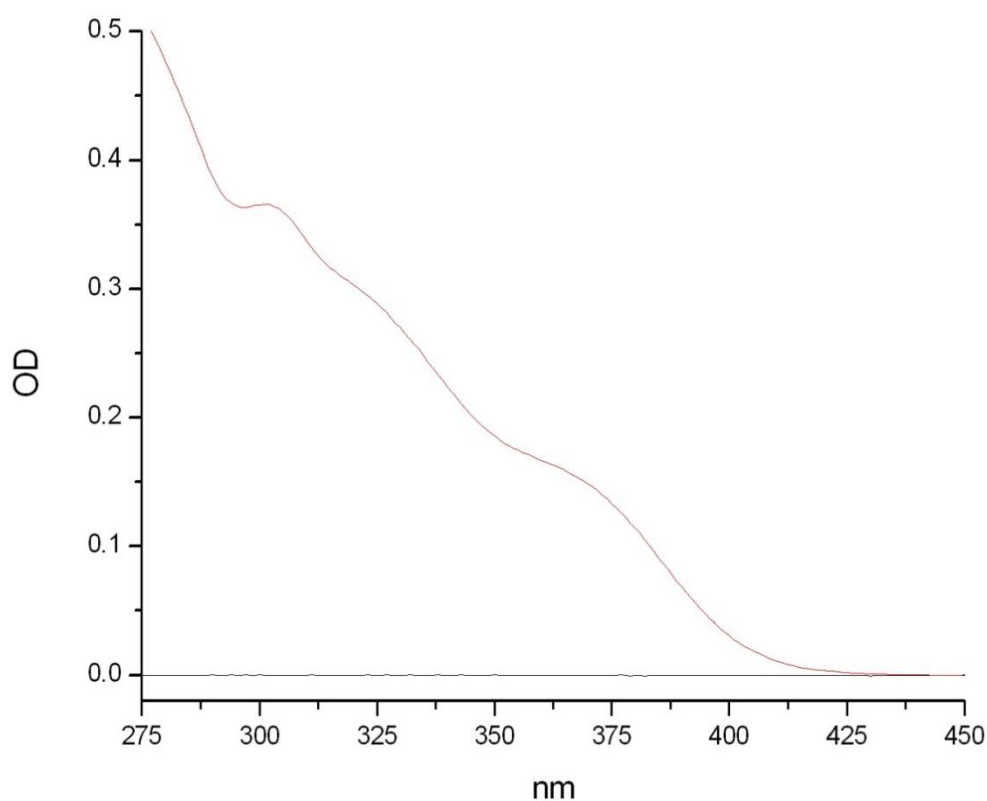


Figure 9 UV/Vis spectrum of CR 19, 2-(2-aminoethyl)-7-hydroxy-3,4-dihydro-2H-pyrido[1,2-a]pyrazine-1,8-dione

The graph shows that the compound has got absorption maxima at 310 and 350nm.

As you can see in the graph the blank does not absorb at any wavelength.

### 4.5.2. Molar Extinction Coefficient

For the molar extinction coefficient determination, cuvettes were set up containing a range of concentrations of the bidentate chelator in 0.1 M MOPS buffer (pH 7.4) from 0.066288 to 0.2651515 mM and the absorbance was measured at different wavelengths, never exceeding 1.000 (see Table 2). The buffer was prepared as described above.

Conc. (mM)	Absorbance 300 nm	Absorbance 320 nm	Absorbance 350 nm	Absorbance 370 nm	Absorbance 380 nm	Absorbance 400 nm
0.066288	0.119	0.045	0.110	0.098	0.079	0.028
0.1060606	0.194	0.145	0.172	0.149	0.118	0.037
0.13257	0.398	0.237	0.225	0.190	0.151	0.043
0.212121	0.586	0.524	0.369	0.299	0.235	0.072
0.2651515	0.746	0.659	0.456	0.372	0.293	0.085
0.3535353	0.913	0.855	0.610	0.499	0.393	0.114

**Table 2** Table of the absorbance of the compound CR 19 at 6 different concentrations and 6 different wavelengths

The concentration was plotted against the absorbance and the slope calculated for each graph (see Figure 10). In a graph absorbance versus concentration the slope is  $\epsilon d$  ( $d=1\text{cm}$ ).

The molar extinction coefficients ( $\text{M}^{-1}\text{cm}^{-1}$ ) at the different wavelengths are 2762.4 (300 nm), 2667.1 (320 nm), 1738.2 (350 nm), 1403.3 (370 nm), 1072.1 (380 nm) and 314.9 (400 nm).

The obtained value of  $2667.1\text{ M}^{-1}\text{cm}^{-1}$  at 320 nm for the synthesized bidentate chelator is lower than the one for the compound 4i of  $3500\text{ M}^{-1}\text{cm}^{-1}$  at 325 nm.

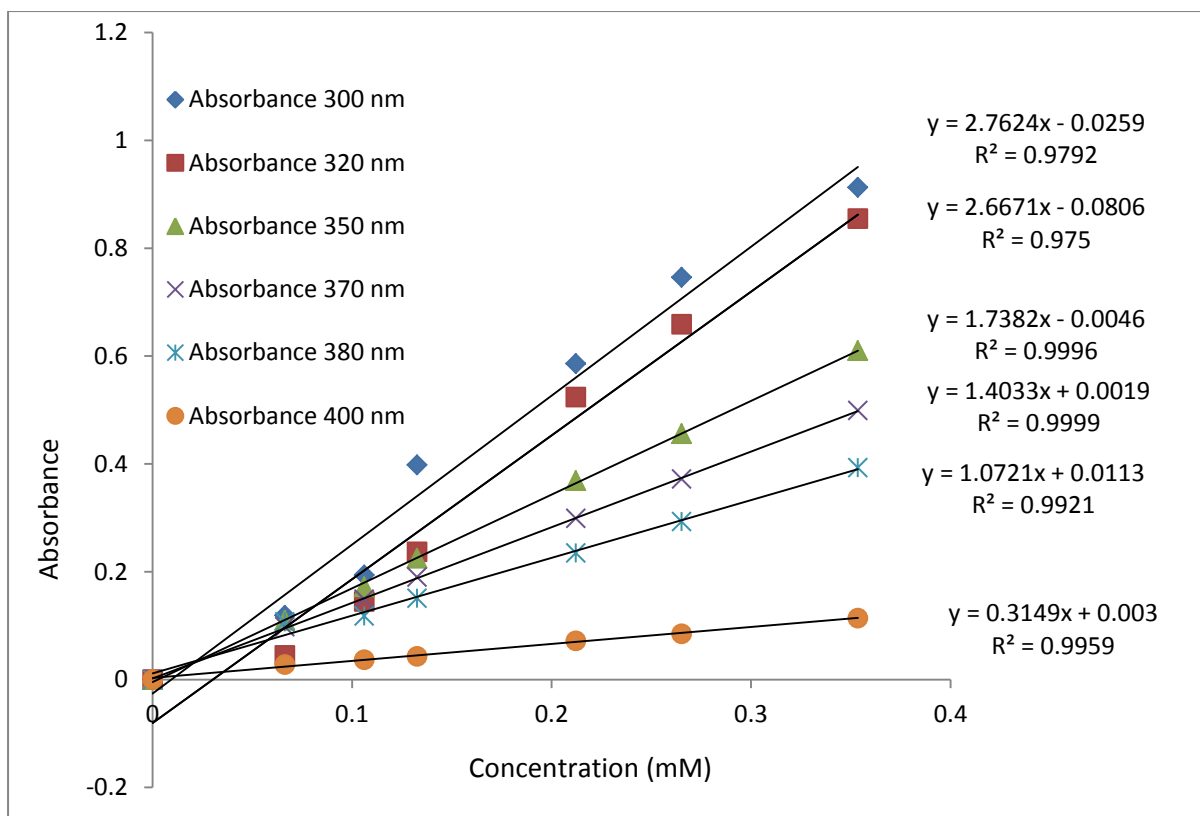


**Figure 10** The different concentrations (mM) plotted against the absorbance (nm) at different wavelengths of the bidentate chelator CR 19 to calculate the slope



## 4.6. Fluorescence emission spectroscopy

The fluorescence emission spectrum of the bicyclic iron chelator at different wavelengths was also performed in MOPS buffer (0.1 molar, at the physiological pH of 7.4) at room temperature. The buffer was again prepared as described above.

The maximum emission wavelength is 469 nm (see Figure 11) which corresponds with the values of compounds 4i and 4j.

As you can see in the graph the blank does not emit fluorescence.

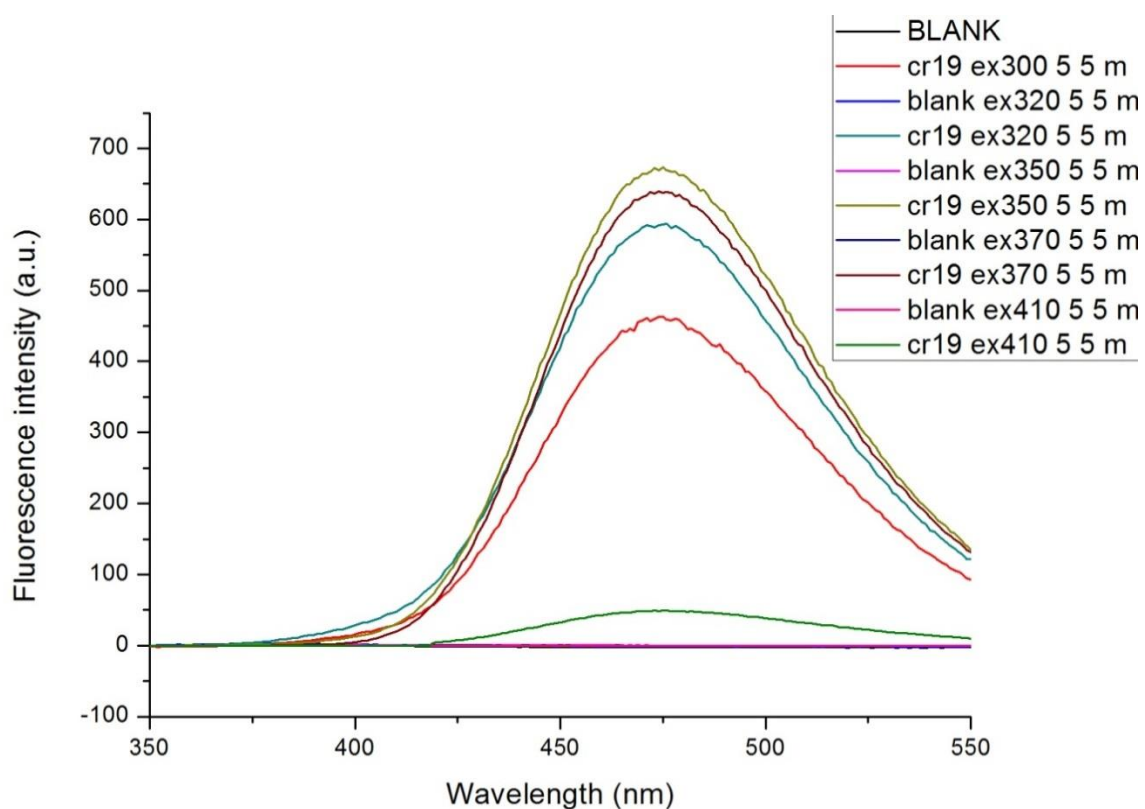
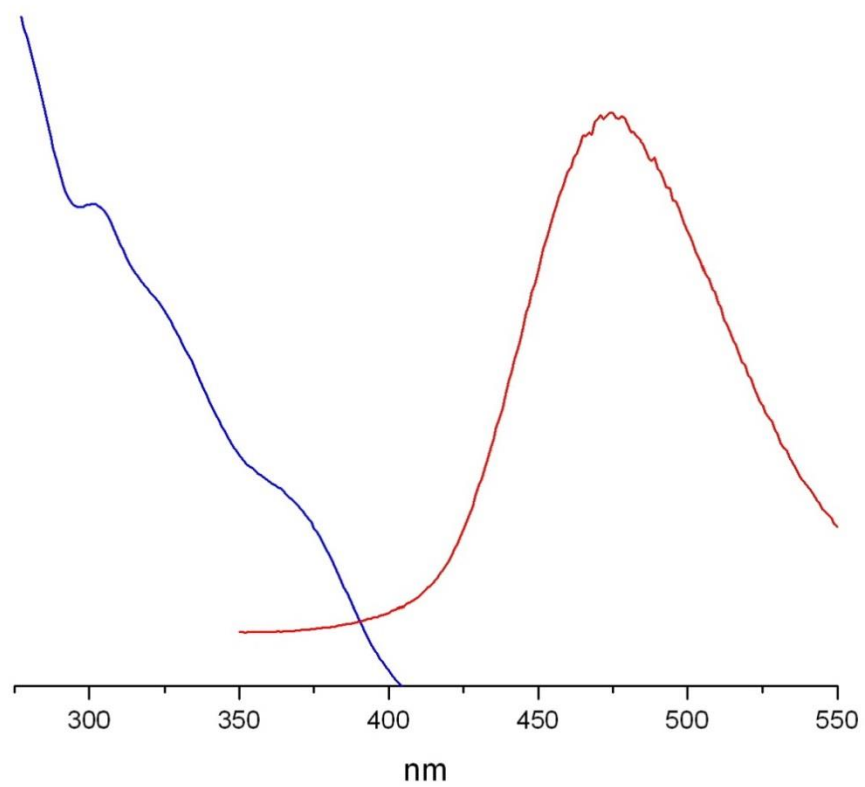


Figure 11 Fluorescence emission spectrum at different wavelengths



**Figure 12 UV/Vis spectrum merged with the fluorescence emission spectrum**

## 4.7. Fluorescence quenching by iron

To determine that the compound chelates iron in a 3:1 ratio, fluorescence quenching by iron was performed in a cell free system.

A 100  $\mu$ M Fe(III)-NTA solution in 100mM MOPS, pH 7.4 was prepared as follows: a stock solution of 100 mM nitrilotriacetic acid (NTA) trisodium salt was prepared in ultra-high pure water. 25  $\mu$ L of this solution were then mixed with 919  $\mu$ L water, followed by 56  $\mu$ L atomic absorption Fe (III) (1000g/L) to give a 1 mM Fe-NTA solution. After mixing it gently for 15 mins, 200  $\mu$ L of this mixture were diluted with 1.8 mL MOPS (0.1 M, pH 7.4) to give the desired target of 100  $\mu$ M Fe(III)-NTA solution.

The concentration of the iron chelator was 20  $\mu$ M in 100 mM MOPS, pH 7.4. In independent cuvettes, to 1.5 mL 100 mM MOPS buffer an appropriate volume was withdrawn and an identical volume was added from the 100  $\mu$ M Fe-NTA solution to give a final desired Fe-NTA concentration; to this solution 1.5 mL aliquots of the probe solutions were added to yield a constant 10  $\mu$ M final probe concentration. The fluorescence emission spectra (maximum emission wavelength 469nm) of the bidentate chelator (10  $\mu$ M) in MOPS buffer (100 mM, pH 7.4) in the presence of 0, 0.3, 0.5, 1.0, 1.5, 2.0, 2.5, 3.0, 5.0, 10.0  $\mu$ M of Fe(III)-NTA were then recorded at 350 nm for each sample to determine the extent of quenching upon probe/Fe(III)-NTA incubation (see Figure 13).

As you can see in the graphs (see Figure 13 and Figure 14) the fluorescence emission spectrum was found to be Fe(III) sensitive. An almost complete fluorescence quenching started at 2.5 to 3  $\mu$ M. When the ratio of the chelator to Fe(III) was less than that, a more or less linear relationship was observed (see Figure 14). When the ratio was higher than 3 to 1 the fluorescence is quenched, suggesting that the type of the chelator is bidentate (Ma, Kong, et al., 2015).

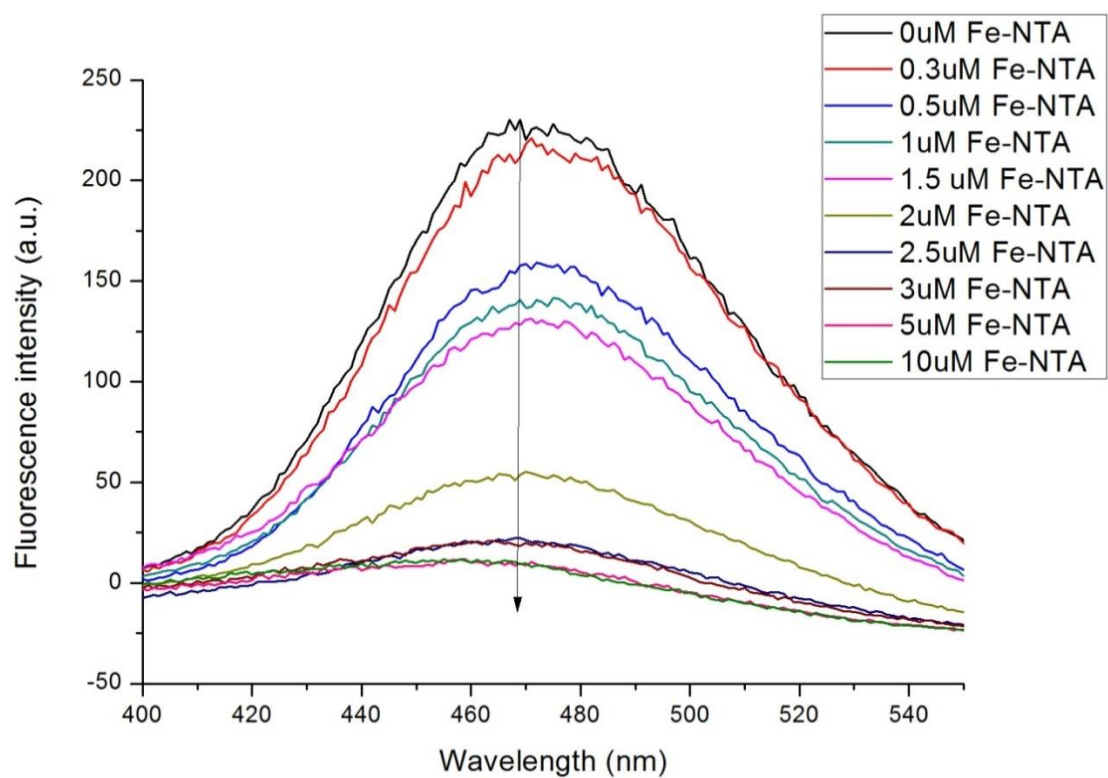


Figure 13 Fluorescence quenching by iron with different concentrations of iron

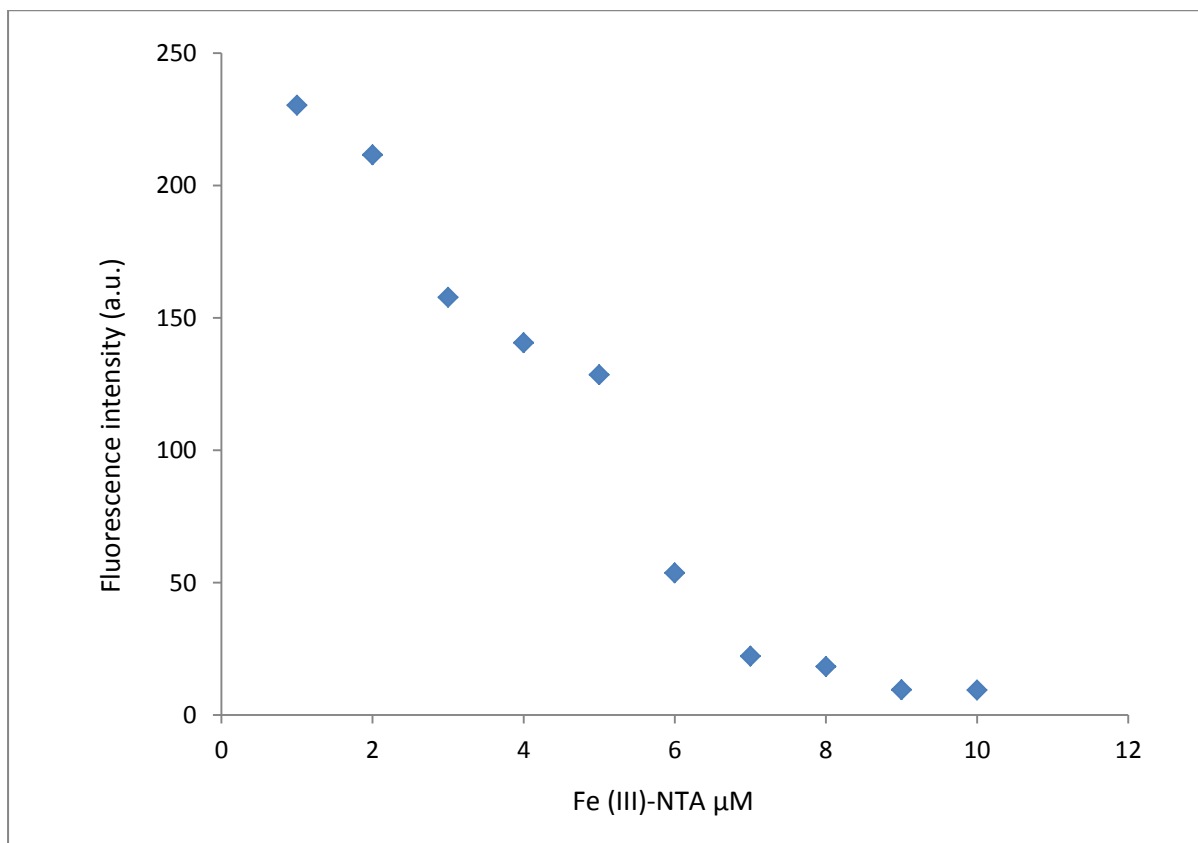


Figure 14 Fluorescence quenching by iron

#### 4.8. Recording of Fluorescence quantum yield ( $\phi_F$ )

To fully characterize a fluorescent compound it is essential to measure its fluorescence quantum yield. Fluorescence quantum yield is the measurement of the fluorescence of one compound. By definition it is the ratio of photons absorbed to photons emitted through fluorescence (Gardens et al., n.d.). It expresses the proportion of excited molecules that deactivate by emitting a fluorescence photon, which means that it indicates the probability of the excited state being deactivated by fluorescence rather than by another, non-radioactive mechanism (Gardens et al., n.d.). The higher the quantum yield is the more fluorescent is the fluorophore. When it reaches a value of 1 all absorbed photons are re-emitted by the compound.

The most reliable method for recording the fluorescence efficiency of the compound is relating it to that of a standard with known  $\phi_F$  values.

In this case Quinine and Norharmane were adopted as standards because they absorb at the excitation wavelength appropriate to the samples, and emit in similar spectral regions (400-600nm and 400-550nm) (Ma, Kong, et al., 2015). The fluorescence of each sample was recorded in a range of 4 concentrations in 0.1M H<sub>2</sub>SO<sub>4</sub> with absorbance values in the range 0.02-0.1 at the excitation wavelength of 320nm (see Table 3 and Table 4). In order to minimize re-absorption effects the absorbance in the 10mm cuvettes should never exceed 0.1 at and above the excitation wavelength (Ma, Kong, et al., 2015). Above this level, nonlinear effects may be observed due to inner filter effects, and the resulting quantum yield values may be perturbed ("Fluorescence Quantum Yield Measurements | HORIBA Jobin Yvon - HORIBA," n.d.).

The recorded fluorescence intensity (see Figure 15 and Figure 16) was integrated with Origin 8 software.

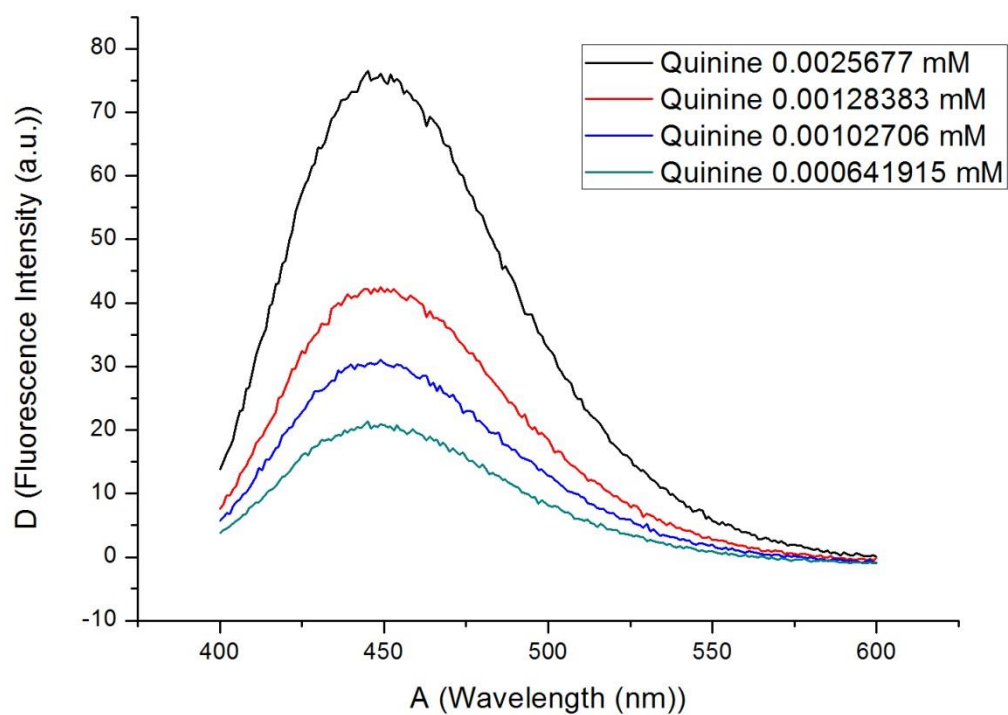


Figure 15 Fluorescence spectrum of quinine

conc. Quinine ( $\mu\text{M}$ )	Absorbance	Integration of the fluorescence intensity
0.6419	0.028	1648.83
1.027	0.049	2502.81
1.28383	0.057	3526.51
2.5677	0.072	6394.38

Table 3 Table of the absorbance and integration of the fluorescence intensity of quinine at different concentrations

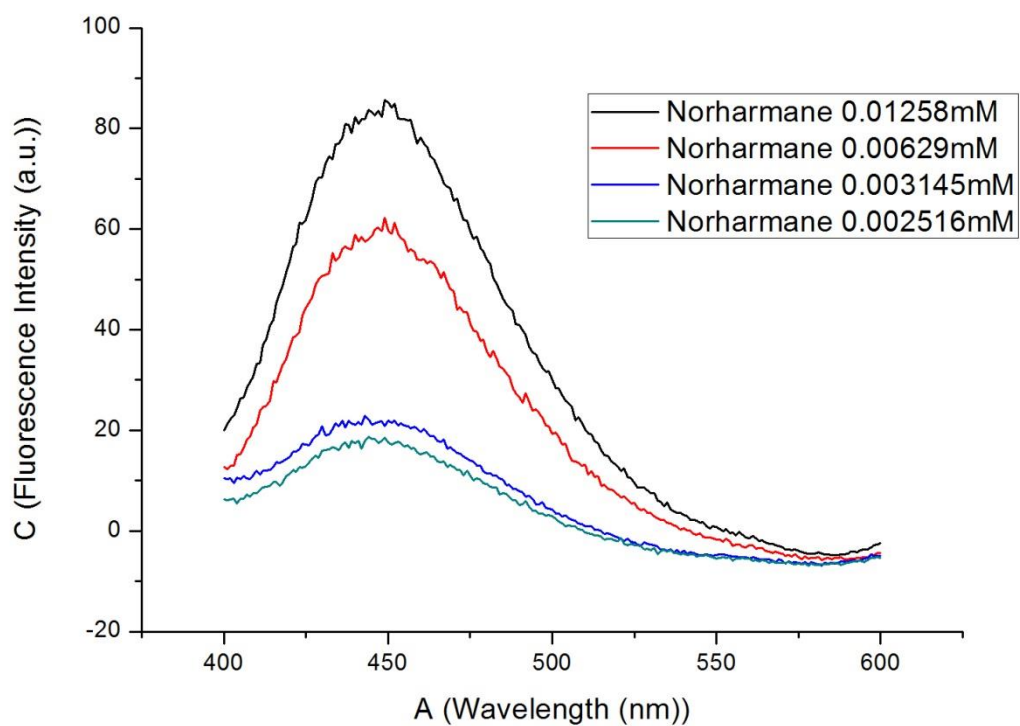


Figure 16 Fluorescence spectrum of norharmane

conc. Norharmane ( $\mu\text{M}$ )	Absorbance	Integration of the fluorescence intensity
2.516	0.033	752.43
3.145	0.038	1153.14
6.29	0.067	4178.59
12.55	0.083	6308.28

Table 4 Table of the absorbance and integration of the fluorescence intensity of norharmane at different concentrations

Two calibration curves, one for each compound were recorded: the integrated fluorescence intensity ( $I_f$ ) was plotted against the absorbance (A), which gave the following equations.

Quinine:  $y = 104535x - 1865.4$

Norharmane:  $y = 110257x - 2993.6$

The gradient of each plot is proportional to the quantum yield of the sample (Ma, Kong, et al., 2015).

The two standard compounds were cross-calibrated by using Equation 2.

$$\Phi_X = \varphi_{st} \left( \frac{\text{Gradient } x}{\text{Gradient } st} \right) \left( \frac{\eta^2 x}{\eta^2 st} \right)$$

#### Equation 2 Calculating fluorescence quantum yield

Two different solvents were used for the measurements, but as they were both blanked at the beginning there was no need to integrate the refractory indices  $\eta$  in the equation.

$$\Phi_X = \varphi_{st} \left( \frac{\text{Gradient } x}{\text{Gradient } st} \right)$$

This means that the quantum yield of each standard sample was calculated relative to the other (Ma, Kong, et al., 2015). First Quinine was treated as the standard (ST) and Norharmane as the test sample (X), and the literature quantum yield for Quinine was used. Then the process was reversed and so the quantum yields of both standards were calculated relative one to another.

Literature quantum yields: Quinine Sulfate: 0.54; Norharmane 0.58

The calibrated values of  $\varphi_F$  (Quinine): 0.5499;  $\varphi_F$  (Norharmane): 0.5696

As the experimental quantum yields match the literature with +/- 10% the values are acceptable.

Once the calibration of the UV spectrophotometer and the fluorimeter was verified with the two standards, the measurements of the fluorescent chelator 2-(2-aminoethyl)-7-hydroxy-3,4-dihydro-2H-pyrido[1,2-a]pyrazine-1,8-dione were carried out (Ma, Kong, et al., 2015). Solutions in 100mM MOPS (pH 7.4) at the following 5 concentrations with absorbance values between 1.000 and 0.010 at the excitation wavelength of 320nm were prepared and measured (see Table 5 and Figure 17). The integration was again calculated with Origin 8:



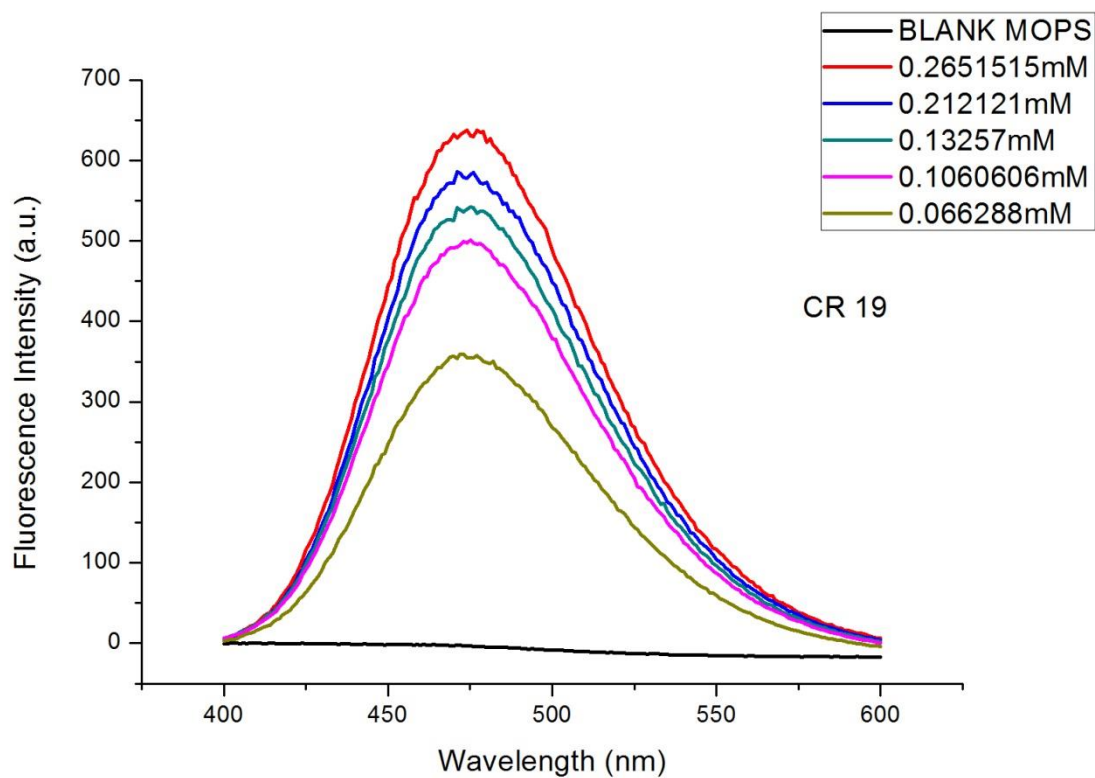


**Figure 17** Fluorescence spectrum of the bidentate chelator CR 19

Concentration of CR 19 (mM)	Absorbance	Integration of the Fluorescence intensity
0.066288	0.045	29046.925225739
0.1060606	0.145	41068.149740613
0.13257	0.237	44699.37283658
0.212121	0.524	48225.111879139
0.2651515	0.659	52846.003755916

**Table 5** Table of the absorbance and integration of the fluorescence intensity of the bidentate chelator CR 19 at different concentrations

Plotting again absorbance versus concentration gave the following equation for the fluorescent chelator:

$$y = 31285x + 33103$$

Then the two  $\phi_F$  values for the compound relevant to each other were obtained for the two standards.

$\phi_F$  relatively to Quinine: 0.1646

$\phi_F$  relatively to Norharmane: 0.1616

The average of 0.16 of these two values represents the quantum yield of the fluorescent iron chelator. This corresponds with the value of 0.12 of the compound 4i.

## 4.9. $pK_a$ (ionization constants)

HPOs are monoprotic acids at pH 7.0 and thus form neutral tris-iron(III) complexes. The  $pK_a$  values of the chelating oxygen atoms reflect the affinity of HPOs for ferric iron: the higher the affinity for ferric iron, the higher the  $pK_a$  value is (Liu & Hider, 2002a).

The chelator was investigated by spectrophotometric titration which demonstrates the pH dependence of the ligand ionization equilibrium (Ma, Kong, et al., 2015). The experiment was carried out with a ligand concentration of 108.4  $\mu\text{M}$  starting in 15.81 mL 0.1M KCl at 25 °C. The pH of the solution continuously increased from 2.38 to 10.97 by the addition of KOH from an autoburette and the total points is 43. The pH-dependent UV/Vis spectra were measured in a 50 mm path length cuvette in a range from 200 to 500 nm. The maximum absorption wavelength is shifted to around 360 nm which corresponds with the values of related compounds 4i and 4j. The calculated spectra of the four species,  $\text{LH}_1$ ,  $\text{LH}_2$ , LH and L are presented in Figure 18. The associated speciation plot is presented in Figure 19. The HPO derivative possesses three  $pK_a$  values at 10.43, which represents the dissociation of the amine group (LH, blue line of the graph), 7.45 from the dissociation of the 3-hydroxyl group ( $\text{LH}_2$ , red line) and 2.34 which corresponds to the protonation of the 4-oxo group ( $\text{LH}_3$ , green line). The brown line derives from the ligand. They were obtained from non-linear least square regression analysis of the spectra taken over the pH range 2.38 – 10.97 (Ma, Kong, et al., 2015).

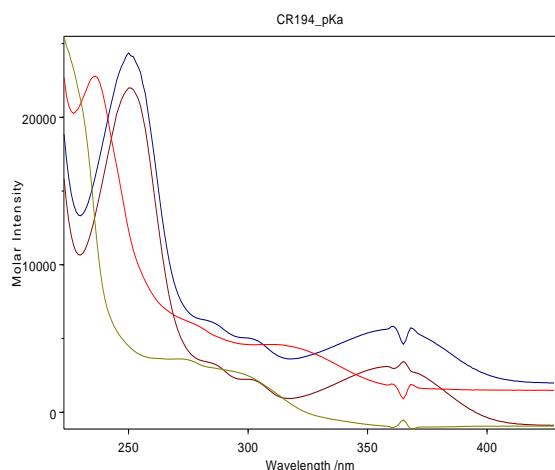


Figure 18 pH dependence of the UV absorbance spectra of the bidentate chelator over the pH range 2.38 to 10.97

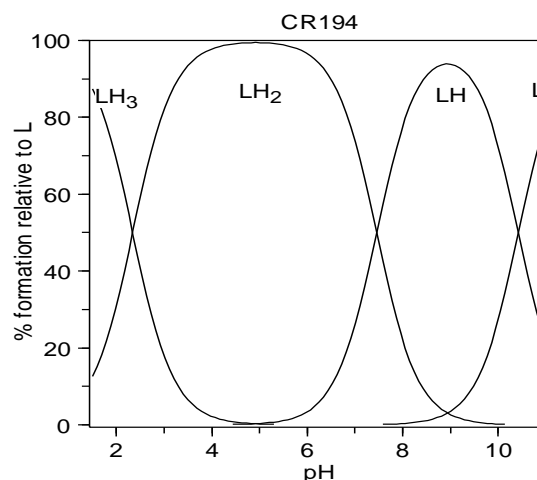


Figure 19 speciation plot of the bidentate chelator CR 19

#### 4.10. $pFe^{3+}$ determination

The stability constant of an iron-ligand complex is one of the key parameters related to the efficacy of an iron chelator. The cumulative stability constants of the ligands can be theoretically determined by spectrophotometric titration. The  $pFe^{3+}$  value is defined as the negative logarithm of the concentration of the free ferric iron in solution and calculated for  $ligand_{[total]} = 10^{-5}M$ ,  $iron_{[total]} = 10^{-6}$  at pH 7.4 (Ma, Kong, et al., 2015).

The calculated spectra of the three iron complexes of CR 19,  $FeLH_1$ ,  $Fe(LH)_2$  and  $Fe(LH)_3$  are presented in Figure 20. The speciation plot of iron III ( $1\mu M$ ) in presence of CR 19 ( $5\mu M$ ) is presented in Figure 21.

For the newly synthesized chelator the obtained  $pFe^{3+}$  value is 18.46 which is slightly lower compared to the ones of 4i (21.4) and 4j (20.4).

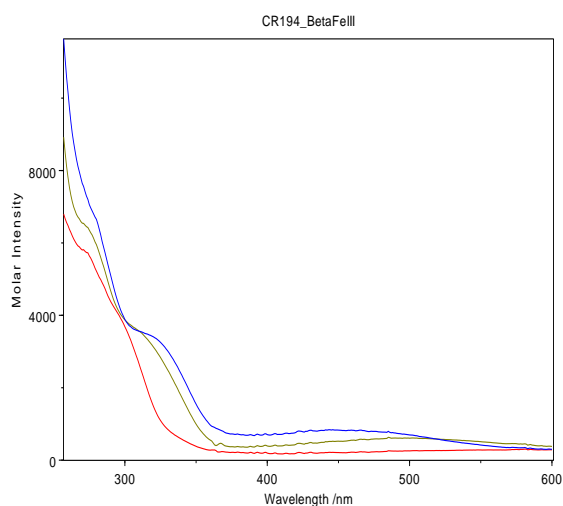


Figure 20 The calculated spectra of the three iron complexes of CR 19;  $FeLH_1$ ,  $Fe(LH)_2$ ,  $Fe(LH)_3$

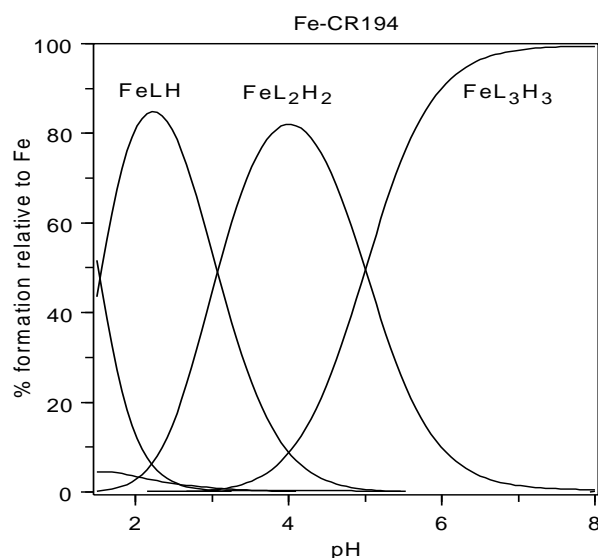


Figure 21 Speciation of iron III ( $1\mu M$ ) in presence of CR 19 ( $5\mu M$ )

## 5. Analytical and Chemicals

### 5.1. High performance liquid chromatography (HPLC)

The purity of the compounds was determined via RP-HPLC analysis. The samples were analyzed on a HP1050 HPLC system equipped with an autosampler, a quaternary pump and a Diode-Array Detector. A Zorbax SB C-18 2.1mm x 10cm (particle size 3.5 micron) column was employed. The flow rate was 0.2mL/min and the eluents were monitored at wavelengths between 210-280 nm. A linear gradient of mobile phase B (acetonitrile containing 0.1% TFA) over mobile phase A (0.1% TFA in water) from 0-90% B in 20 minutes was performed. Data were collected and analyzed using ChemStation software.

### 5.2. Electrospray Ionisation Mass Spectrometry (ESI-MS)

Mass spectra were obtained by infusing samples into a Waters Micromass Z-instrument using ESI positive or negative ionization. MS samples were prepared by dissolving 0.1 mg compound in 1 mL. The mobile phase was H<sub>2</sub>O:MeOH 1:1 containing 0.1% FA.

Samples were injected via a direct infusion trough a 100µL syringe.

Calculated m/z values were obtained via the software Chem Bio Draw Ultra 14.0.

### 5.3. Chromatography

Silica gel 60 with fluorescent indicator F<sub>254</sub> coated aluminium plates were used for thin layer chromatography (TLC). Purifications with Column Chromatography (CC) were performed on Merck silica gel 60 (40-63 µm).

### 5.4. Nuclear Magnetic Resonance (NMR)

The <sup>1</sup>H and <sup>13</sup>C NMR spectra were recorded using a Bruker Avance 400 (400 MHz) NMR spectrometer at Britannia House of King's College London. Chemical shifts are reported in ppm downfield and the notations s (singlet), d (doublet), t (triplet), q (quartet) and m (multiplet) were used to describe the resonance patterns. <sup>13</sup>C-NMR samples were prepared by dissolving about 40 mg compound in 0.75 mL of deuterated solvent, <sup>1</sup>H-NMR with about 5 mg compound. Data from the spectrometer was analysed using the software Topspin.

## **5.5. High resolution Mass spectrometry (HRMS)**

HRMS were monitored on a MicroMass Q-TOF instrument.

## **5.6. UV/Vis spectrometry**

The UV/Vis spectrum was recorded using a Perkin Elmer spectrophotometer (type UV/VIS Lambda 2S) and performed in 0.1 M MOPS buffer (pH 7.4) or 0.1M H<sub>2</sub>SO<sub>4</sub> at room temperature.

Single measurements were recorded on JENWAY 2000 spectrophotometer.

Data was analysed with Excel software.

## **5.7. Fluorescence Emission**

A VARIAN Cary Eclipse fluorescence spectrofluorometer was used to record fluorescence emission spectra operating a scan rate of 120 nm/min and performed in MOPS buffer (pH 7.4) at room temperature. Spectra were not corrected for light intensity or detector sensitivity.

The integration was calculated with OriginPro 8 and the data analysed by Excel software.

## **5.8. pK<sub>a</sub> and iron stability constant determinations**

The automatic titration system comprised an autoburette (Metrohm Dosimat 765 liter mL syringe) and Mettler Toledo MP230 pH meter with Metrohm pH electrode and a reference electrode. The temperature was maintained at 25°C +/- 0.1°C by using a Techne TE-8J temperature controller. A Gilson Mini-plus#3 pump with speed capability (20 mL/min) was used to circulate the test solution through a Hellem quartz flow cuvette. The flow cuvette was mounted on an HP 8453 UV/Vis spectrophotometer. All instruments were interfaced to a computer and controlled by a Visual Basic programme. All the titration data were analysed with the HYSS programme (Ma, Kong, et al., 2015).

## **5.9. Chemicals**

Kojic acid and reagents were purchased from Sigma-Aldrich or Fisher Chemicals. They were reagent grade or better and used as received without further purification.

## 6. Discussion

The aim of this project at the Department of Medicinal Chemistry of KCL was to synthesize and characterize a novel bidentate, fluorescent iron chelator, where the fluorescent and the chelating entity merge.

The compound has a primary amine as functional group on the side chain. Due to this functional group the chelator is quite polar, charged at pH 7.4 and will not permeate membranes at this pH compared to previous similarly synthesized analogues. In future organic synthesis work the chelator could be made more lipophilic via esterification to improve the oral bioavailability.

But the primary amine functional group brings another great advantage: it can be coupled to carboxylic functional groups to make amide formations. A similar, bidentate, fluorescent chelator **4j** (see Overview Statement Formula 6) (Ma, Kong et al. 2015) also possesses a secondary amine but has the disadvantage that the chelating alcohol functional group must be deprotected in order to make the Mannich reaction work. As soon as chelating compounds are deprotected they are very inconvenient to work with as they are highly sensitive to metals in the environment.

The compound was synthesized in a 4 step reaction (see Synthetic schemes Scheme 1) from the commercially available starting material kojic acid: The first one was a benzylation reaction via NaOH and BnCl to protect the 5-OH group. Then the oxidation of the other alcohol group to the carboxylic acid via Jones Reagent followed. An amine insertion reaction with diethylenetriamine formed the bicyclic compound, and the last step was the deprotection of the benzyl group. After several attempts with BCl<sub>3</sub> in DCM and hydrogenation with Pd/C (w/w) with different concentrations of catalyst (5 and 10%) and different solvents (EtOH and MeOH) it seemed to work best when dissolving the compound in MeOH and hydrogenate it with 10% Pd/C (w/w) overnight.

The comparison of the physicochemical characterization of the compound with previously similarly synthesized ones showed that the results were similar (see Characterization of CR 19 Table 1). The results of the molecular weight (MW), maximum absorption wavelength (abs), maximum emission wavelength (em) and fluorescence quantum yield ( $\phi_f$ ) correspond with the previously obtained ones. The molar extinction coefficient  $\epsilon$  and pFe<sup>3+</sup> value are slightly lower and the ClogP and all pK<sub>a</sub> values are somewhat higher.

It was confirmed that the synthesized compound is a fluorescent, bidentate iron chelator.

Various attempts of coupling the bidentate chelator to a tripodal acid to obtain the hexadentate chelator were undertaken. Two different tripodal acids were used and the reaction conditions were modified (see Synthetic Schemes Scheme 6) .

For the duration of the reaction it seemed to work best to incubate the tripodal acid with the activating reagents in an oxygen free environment, adding the amine after 2h and leaving the reaction mixture to stir at room temperature for 2 days. All trial conditions showed the desired protected product as detected by MS.

However, it was difficult to obtain the hexadentate chelator and the synthesis could not be completed due to the limited time I had available for my project at KCL. At the present time the chelator has not been prepared in an acceptable yield and the optimal way of deprotection and purification needs further investigation. The conditions of the coupling reaction, such as which activating reagents and solvents to use, must be further improved.

One of the problems was that the bidentate, protected chelator was not soluble in DMF but only in DMSO. The advantage of the deprotected chelator is its solubility in water, these reaction conditions should be investigated further. As the reaction rate slows down after the first and especially the second amide formation mainly the two-arms coupling product was formed and it might be difficult to obtain the hexadentate chelator. The via preparative HPLC using a prep C18 column and an acetonitrile/water gradient collected two-armed product showed a peak at 16mins in the RP-HPLC. This indicates that in previous trials, which always showed a peak at 16 mins, mainly the two-armed product was formed. Due to the right m/z shown in the MS it was erroneously supposed that all three carboxylic acids had been coupled to the amines. This problem could be solved by not adding all amine at once.

The possibility of purification via CC needs further investigation by finding a suitable TLC system, which was difficult to detect due to the high polarity of the compound. Many different mobile phases were tested and the best way appeared to be 1:1 CHCl<sub>3</sub>:MeOH + 1% of AA.



## Appendix

### Table of Images

Image 1 Schematic representation of chelate ring formation in metal-ligand complexes (Liu and Hider 2002) .....	8
---	---

### Table of Formulas

Formula 1 Deferrioxamine B (Liu & Hider, 2002a).....	9
Formula 2 Hydroxypyridinone .....	10
Formula 3 Deferiprone (Liu & Hider, 2002a) .....	10
Formula 4 Deferasirox (Cappellini & Pattoneri, 2009).....	11
Formula 5 Structure of the desired iron chelator .....	13
Formula 6 Structure of compound 4j (Ma, Kong, et al., 2015) .....	13
Formula 7 The chelator after esterification .....	44

### Table of Tables: Characterization of 2-(2-aminoethyl)-7-hydroxy-3,4-dihydro-2H-pyrido[1,2-a]pyrazine-1,8-dione

Table 1 Table of the characterization of the synthesized bidentate chelator CR 19 .....	43
Table 2 Table of the absorbance of the compound CR 19 at 6 different concentrations and 6 different wavelengths .....	53
Table 3 Table of the absorbance and integration of the fluorescence intensity of quinine at different concentrations .....	60
Table 4 Table of the absorbance and integration of the fluorescence intensity of norharmane at different concentrations .....	61
Table 5 Table of the absorbance and integration of the fluorescence intensity of the bidentate chelator CR 19 at different concentrations .....	63

### Table of Figures: Characterization of 2-(2-aminoethyl)-7-hydroxy-3,4-dihydro-2H-pyrido[1,2-a]pyrazine-1,8-dione

Figure 1 HRMS of 2-(2-aminoethyl)-7-hydroxy-3,4-dihydro-2H-pyrido[1,2-a]pyrazine-1,8-dione .....	45
Figure 2 HRMS of the isotopes of 2-(2-aminoethyl)-7-hydroxy-3,4-dihydro-2H-pyrido[1,2-a]pyrazine-1,8-dione .....	45
Figure 3 <sup>1</sup> H-NMR of 2-(2-aminoethyl)-7-hydroxy-3,4-dihydro-2H-pyrido[1,2-a]pyrazine-1,8-dione ...	47
Figure 4 overlap of the <sup>1</sup> H-NMRs of the benzyl-protected CR 6 and the bidentate chelator CR 19.....	48

Figure 5 <sup>13</sup> C-NMR CR, 19 2-(2-aminoethyl)-7-hydroxy-3,4-dihydro-2H-pyrido[1,2-a]pyrazine-1,8-dione .....	49
Figure 6 <sup>13</sup> C-NMR DEPT of 2-(2-aminoethyl)-7-hydroxy-3,4-dihydro-2H-pyrido[1,2-a]pyrazine-1,8-dione .....	49
Figure 7 HPLC of CR 6, 2-(2-aminoethyl)-7-(benzyloxy)-3,4-dihydro-2H-pyrido[1,2-a]pyrazine-1,8-dione .....	51
Figure 8 HPLC of CR 19, 2-(2-aminoethyl)-7-hydroxy-3,4-dihydro-2H-pyrido[1,2-a]pyrazine-1,8-dione .....	51
Figure 9 UV/Vis spectrum of CR 19, 2-(2-aminoethyl)-7-hydroxy-3,4-dihydro-2H-pyrido[1,2-a]pyrazine-1,8-dione .....	52
Figure 10 The different concentrations (mM) plotted against the absorbance (nm) at different wavelengths of the bidentate chelator CR 19 to calculate the slope .....	54
Figure 11 Fluorescence emission spectrum at different wavelengths .....	55
Figure 12 UV/Vis spectrum merged with the fluorescence emission spectrum .....	56
Figure 13 Fluorescence quenching by iron with different concentrations of iron .....	58
Figure 14 Fluorescence quenching by iron .....	58
Figure 15 Fluorescence spectrum of quinine .....	60
Figure 16 Fluorescence spectrum of norharmane .....	61
Figure 17 Fluorescence spectrum of the bidentate chelator CR 19 .....	63
Figure 18 pH dependence of the UV absorbance spectra of the bidentate chelator over the pH range 2.38 to 10.97 .....	65
Figure 19 speciation plot of the bidentate chelator CR 19 .....	65
Figure 20 The calculated spectra of the three iron complexes of CR 19; FeLH <sub>1</sub> , Fe(LH) <sub>2</sub> , Fe(LH) <sub>3</sub> .....	66
Figure 21 Speciation of iron III (1μM) in presence of CR 19 (5μM) .....	66

## Table of Equitations

Equation 1 Fenton reaction (Altamura & Muckenthaler, 2009) .....	2
Equation 2 Calculating fluorescence quantum yield .....	62

## Table of Schemes

Scheme 1 Scheme of the synthetic steps from kojic acid to the desired iron chelator .....	14
Scheme 2 Synthesis of 5-benzyloxy-2-hydroxymethyl-4H-pyran-4-one .....	15
<b>Scheme 3 Synthesis of 5-(benzyloxy)-4-oxo-4H-pyran-2-carboxylic acid</b> .....	16
Scheme 4 Synthesis of 2-(2-aminoethyl)-7-(benzyloxy)-3,4-dihydro-2H-pyrido[1,2-a]pyrazine-1,8-dione .....	17
Scheme 5 Synthesis of 2-(2-aminoethyl)-7-hydroxy-3,4-dihydro-2H-pyrido[1,2-a]pyrazine-1,8-dione .....	19
Scheme 6 Scheme of the synthetic steps to form the hexadentate chelators .....	22
Scheme 7 Attempted synthesis of N1,N7-bis(2-(7-(benzyloxy)-1,8-dioxo-1,3,4,8-tetrahydro-2H-pyrido[1,2-a]pyrazin-2-yl)ethyl)-4-(3-((2-(7-(benzyloxy)-1,8-dioxo-1,3,4,8-tetrahydro-2H-pyrido[1,2-	

a]pyrazin-2-yl)ethyl)amino)-3-oxopropyl)-4-(3-(1,3-dioxoisindolin-2-yl)propanamido)heptanediamide .....	23
Scheme 8 Attempted Synthesis of 4-(3-aminopropanamido)-N1,N7-bis(2-(7-(benzyloxy)-1,8-dioxo-1,3,4,8-tetrahydro-2H-pyrido[1,2-a]pyrazin-2-yl)ethyl)-4-(3-((2-(7-(benzyloxy)-1,8-dioxo-1,3,4,8-tetrahydro-2H-pyrido[1,2-a]pyrazin-2-yl)ethyl)amino)-3-oxopropyl)heptanediamide.....	25
<b>Scheme 9 Synthesis of di-tert-butyl 4-acetamido-4-(3-(tert-butoxy)-3-oxopropyl)heptanedioate..</b>	26
Scheme 10 Synthesis of 4-acetamido-4-(2-carboxyethyl)heptanedioic acid.....	28
Scheme 11 Attempted synthesis of 4-acetamido-N1,N7-bis(2-(7-(benzyloxy)-1,8-dioxo-1,3,4,8-tetrahydro-2H-pyrido[1,2-a]pyrazin-2-yl)ethyl)-4-(3-((2-(7-(benzyloxy)-1,8-dioxo-1,3,4,8-tetrahydro-2H-pyrido[1,2-a]pyrazin-2-yl)ethyl)amino)-3-oxopropyl)heptanediamide .....	29
Scheme 12 Attempted synthesis of 4-acetamido-N1,N7-bis(2-(7-hydroxy-1,8-dioxo-1,3,4,8-tetrahydro-2H-pyrido[1,2-a]pyrazin-2-yl)ethyl)-4-(3-((2-(7-hydroxy-1,8-dioxo-1,3,4,8-tetrahydro-2H-pyrido[1,2-a]pyrazin-2-yl)ethyl)amino)-3-oxopropyl)heptanediamide .....	31

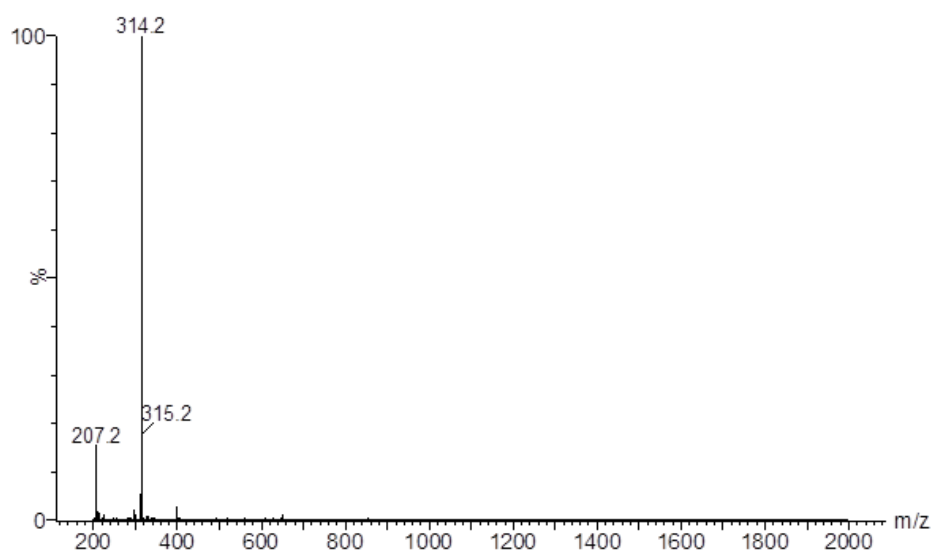
## Table of Selected Data

1 MS of Compound CR 6, 2-(2-aminoethyl)-7-(benzyloxy)-3,4-dihydro-2H-pyrido[1,2-a]pyrazine-1,8-dione .....	VI
2 MS of Compound CR 8, N1,N7-bis(2-(7-(benzyloxy)-1,8-dioxo-1,3,4,8-tetrahydro-2H-pyrido[1,2-a]pyrazin-2-yl)ethyl)-4-(3-((2-(7-(benzyloxy)-1,8-dioxo-1,3,4,8-tetrahydro-2H-pyrido[1,2-a]pyrazin-2-yl)ethyl)amino)-3-oxopropyl)-4-(3-(1,3-dioxoisindolin-2-yl)propanamido)heptanediamide .....	VI
3 MS of Compound CR 14, di-tert-butyl 4-acetamido-4-(3-(tert-butoxy)-3-oxopropyl)heptanedioate .....	VII
4 MS of Compound CR 15, 4-acetamido-4-(2-carboxyethyl)heptanedioic acid .....	VII
5 MS of Compound CR 16, 4-acetamido-N1,N7-bis(2-(7-(benzyloxy)-1,8-dioxo-1,3,4,8-tetrahydro-2H-pyrido[1,2-a]pyrazin-2-yl)ethyl)-4-(3-((2-(7-(benzyloxy)-1,8-dioxo-1,3,4,8-tetrahydro-2H-pyrido[1,2-a]pyrazin-2-yl)ethyl)amino)-3-oxopropyl)heptanediamide .....	VIII
6 HRMS of CR 16 4-acetamido-N1,N7-bis(2-(7-(benzyloxy)-1,8-dioxo-1,3,4,8-tetrahydro-2H-pyrido[1,2-a]pyrazin-2-yl)ethyl)-4-(3-((2-(7-(benzyloxy)-1,8-dioxo-1,3,4,8-tetrahydro-2H-pyrido[1,2-a]pyrazin-2-yl)ethyl)amino)-3-oxopropyl)heptanediamide after 30min .....	IX
7 HRMS of CR 16 4-acetamido-N1,N7-bis(2-(7-(benzyloxy)-1,8-dioxo-1,3,4,8-tetrahydro-2H-pyrido[1,2-a]pyrazin-2-yl)ethyl)-4-(3-((2-(7-(benzyloxy)-1,8-dioxo-1,3,4,8-tetrahydro-2H-pyrido[1,2-a]pyrazin-2-yl)ethyl)amino)-3-oxopropyl)heptanediamide after 1h .....	X
8 <sup>1</sup> H-NMR CR 0 5-benzyloxy-2-hydroxymethyl-4H-pyran-4-one .....	XI
9 <sup>1</sup> H-NMR of CR 4, 5-(benzyloxy)-4-oxo-4H-pyran-2-carboxylic acid .....	XI
10 <sup>1</sup> H-NMR CR 6, 2-(2-aminoethyl)-7-(benzyloxy)-3,4-dihydro-2H-pyrido[1,2-a]pyrazine-1,8-dione ..	XII
11 <sup>13</sup> C-NMR, CR 6 2-(2-aminoethyl)-7-(benzyloxy)-3,4-dihydro-2H-pyrido[1,2-a]pyrazine-1,8-dione ..	XII
12 <sup>13</sup> C-NMR DEPT mode, CR 6 2-(2-aminoethyl)-7-(benzyloxy)-3,4-dihydro-2H-pyrido[1,2-a]pyrazine-1,8-dione .....	XIII
13 <sup>1</sup> H-NMR of CR 19 after the treatment with BCl <sub>3</sub> .....	XIII
14 <sup>13</sup> C-NMR of CR 19 after the treatment with BCl <sub>3</sub> .....	XIV
15 <sup>1</sup> H-NMR of CR 19 after the treatment with 5% Pd/C .....	XIV
16 C-NMR of CR 19 after the treatment with 5% Pd/C .....	XV
17 <sup>1</sup> H-NMR of CR 8, N1,N7-bis(2-(7-(benzyloxy)-1,8-dioxo-1,3,4,8-tetrahydro-2H-pyrido[1,2-a]pyrazin-2-yl)ethyl)-4-(3-((2-(7-(benzyloxy)-1,8-dioxo-1,3,4,8-tetrahydro-2H-pyrido[1,2-a]pyrazin-2-yl)ethyl)amino)-3-oxopropyl)-4-(3-(1,3-dioxoisindolin-2-yl)propanamido)heptanediamide .....	XV
18 <sup>13</sup> C-NMR CR 8, N1,N7-bis(2-(7-(benzyloxy)-1,8-dioxo-1,3,4,8-tetrahydro-2H-pyrido[1,2-a]pyrazin-2-yl)ethyl)-4-(3-((2-(7-(benzyloxy)-1,8-dioxo-1,3,4,8-tetrahydro-2H-pyrido[1,2-a]pyrazin-2-yl)ethyl)amino)-3-oxopropyl)-4-(3-(1,3-dioxoisindolin-2-yl)propanamido)heptanediamide .....	XVI
19 <sup>13</sup> C-NMR DEPT mode CR 8, N1,N7-bis(2-(7-(benzyloxy)-1,8-dioxo-1,3,4,8-tetrahydro-2H-pyrido[1,2-a]pyrazin-2-yl)ethyl)-4-(3-((2-(7-(benzyloxy)-1,8-dioxo-1,3,4,8-tetrahydro-2H-pyrido[1,2-a]pyrazin-2-yl)ethyl)amino)-3-oxopropyl)-4-(3-(1,3-dioxoisindolin-2-yl)propanamido)heptanediamide .....	XVI
20 <sup>1</sup> H-NMR of CR 14, di-tert-butyl 4-acetamido-4-(3-(tert-butoxy)-3-oxopropyl)heptanedioate .....	XVII
21 <sup>1</sup> H-NMR of CR 15, 4-acetyl-amido-4-(2-carboxyethyl)heptanedioic acid .....	XVII
22 <sup>1</sup> H-NMR of CR 16 4-acetamido-N1,N7-bis(2-(7-(benzyloxy)-1,8-dioxo-1,3,4,8-tetrahydro-2H-pyrido[1,2-a]pyrazin-2-yl)ethyl)-4-(3-((2-(7-(benzyloxy)-1,8-dioxo-1,3,4,8-tetrahydro-2H-pyrido[1,2-a]pyrazin-2-yl)ethyl)amino)-3-oxopropyl)heptanediamide .....	XVIII

23 <sup>1</sup> H-NMR of CR 17, 4-acetamido-N1,N7-bis(2-(7-hydroxy-1,8-dioxo-1,3,4,8-tetrahydro-2H-pyrido[1,2-a]pyrazin-2-yl)ethyl)-4-(3-((2-(7-hydroxy-1,8-dioxo-1,3,4,8-tetrahydro-2H-pyrido[1,2-a]pyrazin-2-yl)ethyl)amino)-3-oxopropyl)heptanediamide .....	XVIII
24 HPLC CR 0 5-benzyloxy-2-hydroxymethyl-4H-pyran-4-one .....	XIX
25 HPLC of CR 4, 5-(benzyloxy)-4-oxo-4H-pyran-2-carboxylic acid .....	XIX
26 HPLC of CR 8, N1,N7-bis(2-(7-(benzyloxy)-1,8-dioxo-1,3,4,8-tetrahydro-2H-pyrido[1,2-a]pyrazin-2-yl)ethyl)-4-(3-((2-(7-(benzyloxy)-1,8-dioxo-1,3,4,8-tetrahydro-2H-pyrido[1,2-a]pyrazin-2-yl)ethyl)amino)-3-oxopropyl)-4-(3-(1,3-dioxoisindolin-2-yl)propanamido)heptanediamide .....	XX
27 HPLC of CR 8 after prep. HPLC, N1,N7-bis(2-(7-(benzyloxy)-1,8-dioxo-1,3,4,8-tetrahydro-2H-pyrido[1,2-a]pyrazin-2-yl)ethyl)-4-(3-((2-(7-(benzyloxy)-1,8-dioxo-1,3,4,8-tetrahydro-2H-pyrido[1,2-a]pyrazin-2-yl)ethyl)amino)-3-oxopropyl)-4-(3-(1,3-dioxoisindolin-2-yl)propanamido)heptanediamide after prep.HPLC .....	XX
28 HPLC of CR 16, 4-acetamido-N1,N7-bis(2-(7-(benzyloxy)-1,8-dioxo-1,3,4,8-tetrahydro-2H-pyrido[1,2-a]pyrazin-2-yl)ethyl)-4-(3-((2-(7-(benzyloxy)-1,8-dioxo-1,3,4,8-tetrahydro-2H-pyrido[1,2-a]pyrazin-2-yl)ethyl)amino)-3-oxopropyl)heptanediamide .....	XXI

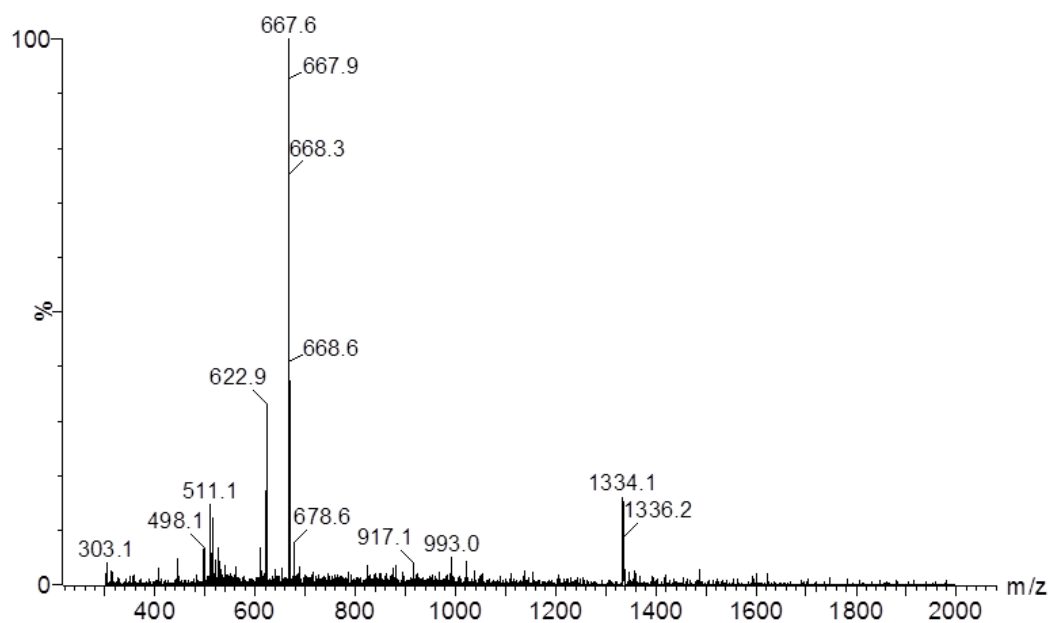
## MS selected data

16-Apr-2015 12:08:00



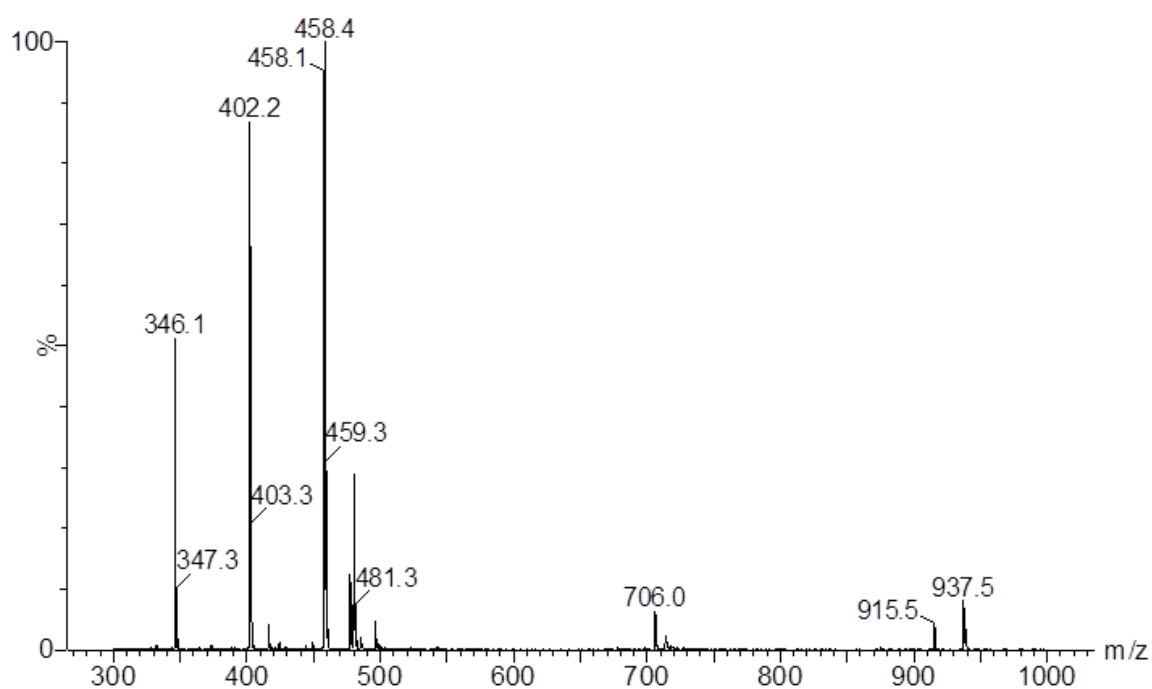
1 MS of Compound CR 6, 2-(2-aminoethyl)-7-(benzyloxy)-3,4-dihydro-2H-pyrido[1,2-a]pyrazine-1,8-dione

27-Mar-2015 11:48:44



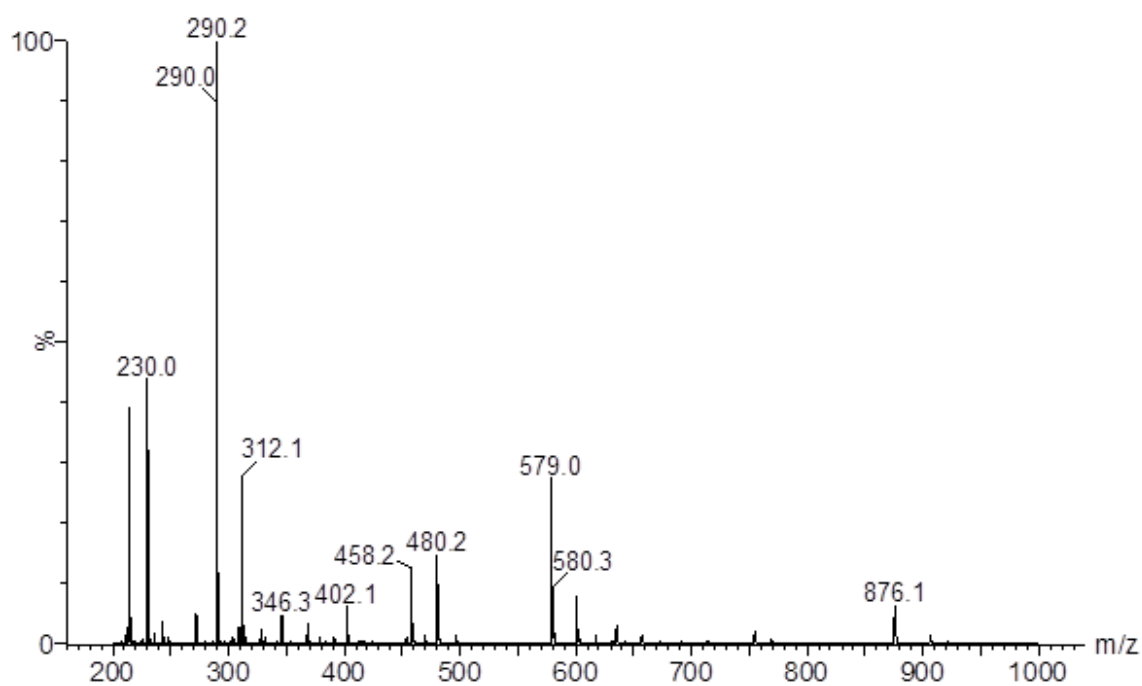
2 MS of Compound CR 8, N1,N7-bis(2-(7-(benzyloxy)-1,8-dioxo-1,3,4,8-tetrahydro-2H-pyrido[1,2-a]pyrazin-2-yl)ethyl)-4-(3-((2-(7-(benzyloxy)-1,8-dioxo-1,3,4,8-tetrahydro-2H-pyrido[1,2-a]pyrazin-2-yl)ethyl)amino)-3-oxopropyl)-4-(3-(1,3-dioxoisindolin-2-yl)propanamido)heptanediamide

24-Mar-2015 13:44:40

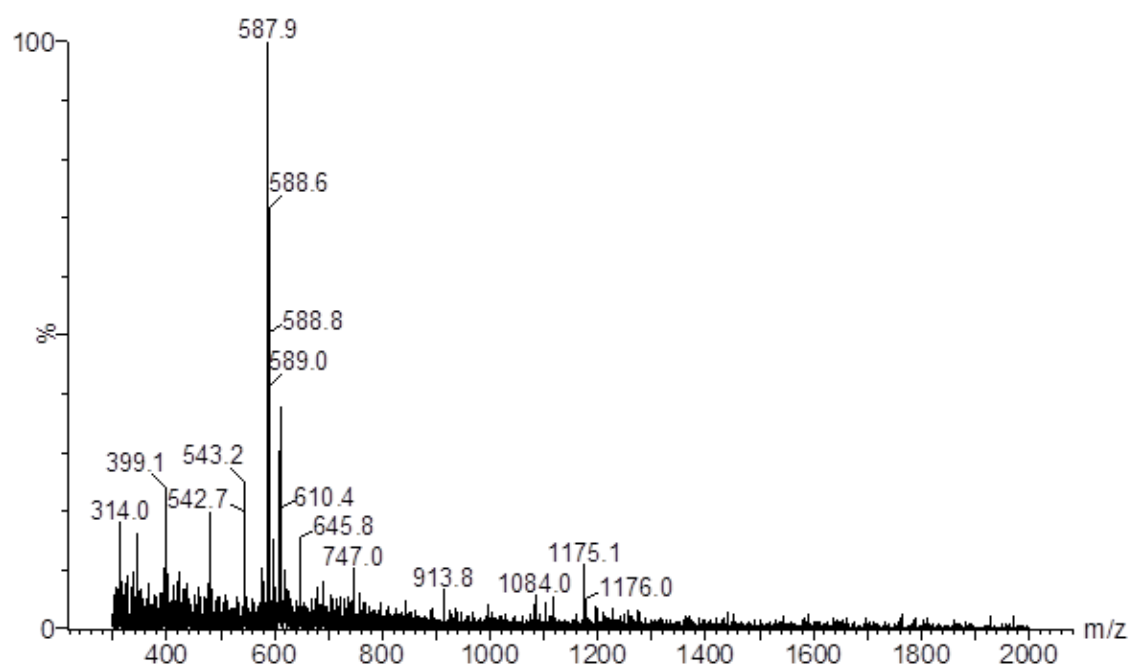


3 MS of Compound CR 14, di-tert-butyl 4-acetamido-4-(3-(tert-butoxy)-3-oxopropyl)heptanedioate

25-Mar-2015 10:48:39



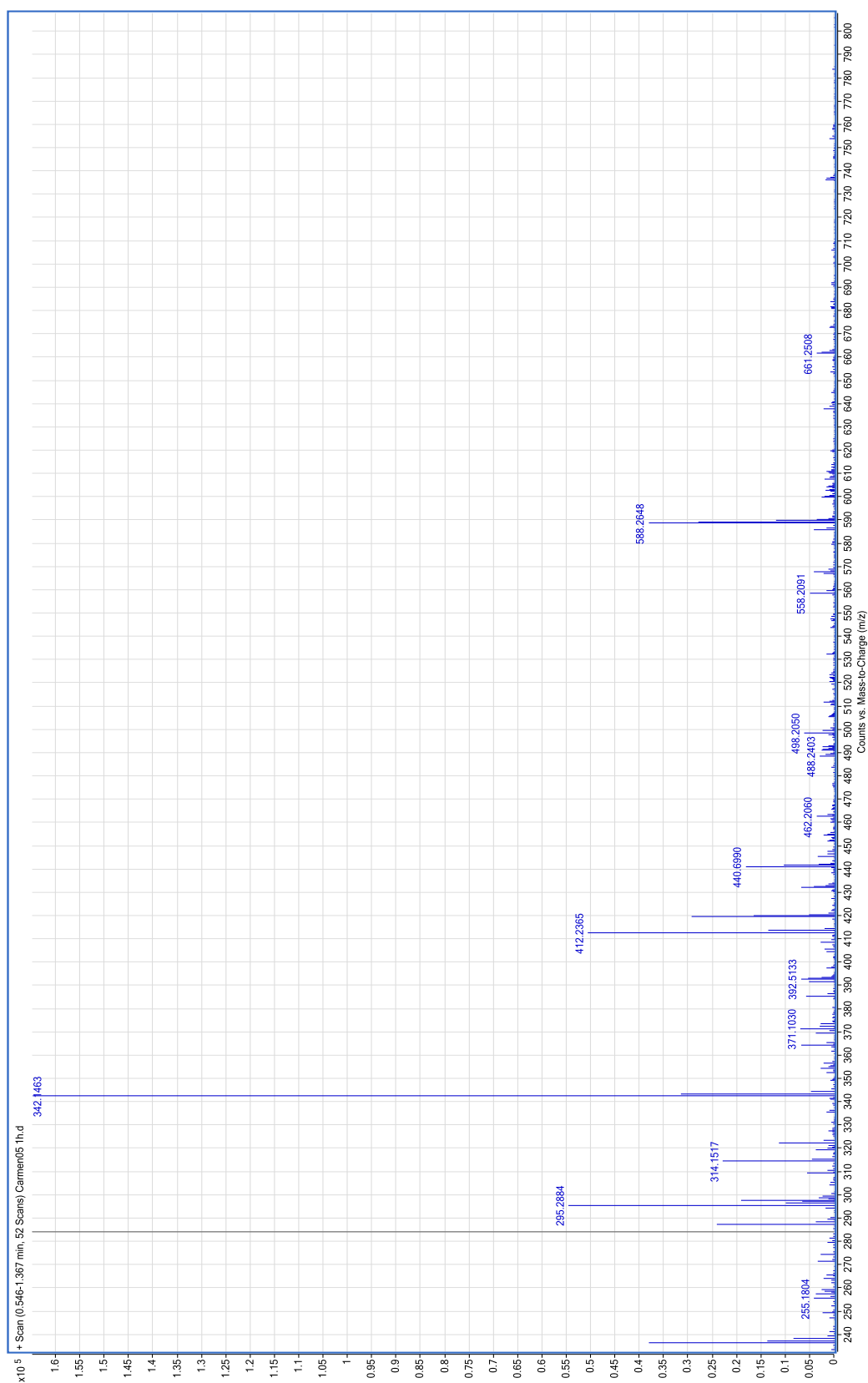
4 MS of Compound CR 15, 4-acetamido-4-(2-carboxyethyl)heptanedioic acid



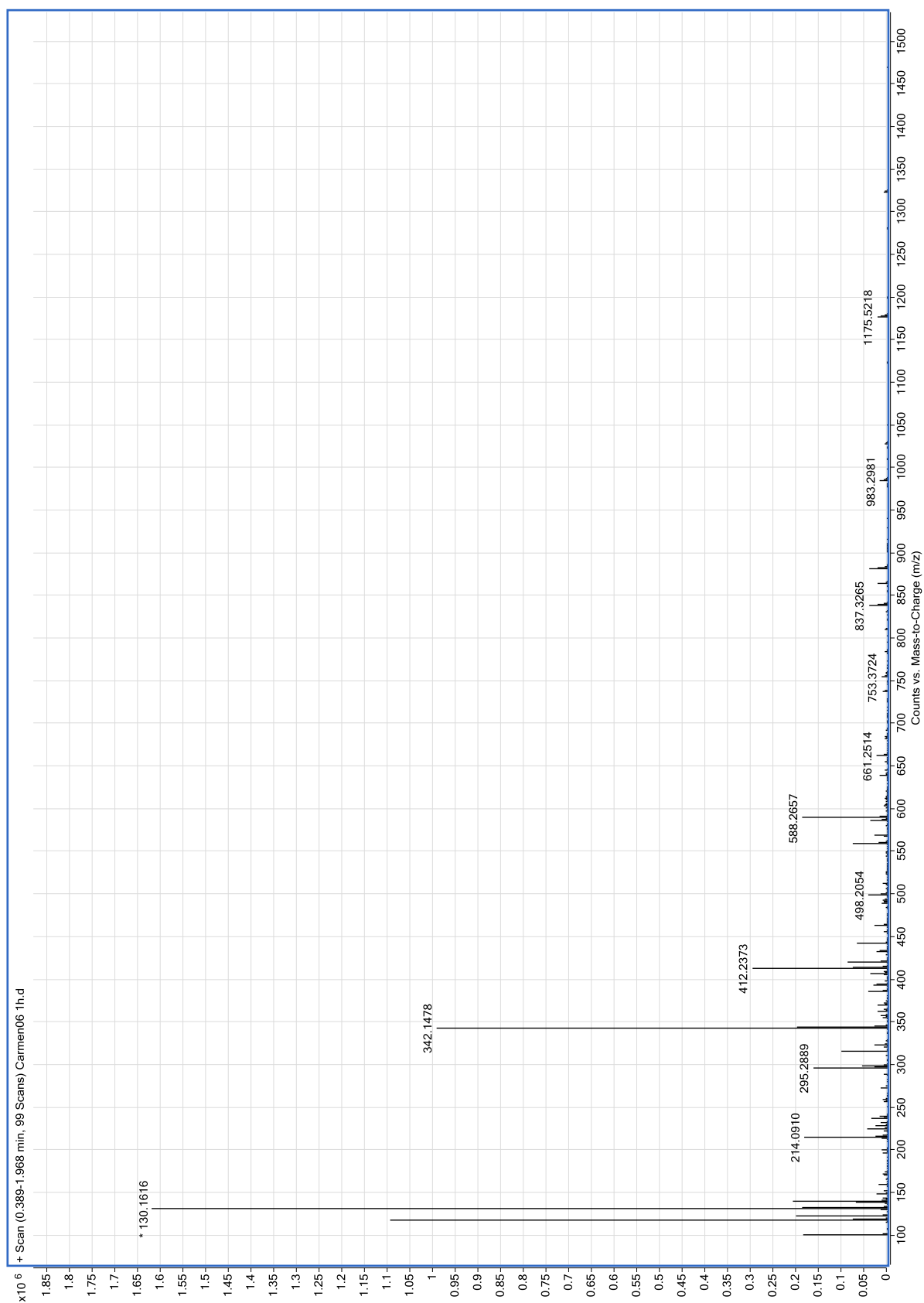
5 MS of Compound CR 16, 4-acetamido-N1,N7-bis(2-(7-(benzyloxy)-1,8-dioxo-1,3,4,8-tetrahydro-2H-pyrido[1,2-a]pyrazin-2-yl)ethyl)-4-(3-((2-(7-(benzyloxy)-1,8-dioxo-1,3,4,8-tetrahydro-2H-pyrido[1,2-a]pyrazin-2-yl)ethyl)amino)-3-oxopropyl)heptanediamide



## HRMS selected data

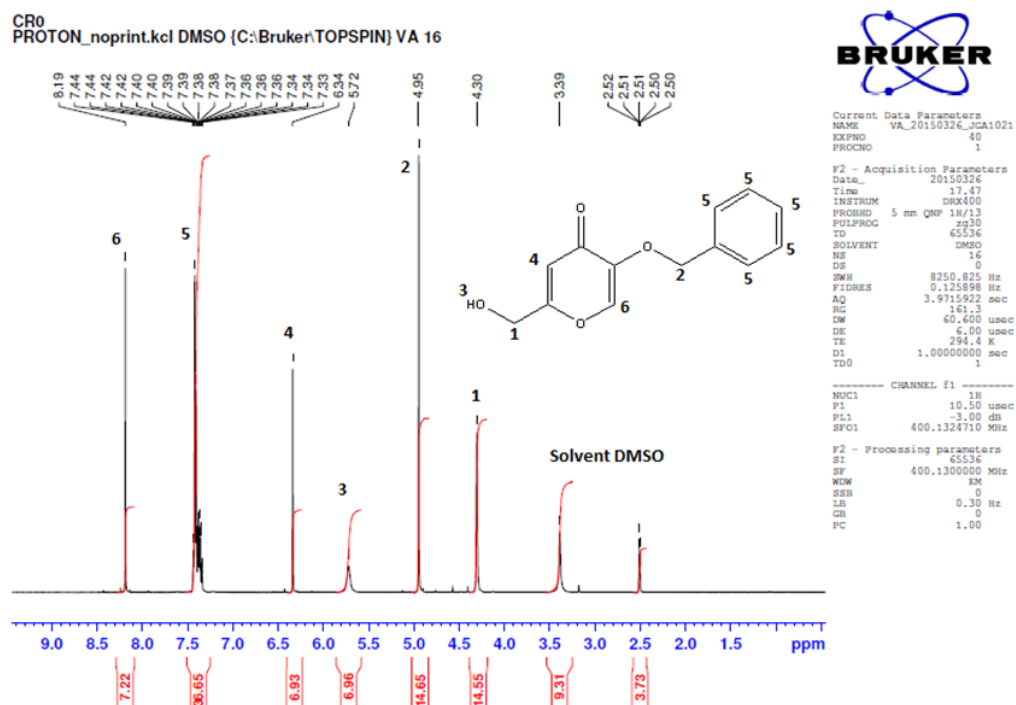


6 HRMS of CR 16 4-acetamido-N1,N7-bis(2-(7-(benzyloxy)-1,8-dioxo-1,3,4,8-tetrahydro-2H-pyrido[1,2-a]pyrazin-2-yl)ethyl)-4-(3-((2-(7-(benzyloxy)-1,8-dioxo-1,3,4,8-tetrahydro-2H-pyrido[1,2-a]pyrazin-2-yl)ethyl)amino)-3-oxopropyl)heptanediamide after 30min

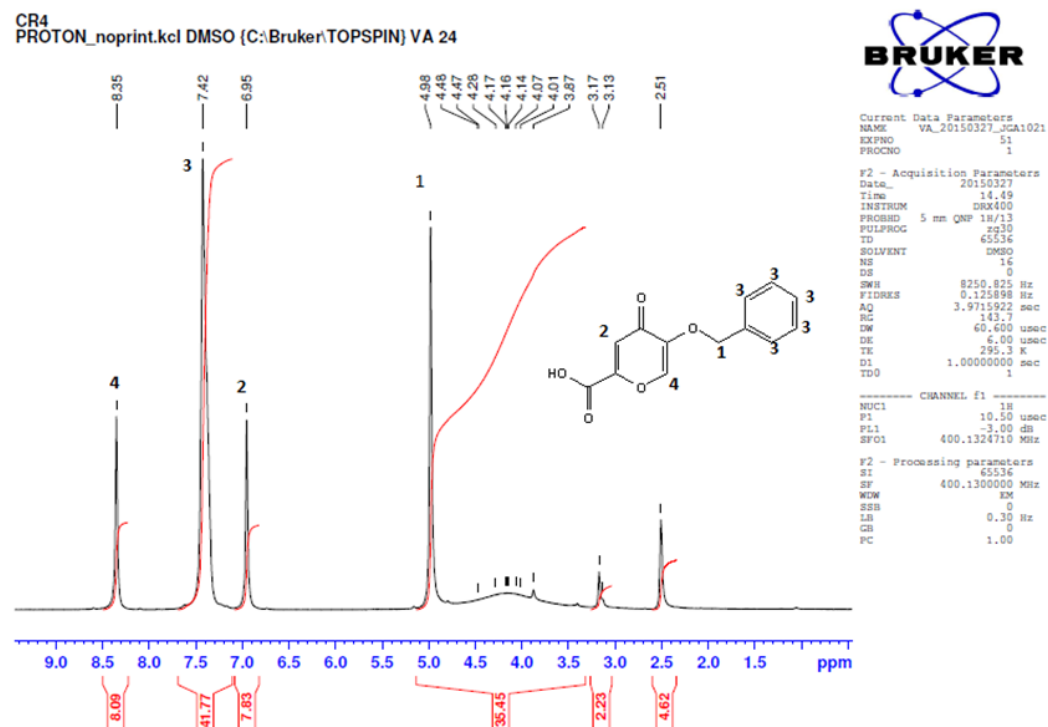


7 HRMS of CR 16 4-acetamido-N1,N7-bis(2-(7-(benzyloxy)-1,8-dioxo-1,3,4,8-tetrahydro-2H-pyrido[1,2-a]pyrazin-2-yl)ethyl)-4-(3-((2-(7-(benzyloxy)-1,8-dioxo-1,3,4,8-tetrahydro-2H-pyrido[1,2-a]pyrazin-2-yl)ethyl)amino)-3-oxopropyl)heptanediamide after 1h

## NMR selected data

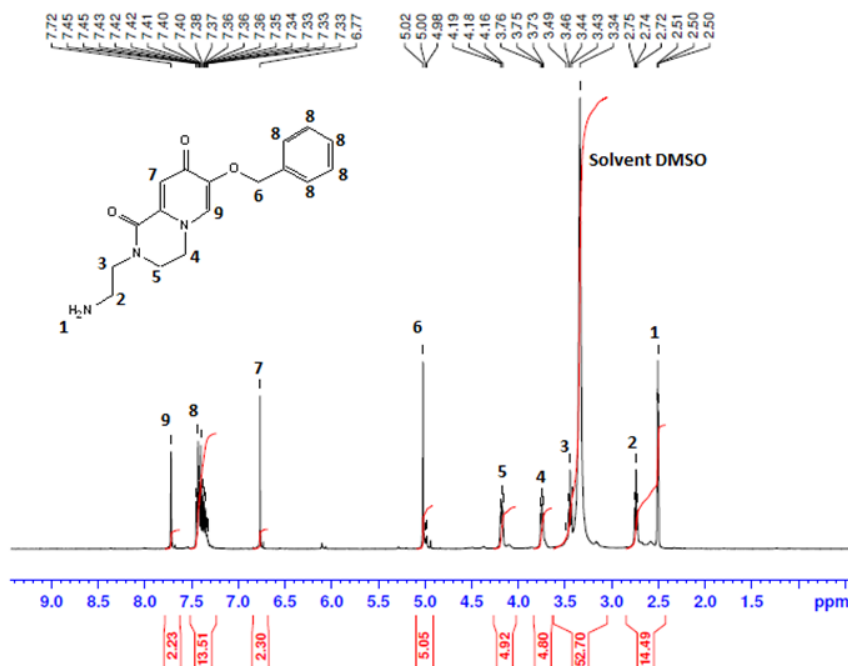


<sup>8</sup> <sup>1</sup>H-NMR CR 0 5-benzyloxy-2-hydroxymethyl-4H-pyran-4-one



<sup>9</sup> <sup>1</sup>H-NMR of CR 4, 5-(benzyloxy)-4-oxo-4H-pyran-2-carboxylic acid

CR6  
PROTON\_noprint.kcl DMSO (C:\Bruker\TOPSPIN) VA 37



Current Data Parameters  
NAME VA\_20150310\_JCA1021  
EXPNO 40  
PROCNO 1

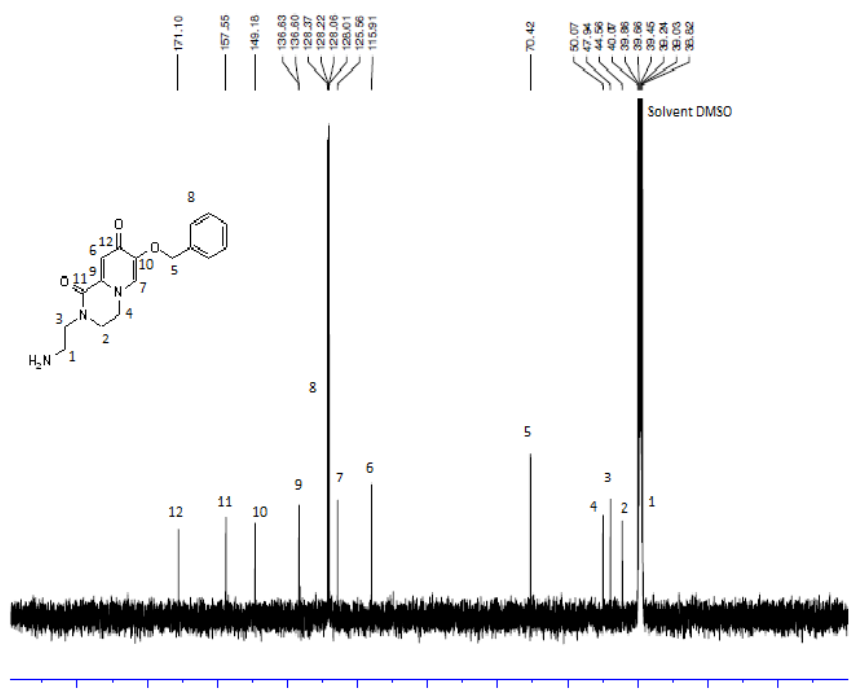
F2 - Acquisition Parameters  
Date\_ 20150310  
Time 10.52  
INSTRUM DRX400  
PROBHD 5 mm QNP 1H/13  
PULPROG zgpg30  
TD 65536  
SOLVENT DMSO  
NS 16  
DS 0  
SWH 8250.825 Hz  
FIDRES 0.125898 Hz  
AQ 3.9715922 sec  
RG 256  
DW 60.600 usec  
DE 6.00 usec  
TE 295.9 K  
D1 1.00000000 sec  
TD0 1

===== CHANNEL f1 =====  
NUC1 1H  
P1 10.50 usec  
PL1 -3.00 dB  
SFO1 400.1324710 MHz

F2 - Processing parameters  
SI 65536  
SF 400.1300012 MHz  
WDW EM  
SSB 0  
LB 0.30 Hz  
GB 0  
PC 1.00

10 <sup>1</sup>H-NMR CR 6, 2-(2-aminoethyl)-7-(benzyloxy)-3,4-dihydro-2H-pyrido[1,2-a]pyrazine-1,8-dione

CR6  
C13CPD\_noprint.kcl DMSO (C:\Bruker\TOPSPIN) VA 37



Current Data Parameters  
NAME VA\_20150310\_JCA1021  
EXPNO 41  
PROCNO 1

F2 - Acquisition Parameters  
Date\_ 20150310  
Time 11.23  
INSTRUM DRX400  
PROBHD 5 mm QNP 1H/13  
PULPROG zgpg30  
TD 65536  
SOLVENT DMSO  
NS 512  
DS 4  
SWH 24039.461 Hz  
FIDRES 0.366798 Hz  
AQ 1.3632196 sec  
RG 2298.8  
DW 20.800 usec  
DE 6.00 usec  
TE 296.1 K  
D1 2.00000000 sec  
d11 0.03000000 sec  
DELTA 1.89999999 sec  
TD0 1

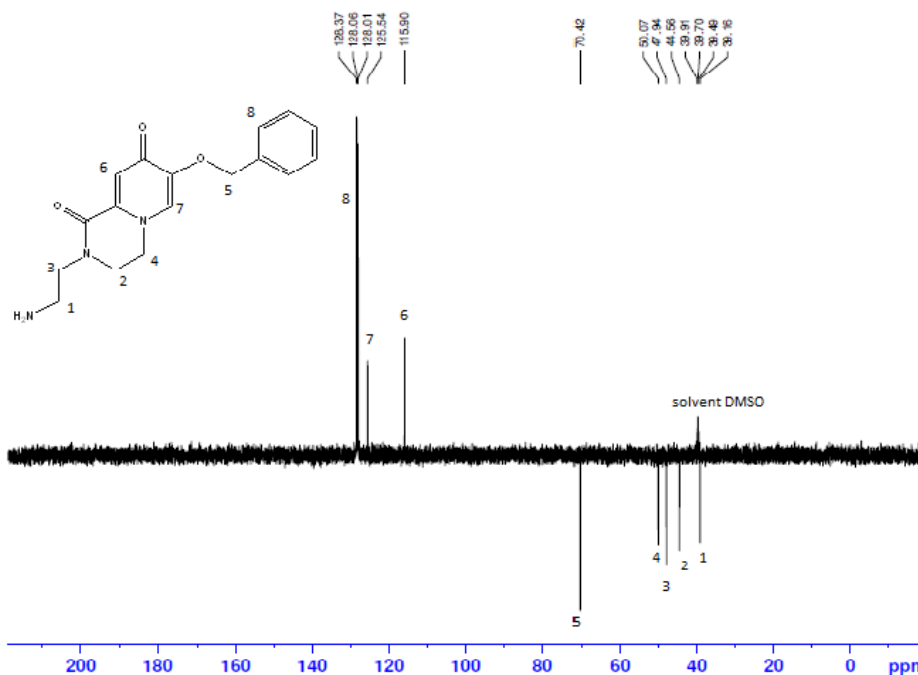
===== CHANNEL F1 =====  
NUC1 13C  
P1 9.50 usec  
PL1 -5.00 dB  
SFO1 100.6228298 MHz

===== CHANNEL F2 =====  
CPDPRG2 waltz16  
NUC2 1H  
PCPD2 80.00 usec  
PL2 -3.00 dB  
PL12 15.28 dB  
PL13 16.00 dB  
SFO2 400.1316005 MHz

F2 - Processing parameters  
SI 32768  
SF 100.6128193 MHz  
WDW BM  
SSB 0  
LB 1.00 Hz  
GB 0  
PC 1.40

11 <sup>13</sup>C-NMR, CR 6 2-(2-aminoethyl)-7-(benzyloxy)-3,4-dihydro-2H-pyrido[1,2-a]pyrazine-1,8-dione

CR6  
C13DEPT135\_noprint.kcl DMSO (C:\Bruker\TOPSPIN) VA 37



Current Data Parameters  
NAME VA\_20150310\_JCA1021  
EXPNO 42  
PROCNO 1

F2 - Acquisition Parameters  
Date\_ 20150310  
Time 12.05  
INSTRUM DRX400  
PROBHD 5 mm QNP 1H/13  
PULPROG zgpg30  
TD 65536  
SOLVENT DMSO  
NS 512  
DS 2  
SWH 24039.441 Hz  
FIDRES 0.366798 Hz  
AQ 1.3632196 sec  
RG 7298.2  
DW 20.800 usec  
DE 6.00 usec  
TE 299.2 K  
CNST2 145.0000000  
D1 2.00000000 sec  
d2 0.00344828 sec  
d12 0.00002000 sec  
FWE1TA 0.00001710 sec  
TD0 1

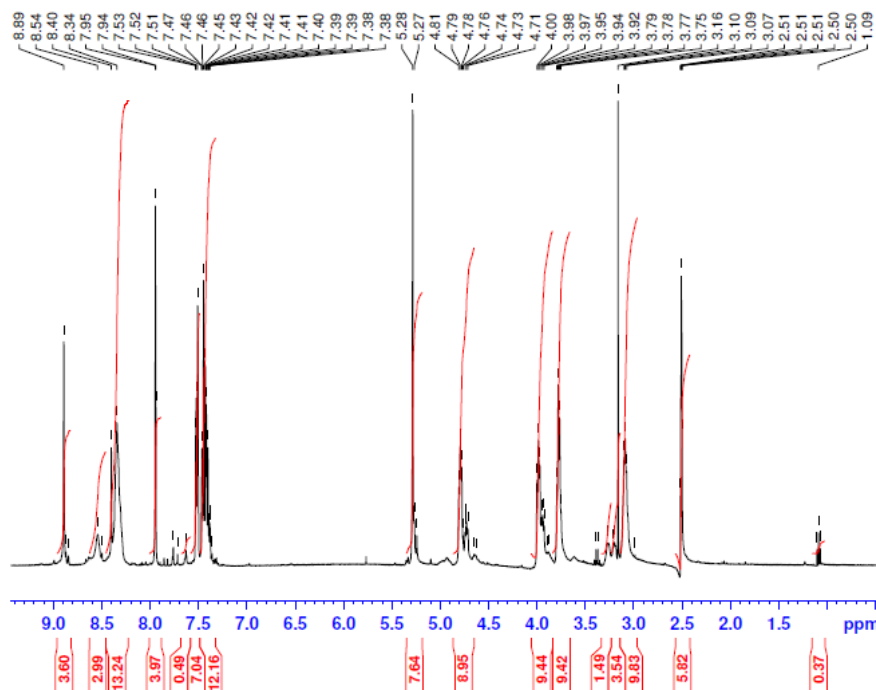
CHANNEL F1  
NUC1 13C  
P1 9.50 usec  
PL1 2000.00 dB  
PL0 120.00 dB  
PL1 100.6228276 MHz  
SFO1 3.60 dB  
SPNAM2 Crp60comp.4  
SPQAL2 0.500  
SFOFFS2 0.00 Hz

CHANNEL F2  
CPDPRG2 waltz16  
NUC2 1H  
P3 9.75 usec  
P4 19.50 usec  
PL2 80.00 usec  
PL2 3.00 dB  
PL12 15.28 dB  
SFO2 400.1316005 MHz

F2 - Processing parameters  
SI 32768  
SF 100.6128193 MHz  
WOW RM  
SSB 0  
LB 1.00 Hz

12 <sup>13</sup>C-NMR DEPT mode, CR 6 2-(2-aminoethyl)-7-(benzyloxy)-3,4-dihydro-2H-pyrido[1,2-a]pyrazine-1,8-dione

CR19.2 BC13  
PROTON\_noprint.kcl DMSO (C:\Bruker\TOPSPIN) VA 37



Current Data Parameters  
NAME VA\_20150528\_JCA1021  
EXPNO 30  
PROCNO 1

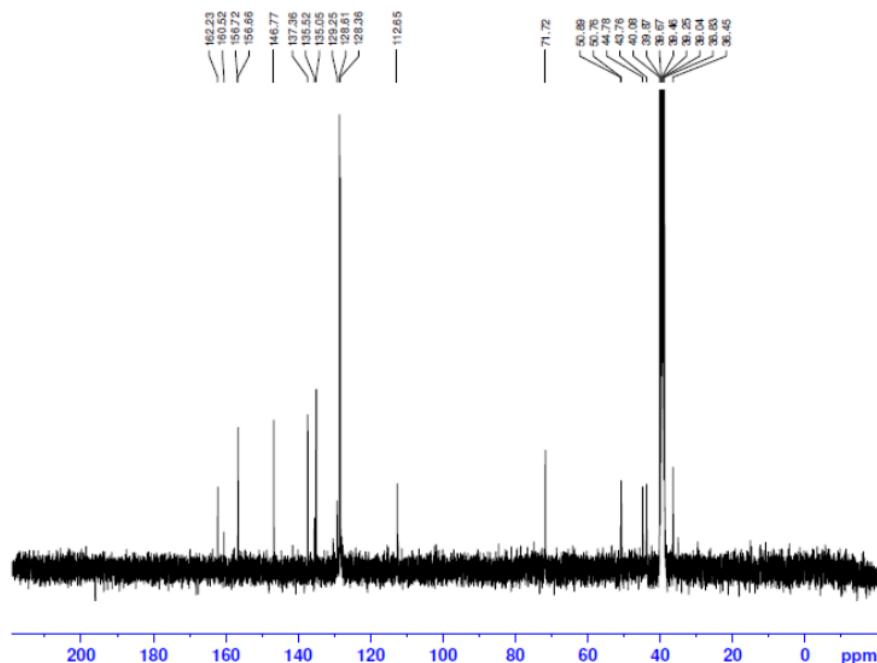
F2 - Acquisition Parameters  
Date\_ 20150528  
Time 15.15  
INSTRUM DRX400  
PROBHD 5 mm QNP 1H/13  
PULPROG zg30  
TD 65536  
SOLVENT DMSO  
NS 16  
DS 0  
SWH 8250.825 Hz  
FIDRES 0.125898 Hz  
AQ 3.9715922 sec  
RG 362  
DW 60.600 usec  
DE 5.00 usec  
TE 297.1 K  
D1 1.00000000 sec  
TD0 1

CHANNEL F1  
NUC1 1H  
P1 10.50 usec  
PL1 -3.00 dB  
SFO1 400.1324710 MHz

F2 - Processing parameters  
SI 65536  
SF 400.1300000 MHz  
WOW RM  
SSB 0  
LB 0.30 Hz  
GB 0  
PC 1.00

13 <sup>1</sup>H-NMR of CR 19 after the treatment with BC13

CR19.2 BCI3  
C13CPD\_noprint.kcl DMSO [C:\Bruker\TOPSPIN] VA 37



Current Data Parameters  
NAME VA\_20150528\_JCA1021  
EXPNO 32  
PROCNO 1

F2 - Acquisition Parameters  
Date\_ 20150528  
Time 16.39  
INSTRUM DRX400  
PROBHD 5 mm QNP 1H/13  
PULPROG zgpg30  
TD 65536  
SOLVENT DMSO  
NS 512  
DS 4  
SWH 24039.461 Hz  
FIDRES 0.366798 Hz  
AQ 1.3632196 sec  
RG 1024  
DW 20.800 usec  
DE 6.00 usec  
TE 297.3 K  
D1 2.00000000 sec  
d11 0.03000000 sec  
DELTA 1.89999998 sec  
TD0 1

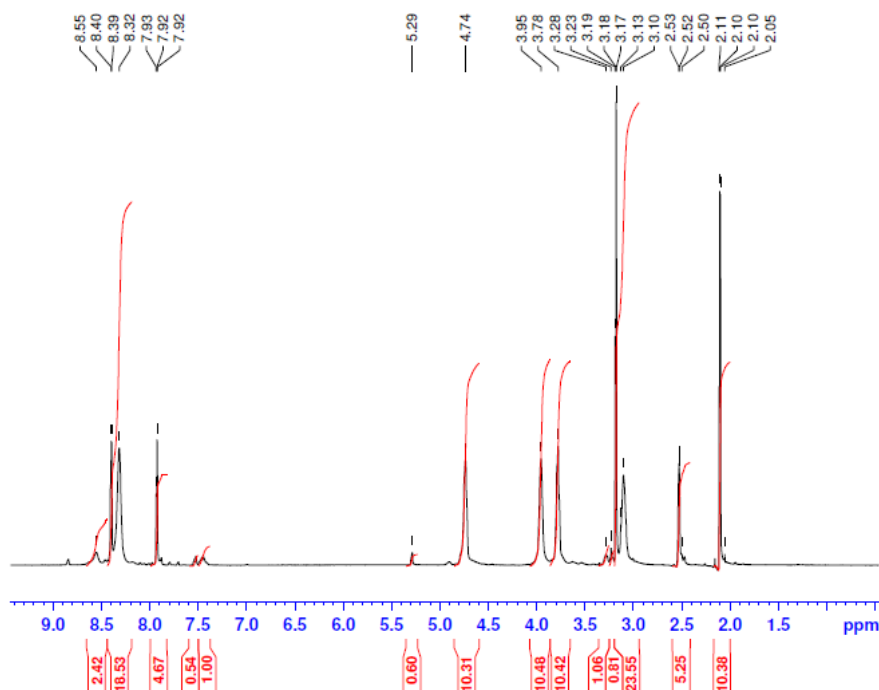
===== CHANNEL f1 =====  
NUC1 13C  
P1 9.50 usec  
PL1 -5.00 dB  
SFO1 100.6228298 MHz

===== CHANNEL f2 =====  
CPDPRG2 waltz16  
NUC2 1H  
PCPD2 80.00 usec  
PL2 3.00 dB  
PL12 15.28 dB  
PL13 16.00 dB  
SFO2 400.1316005 MHz

F2 - Processing parameters  
SI 32768  
SF 100.6128193 MHz  
WDW EM  
SSB 0  
LB 1.00 Hz  
GB 0  
PC 1.40

14 <sup>13</sup>C-NMR of CR 19 after the treatment with BCI3

CR19  
PROTON\_noprint.kcl DMSO [C:\Bruker\TOPSPIN] VA 18



Current Data Parameters  
NAME VA\_20150528\_JCA1021  
EXPNO 10  
PROCNO 1

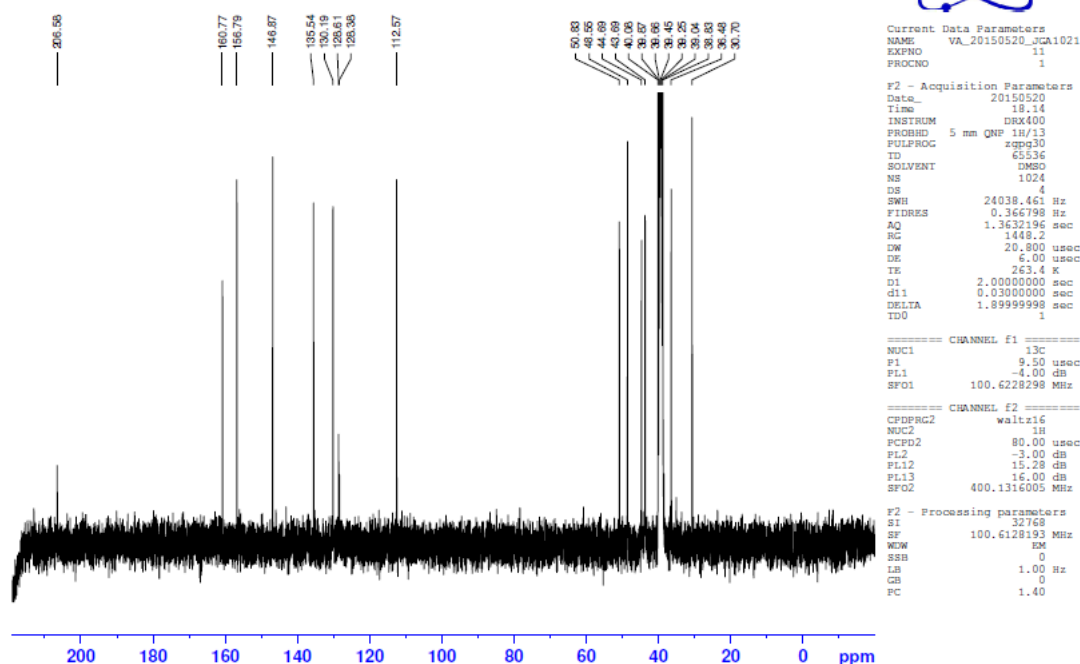
F2 - Acquisition Parameters  
Date\_ 20150520  
Time 17.14  
INSTRUM DRX400  
PROBHD 5 mm QNP 1H/13  
PULPROG zg30  
TD 65536  
SOLVENT DMSO  
NS 16  
DS 0  
SWH 8250.825 Hz  
FIDRES 0.125898 Hz  
AQ 3.9715922 sec  
RG 203.2  
DW 60.600 usec  
DE 5.00 usec  
TE 263.3 K  
D1 1.00000000 sec  
TD0 1

===== CHANNEL f1 =====  
NUC1 1H  
P1 10.50 usec  
PL1 -3.00 dB  
SFO1 400.1324710 MHz

F2 - Processing parameters  
SI 65536  
SF 400.1300000 MHz  
WDW EM  
SSB 0  
LB 0.30 Hz  
GB 0  
PC 1.00

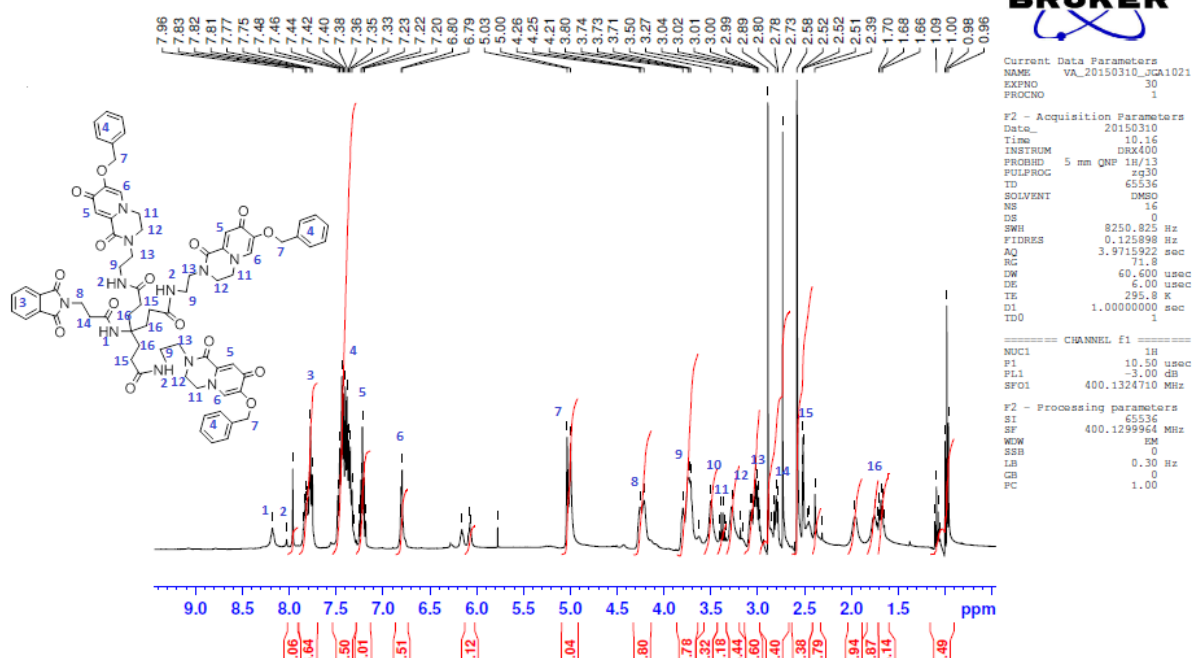
15 <sup>1</sup>H-NMR of CR 19 after the treatment with 5% Pd/C

CR19  
C13CPD\_noprint.kcl DMSO (C:\Bruker\TOPSPIN) VA 18

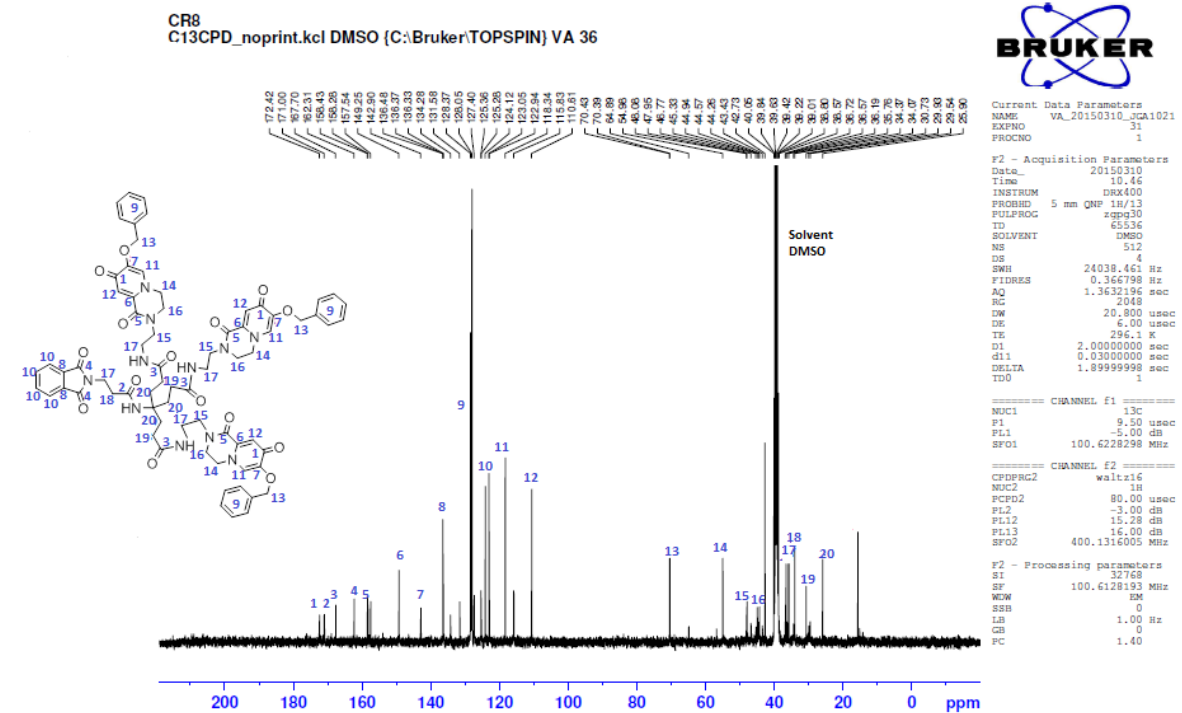


16 C-NMR of CR 19 after the treatment with 5% Pd/C

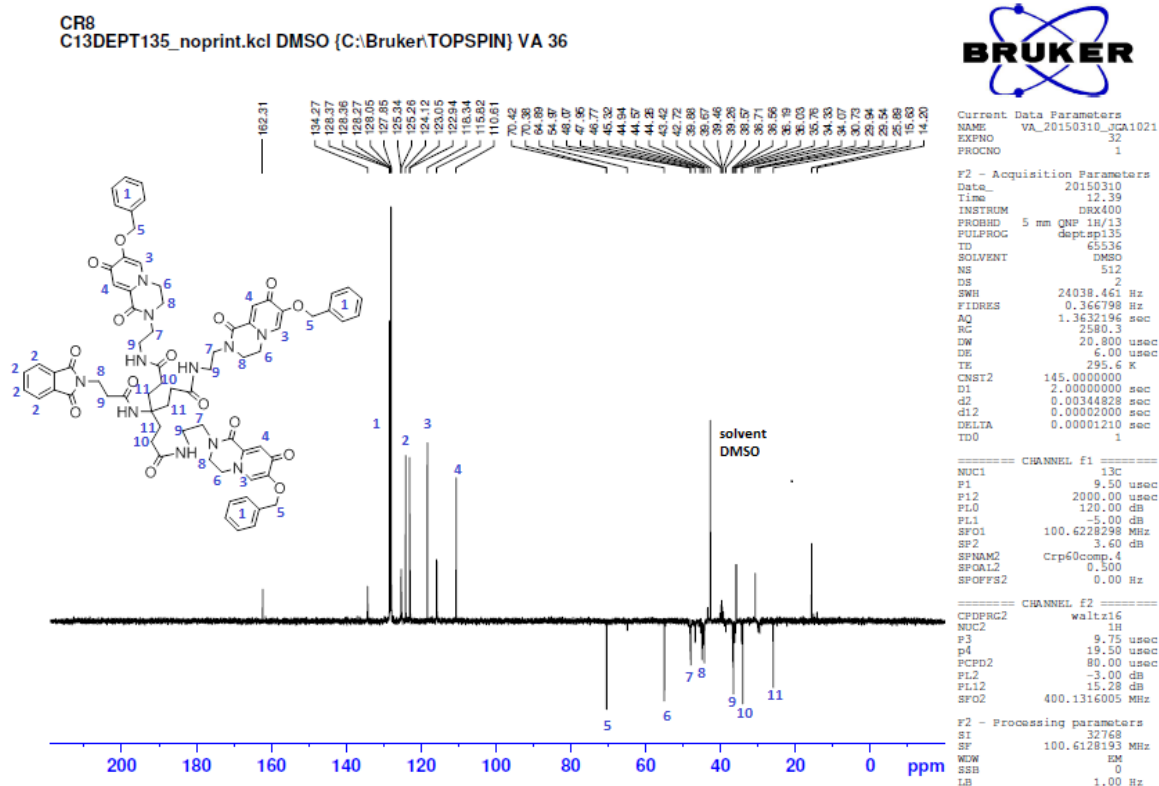
CR8  
PROTON\_noprint.kcl DMSO (C:\Bruker\TOPSPIN) VA 36



17 <sup>1</sup>H-NMR of CR 8, N1,N7-bis(2-(7-(benzyloxy)-1,8-dioxo-1,3,4,8-tetrahydro-2H-pyrido[1,2-a]pyrazin-2-yl)ethyl)-4-(3-((2-(7-(benzyloxy)-1,8-dioxo-1,3,4,8-tetrahydro-2H-pyrido[1,2-a]pyrazin-2-yl)amino)-3-oxopropyl)-4-(3-(1,3-dioxoisindolin-2-yl)propanamido)heptanediamide



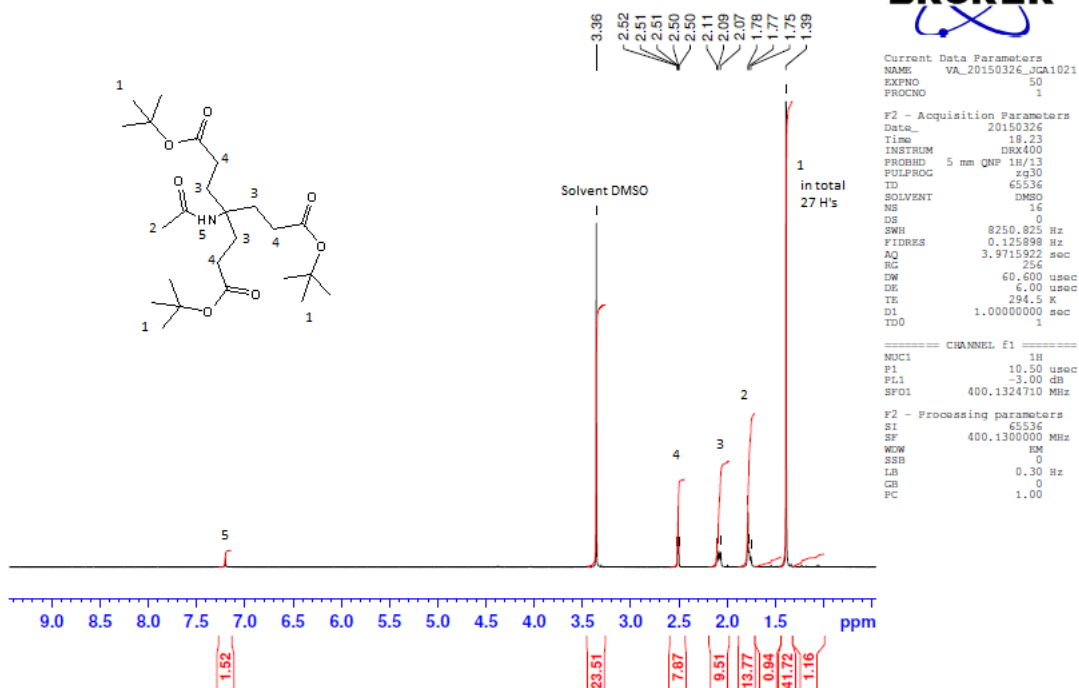
18 <sup>13</sup>C-NMR CR 8, N1,N7-bis(2-(7-(benzyloxy)-1,8-dioxo-1,3,4,8-tetrahydro-2H-pyrido[1,2-a]pyrazin-2-yl)ethyl)-4-(3-((2-(7-(benzyloxy)-1,8-dioxo-1,3,4,8-tetrahydro-2H-pyrido[1,2-a]pyrazin-2-yl)ethyl)amino)-3-oxopropyl)-4-(3-(1,3-dioxoisindolin-2-yl)propanamido)heptanediamide



19 <sup>13</sup>C-NMR DEPT mode CR 8, N1,N7-bis(2-(7-(benzyloxy)-1,8-dioxo-1,3,4,8-tetrahydro-2H-pyrido[1,2-a]pyrazin-2-yl)ethyl)-4-(3-((2-(7-(benzyloxy)-1,8-dioxo-1,3,4,8-tetrahydro-2H-pyrido[1,2-a]pyrazin-2-yl)ethyl)amino)-3-oxopropyl)-4-(3-(1,3-dioxoisindolin-2-yl)propanamido)heptanediamide

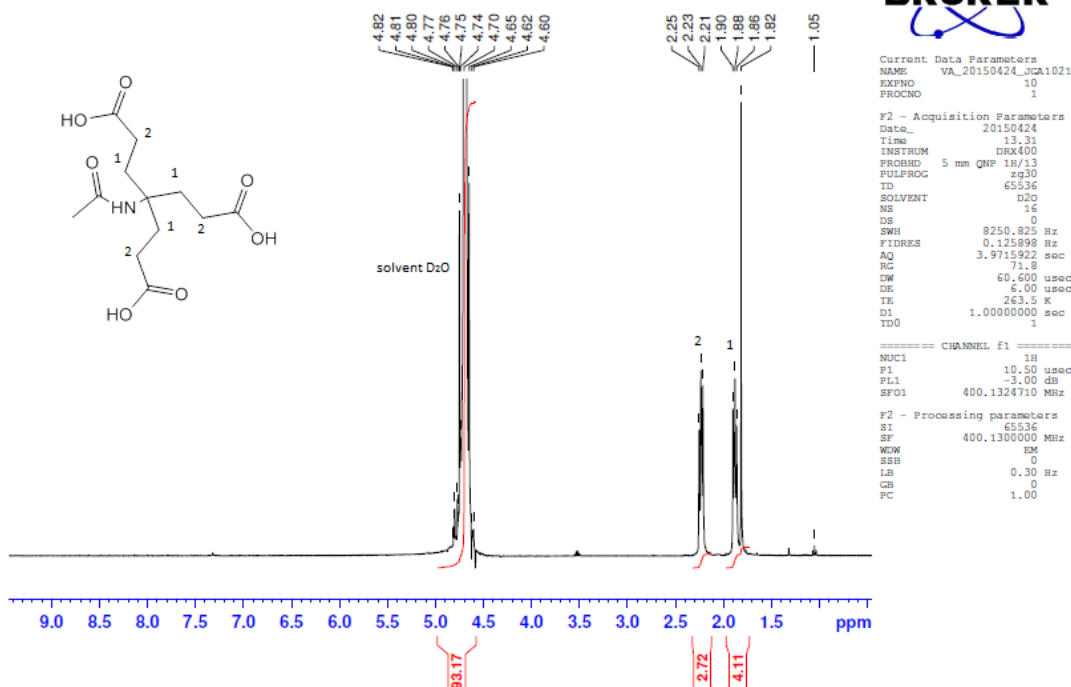


CR14  
PROTON\_noprint.kcl DMSO (C:\Bruker\TOPSPIN) VA 17

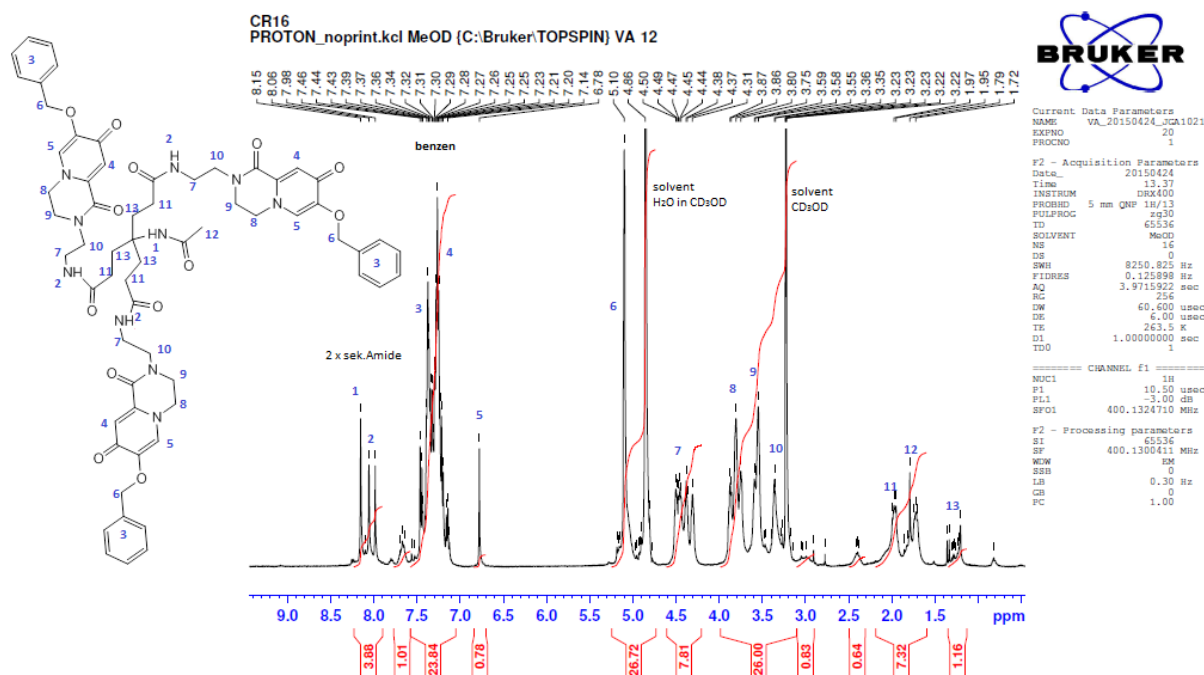


20 <sup>1</sup>H-NMR of CR 14, di-tert-butyl 4-acetamido-4-(3-(tert-butoxy)-3-oxopropyl)heptanedioate

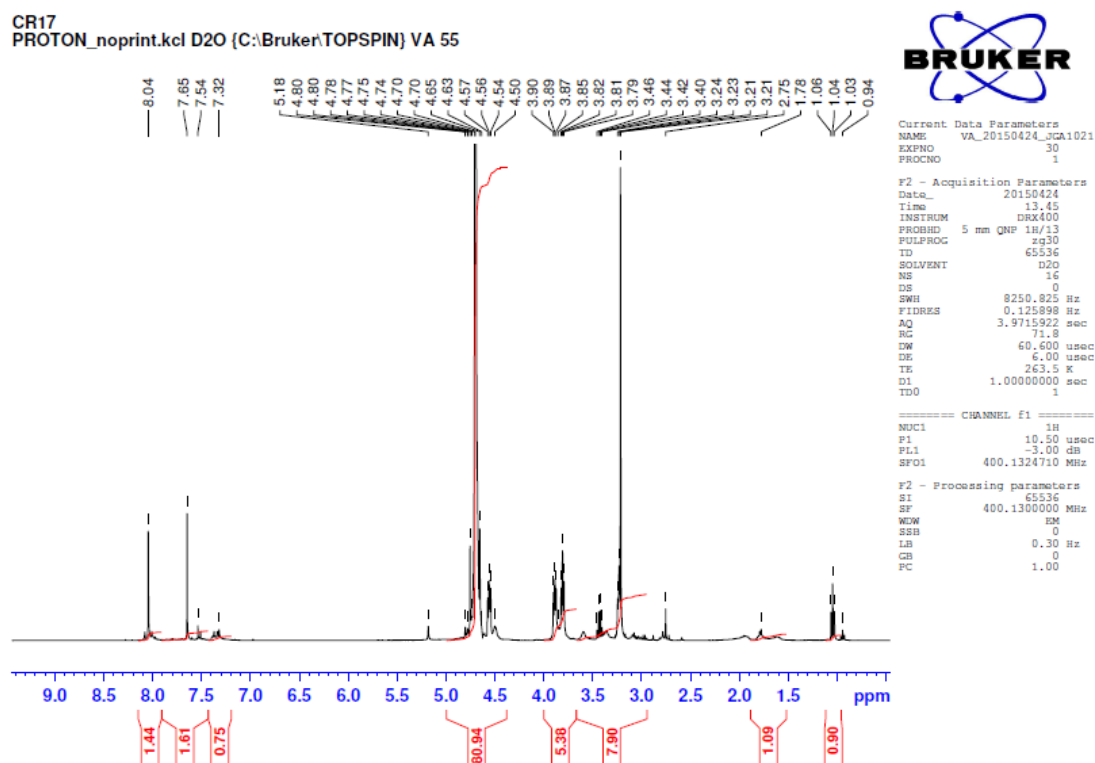
CR15  
PROTON\_noprint.kcl D2O (C:\Bruker\TOPSPIN) VA 11



21 <sup>1</sup>H-NMR of CR 15, 4-acetyl-amido-4-(2-carboxyethyl)heptanedioic acid

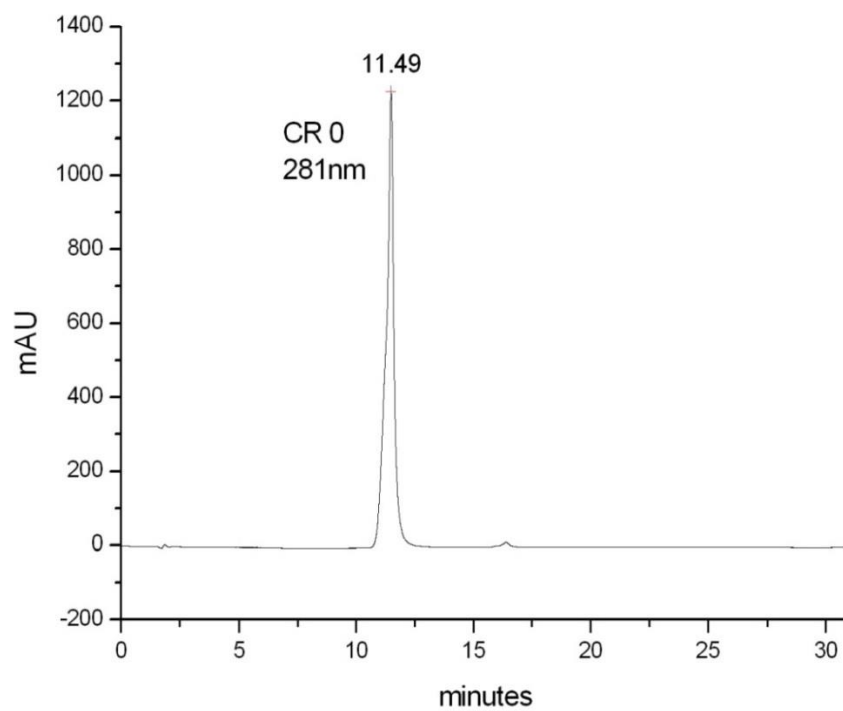


22 <sup>1</sup>H-NMR of CR 16 4-acetamido-N1,N7-bis(2-(7-(benzyloxy)-1,8-dioxo-1,3,4,8-tetrahydro-2H-pyrido[1,2-a]pyrazin-2-yl)ethyl)-4-(3-((2-(7-(benzyloxy)-1,8-dioxo-1,3,4,8-tetrahydro-2H-pyrido[1,2-a]pyrazin-2-yl)ethyl)amino)-3-oxopropyl)heptanediamide

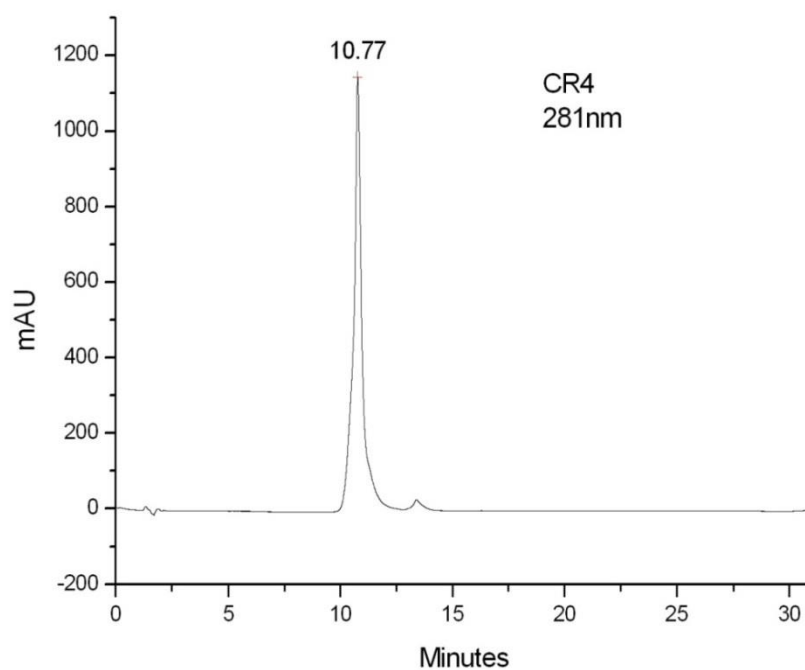


23 <sup>1</sup>H-NMR of CR 17, 4-acetamido-N1,N7-bis(2-(7-hydroxy-1,8-dioxo-1,3,4,8-tetrahydro-2H-pyrido[1,2-a]pyrazin-2-yl)ethyl)-4-(3-((2-(7-hydroxy-1,8-dioxo-1,3,4,8-tetrahydro-2H-pyrido[1,2-a]pyrazin-2-yl)ethyl)amino)-3-oxopropyl)heptanediamide

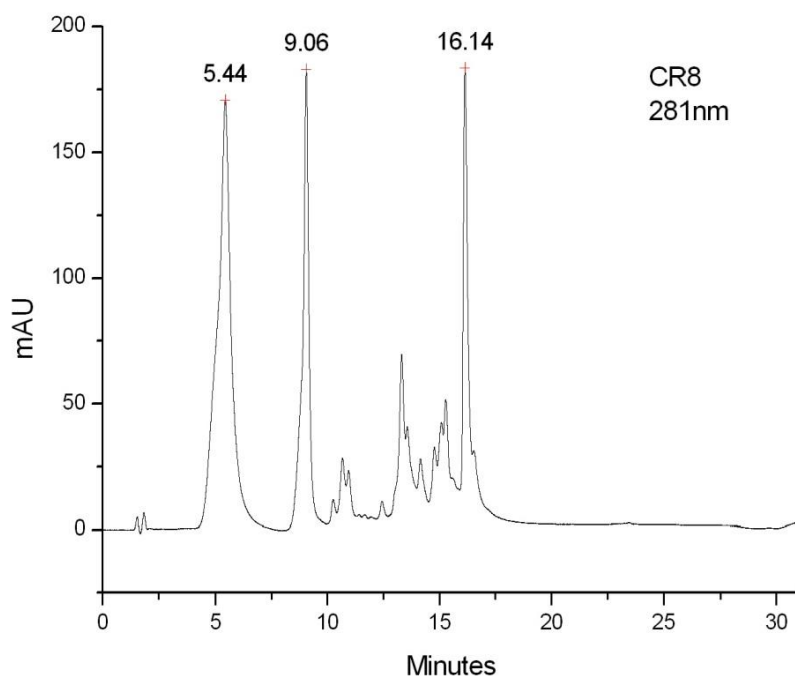
## HPLC selected data



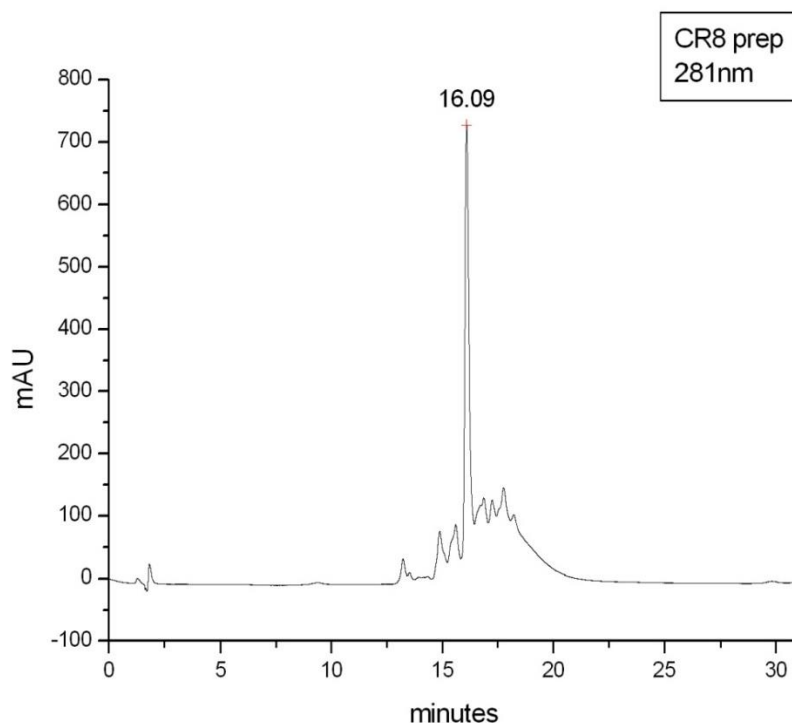
24 HPLC CR 0 5-benzyloxy-2-hydroxymethyl-4H-pyran-4-one



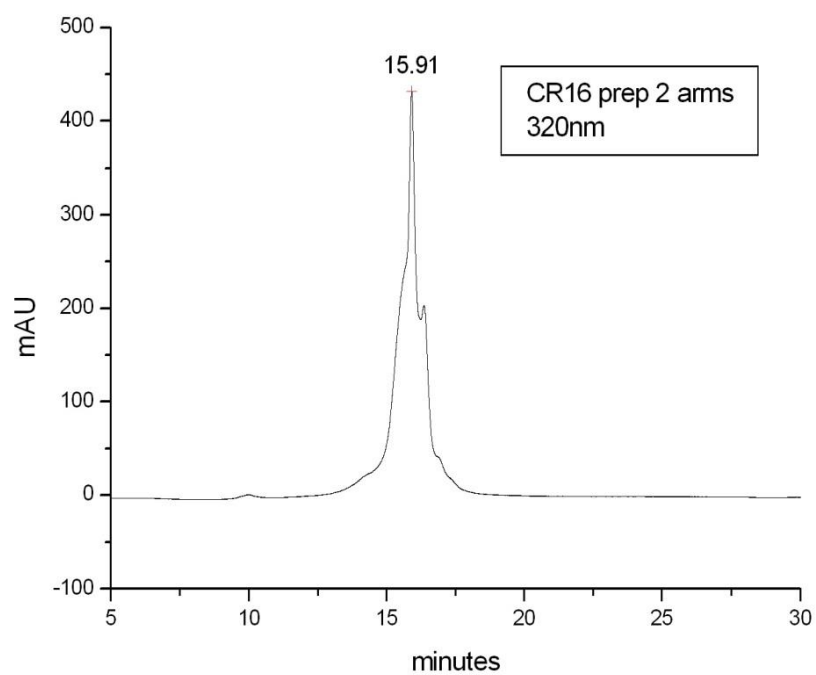
25 HPLC of CR 4, 5-(benzyloxy)-4-oxo-4H-pyran-2-carboxylic acid



**26 HPLC of CR 8, N1,N7-bis(2-(7-(benzyloxy)-1,8-dioxo-1,3,4,8-tetrahydro-2H-pyrido[1,2-a]pyrazin-2-yl)ethyl)-4-(3-((2-(7-(benzyloxy)-1,8-dioxo-1,3,4,8-tetrahydro-2H-pyrido[1,2-a]pyrazin-2-yl)ethyl)amino)-3-oxopropyl)-4-(3-(1,3-dioxoisindolin-2-yl)propanamido)heptanediamide**



**27 HPLC of CR 8 after prep. HPLC, N1,N7-bis(2-(7-(benzyloxy)-1,8-dioxo-1,3,4,8-tetrahydro-2H-pyrido[1,2-a]pyrazin-2-yl)ethyl)-4-(3-((2-(7-(benzyloxy)-1,8-dioxo-1,3,4,8-tetrahydro-2H-pyrido[1,2-a]pyrazin-2-yl)ethyl)amino)-3-oxopropyl)-4-(3-(1,3-dioxoisindolin-2-yl)propanamido)heptanediamide after prep.HPLC**



**28 HPLC of CR 16, 4-acetamido-N1,N7-bis(2-(7-(benzyloxy)-1,8-dioxo-1,3,4,8-tetrahydro-2H-pyrido[1,2-a]pyrazin-2-yl)ethyl)-4-(3-((2-(7-(benzyloxy)-1,8-dioxo-1,3,4,8-tetrahydro-2H-pyrido[1,2-a]pyrazin-2-yl)ethyl)amino)-3-oxopropyl)heptanediamide**

## References

- Altamura, S., & Muckenthaler, M. U. (2009). Iron toxicity in diseases of aging: Alzheimer's disease, Parkinson's disease and atherosclerosis. *Journal of Alzheimer's Disease : JAD*, 16(4), 879–95. <http://doi.org/10.3233/JAD-2009-1010>
- Berry, D. J., Ma, Y., Ballinger, J. R., Tavaré, R., Koers, A., Sunassee, K., ... Blower, P. J. (2011). Efficient bifunctional gallium-68 chelators for positron emission tomography: tris(hydroxypyridinone) ligands. *Chemical Communications (Cambridge, England)*, 47(25), 7068–70. <http://doi.org/10.1039/c1cc12123e>
- Beutler, E., Hoffbrand, a V., & Cook, J. D. (2003). Iron deficiency and overload. *Hematology / the Education Program of the American Society of Hematology. American Society of Hematology. Education Program*, 40–61. <http://doi.org/10.1182/asheducation-2003.1.40>
- Boddaert, N., Sang, K. H. L. Q., Rötig, A., Leroy-Willig, A., Gallet, S., Brunelle, F., ... Cabantchik, Z. I. (2007). Selective iron chelation in Friedreich ataxia: Biologic and clinical implications. *Blood*, 110(1), 401–408. <http://doi.org/10.1182/blood-2006-12-065433>
- Cacciatore, I., Baldassarre, L., Fornasari, E., Mollica, A., & Pinnen, F. (2012). Recent advances in the treatment of neurodegenerative diseases based on GSH delivery systems. *Oxidative Medicine and Cellular Longevity*, 2012(12), 240146. <http://doi.org/10.1155/2012/240146>
- Camaschella, C., & Strati, P. (2010). Recent advances in iron metabolism and related disorders. *Internal and Emergency Medicine*, 5(5), 393–400. <http://doi.org/10.1007/s11739-010-0387-4>
- Cappellini, M. D., & Pattoneri, P. (2009). Oral iron chelators. *Annual Review of Medicine*, 60, 25–38. <http://doi.org/10.1146/annurev.med.60.041807.123243>
- Dubey, a P., Sudha, S., & Parakh, A. (2007). Deferasirox: the new oral iron chelator. *Indian Pediatrics*, 44(8), 603–607.
- Fakih, S., Podinovskaia, M., Kong, X., Collins, H. L., Schaible, U. E., & Hider, R. C. (2008). Targeting the lysosome: fluorescent iron(III) chelators to selectively monitor endosomal/lysosomal labile iron pools. *Journal of Medicinal Chemistry*, 51(15), 4539–52. <http://doi.org/10.1021/jm8001247>
- Fluorescence Quantum Yield Measurements | HORIBA Jobin Yvon - HORIBA. (n.d.). Retrieved December 11, 2015, from <http://www.horiba.com/scientific/products/fluorescence-spectroscopy/application-notes/quantum-yields/>
- Gaeta, A., & Hider, R. C. (2005). The crucial role of metal ions in neurodegeneration: the basis for a promising therapeutic strategy. *British Journal of Pharmacology*, 146(8), 1041–1059. <http://doi.org/10.1038/sj.bjp.0706416>
- Galanello, R. (2007). Deferiprone in the treatment of transfusion-dependent thalassemia: a review and perspective. *Therapeutics and Clinical Risk Management*, 3(5), 795–805. Retrieved from <http://www.pubmedcentral.nih.gov/articlerender.fcgi?artid=2376085&tool=pmcentrez&rendertype=abstract>
- Gardens, D., Ha, M., & Fax, B. Q. U. K. (n.d.). A guide to recording quantum yields.
- Gattermann, N. (2009). The treatment of secondary hemochromatosis. *Deutsches Ärzteblatt International*, 106(30), 499–504, I. <http://doi.org/10.3238/arztebl.2009.0499>
- Gille, G., & Reichmann, H. (2011). Iron-dependent functions of mitochondria--relation to neurodegeneration. *Journal of Neural Transmission (Vienna, Austria : 1996)*, 118, 349–359. <http://doi.org/10.1007/s00702-010-0503-7>

- Gkouvatsos, K., Papanikolaou, G., & Pantopoulos, K. (2012). Regulation of iron transport and the role of transferrin. *Biochimica et Biophysica Acta (BBA) - General Subjects*, 1820(3), 188–202. <http://doi.org/10.1016/j.bbagen.2011.10.013>
- Hatcher, H. C., Singh, R. N., Torti, F. M., & Torti, S. V. (2009). Synthetic and natural iron chelators: therapeutic potential and clinical use. *Future Medicinal Chemistry*, 1(9), 1643–70. <http://doi.org/10.4155/fmc.09.121>
- Hersch, S. M., & Rosas, H. D. (2008). Neuroprotection for Huntington's disease: ready, set, slow. *Neurotherapeutics : The Journal of the American Society for Experimental NeuroTherapeutics*, 5(2), 226–36. <http://doi.org/10.1016/j.nurt.2008.01.003>
- Hershko, C., Konijn, A. M., & Link, G. (1998). Iron Chelators for Thalassaemia. *British Journal of Haematology*, 101(3), 399–406. <http://doi.org/10.1046/j.1365-2141.1998.00726.x>
- Hider, R. C. (1995). Potential protection from toxicity by oral iron chelators. *Toxicology Letters*, 82-83, 961–967. [http://doi.org/10.1016/0378-4274\(95\)03606-7](http://doi.org/10.1016/0378-4274(95)03606-7)
- Hider, R. C., & Kong, X. (2010). Chemistry and biology of siderophores. *Natural Product Reports*, 27(5), 637. <http://doi.org/10.1039/b906679a>
- Hider, R. C., Ma, Y., Molina-Holgado, F., Gaeta, A., & Roy, S. (2008). Iron chelation as a potential therapy for neurodegenerative disease. *Biochemical Society Transactions*, 36(Pt 6), 1304–8. <http://doi.org/10.1042/BST0361304>
- Hider, R. C., Roy, S., Ma, Y. M., Le Kong, X., & Preston, J. (2011). The potential application of iron chelators for the treatment of neurodegenerative diseases. *Metallomics : Integrated Biometal Science*, 3(3), 239–249. <http://doi.org/10.1039/c0mt00087f>
- Jang, J. H., Lee, J.-H., Yoon, S.-S., Jo, D.-Y., Kim, H.-J., Chung, J., & Lee, J. W. (2013). Korean guideline for iron chelation therapy in transfusion-induced iron overload. *Journal of Korean Medical Science*, 28(11), 1563–72. <http://doi.org/10.3346/jkms.2013.28.11.1563>
- Jomova, K., & Valko, M. (2011). Importance of iron chelation in free radical-induced oxidative stress and human disease. *Current Pharmaceutical Design*, 17(31), 3460–73. Retrieved from <http://www.ncbi.nlm.nih.gov/pubmed/21902663>
- Jomova, K., Vondrakova, D., Lawson, M., & Valko, M. (2010). Metals, oxidative stress and neurodegenerative disorders. *Molecular and Cellular Biochemistry*, 345(1-2), 91–104. <http://doi.org/10.1007/s11010-010-0563-x>
- Kohgo, Y., Ikuta, K., Ohtake, T., Torimoto, Y., & Kato, J. (2008). Body iron metabolism and pathophysiology of iron overload. *International Journal of Hematology*, 88(1), 7–15. <http://doi.org/10.1007/s12185-008-0120-5>
- Kwiatkowski, J. L. (2008). Oral iron chelators. *Pediatric Clinics of North America*, 55(2), 461–82, x. <http://doi.org/10.1016/j.pcl.2008.01.005>
- Liu, Z. D., & Hider, R. C. (2002a). Design of clinically useful iron(III)-selective chelators. *Medicinal Research Reviews*, 22(1), 26–64. <http://doi.org/10.1002/med.1027>
- Liu, Z. D., & Hider, R. C. (2002b). Design of iron chelators with therapeutic application. *Coordination Chemistry Reviews*, 232(1-2), 151–171. [http://doi.org/10.1016/S0010-8545\(02\)00050-4](http://doi.org/10.1016/S0010-8545(02)00050-4)
- Liu, Z. D., Kayyali, R., Hider, R. C., Porter, J. B., & Theobald, A. E. (2002). Design, synthesis, and evaluation of novel 2-substituted 3-hydroxypyridin-4-ones: structure-activity investigation of metalloenzyme inhibition by iron chelators. *Journal of Medicinal Chemistry*, 45(3), 631–9. Retrieved from <http://www.ncbi.nlm.nih.gov/pubmed/11806714>

- Ma, Y., Abbate, V., & Hider, R. C. (2015). Iron-sensitive fluorescent probes: monitoring intracellular iron pools. *Metallomics : Integrated Biometal Science*, 7(2), 212–22. <http://doi.org/10.1039/c4mt00214h>
- Ma, Y., Kong, X., Abbate, V., & Hider, R. C. (2015). Synthesis and characterization of novel iron-specific bicyclic fluorescent probes. *Sensors and Actuators B: Chemical*, 213, 12–19. <http://doi.org/10.1016/j.snb.2015.02.072>
- Ma, Y., Luo, W., Camplo, M., Liu, Z., & Hider, R. C. (2005). Novel iron-specific fluorescent probes. *Bioorganic & Medicinal Chemistry Letters*, 15(14), 3450–2. <http://doi.org/10.1016/j.bmcl.2005.05.010>
- Ma, Y., Luo, W., Quinn, P. J., Liu, Z., & Hider, R. C. (2004). Design, synthesis, physicochemical properties, and evaluation of novel iron chelators with fluorescent sensors. *Journal of Medicinal Chemistry*, 47(25), 6349–62. <http://doi.org/10.1021/jm049751s>
- Molina-Holgado, F., Hider, R. C., Gaeta, A., Williams, R., & Francis, P. (2007). Metals ions and neurodegeneration. *BioMetals*, 20(3-4), 639–654. <http://doi.org/10.1007/s10534-006-9033-z>
- Neufeld, E. J. (2006). Oral chelators deferasirox and deferiprone for transfusional iron overload in thalassemia major : new data , new questions, 107(9), 3436–3441. <http://doi.org/10.1182/blood-2006-02-002394>.Supported
- Oshiro, S., Morioka, M. S., & Kikuchi, M. (2011). Dysregulation of iron metabolism in Alzheimer's disease, Parkinson's disease, and amyotrophic lateral sclerosis. *Advances in Pharmacological Sciences*, 2011, 378278. <http://doi.org/10.1155/2011/378278>
- Papanikolaou, G., & Pantopoulos, K. (2005). Iron metabolism and toxicity. *Toxicology and Applied Pharmacology*, 202(2), 199–211. <http://doi.org/10.1016/j.taap.2004.06.021>
- Saghaie, L., Sadeghi, M. M., & Nikazma, A. (2006). Synthesis , analysis and determination of partition coefficients of N-arylhydroxypyridinone derivatives as iron chelators. *Res. Pharm. Sci.*, 1(1), 40–48.
- Tilbrook, G. S., & Hider, R. C. (1998). Iron chelators for clinical use. *Metal Ions in Biological Systems*, 35, 691–730. Retrieved from <http://www.ncbi.nlm.nih.gov/pubmed/9444773>
- Zhou, T., Neubert, H., Liu, D. Y., Liu, Z. D., Ma, Y. M., Kong, X. Le, ... Hider, R. C. (2006). Iron binding dendrimers: a novel approach for the treatment of haemochromatosis. *Journal of Medicinal Chemistry*, 49(14), 4171–82. <http://doi.org/10.1021/jm0600949>



## List of Abbreviations

°C – Degrees Celsius  
μL – Micro litre  
μM – Micro molar  
<sup>13</sup>C-NMR – Carbon-13 nuclear magnetic resonance  
<sup>1</sup>H-NMR – Proton-1 nuclear magnetic resonance  
AA – Acetic acid  
AD – Alzheimer's disease  
ALS – Amyotrophic Lateral Sclerosis  
APP – Amyloid-β precursor protein  
ATXN2 – Ataxin 2  
BCl<sub>3</sub> – Borontrichloride  
BnCl – Benzyl chloride  
C – Carbon  
CC – Column chromatography  
CHCl<sub>3</sub> – Chloroform  
d – Deuterated  
D – Deuterium  
D<sub>2</sub>O – Deuterated water  
DCC – Dicyclohexylcarbodiimide  
DCM – Dichloromethane  
DFO – Desferrioxamine  
DFP – Deferiprone  
DIPEA – *N,N*-Diisopropylethylamine  
DMF – Dimethylformamide  
DMSO – Dimethyl sulfoxide  
DNA – Desoxyribonucleic acid  
EDC – 1-Ethyl-3-(3-dimethylaminopropyl)carbodiimide  
eq – Equivalent  
ESI-MS – Electrospray ionization mass spectrometry  
EtOAc – Ethyl acetate  
EtOH – Ethanol  
FA – Friedreich's ataxia or formic acid  
FXN – Frataxin  
g – Gram  
GSH – Glutathione  
h – Hour  
H<sub>2</sub>O – Water  
H<sub>2</sub>SO<sub>4</sub> – Sulfuric acid  
HATU – 2-(1H-7-Azabenzotriazol-1-yl)-1,1,3,3-tetramethyl uronium hexafluorophosphate  
HCl – Hydrochloric acid  
HD – Huntington's disease  
HFE – High Iron Fe (human hemochromatosis protein)  
HH – Hereditary hemochromatosis  
HOBt – Hydroxybenzotriazole  
HPLC – High pressure liquid chromatography  
HPO – 3-Hydroxypyridin-4-one  
IRE – Iron responding elements  
K<sub>a</sub> – Acid dissociation constant  
KCL – King's College London

KOH – Potassium hydroxide  
L – Ligand or litre  
LIP – Labile iron pool  
M – Molar  
m/z – Mass-to-charge ratio  
MeOD – Deuterated methanol  
MeOH – Methanol  
mL – Millilitre  
mM – Milli molar, mMol/Litre  
mMol – Milli mole  
MOPS – 3-(*N*-morpholino)propanesulfonic acid  
mRNA – Messenger ribonucleic acid  
MS – Mass spectrometry  
MW – Molecular weight  
Na<sub>2</sub>SO<sub>4</sub> – Sodium sulfate  
NaCl – Sodium chloride  
NaHCO<sub>3</sub> – Sodium bicarbonate  
NaOH – Sodium hydroxide  
ND – Neurodegenerative disorders or not determined  
NFTs – Neurofibrillary tangles  
nm – Nano meter  
NTBI – Non-transferrin-bound-iron  
Pd – Palladium  
PD – Parkinson's Disease  
pK<sub>a</sub> – the negative decadic logarithm of the ionization constant of an acid  
ppm – Parts per million  
ROS – Reactive oxygen species  
RP-HPLC – Reversed phase high pressure liquid chromatography  
RT – Retention time or room temperature  
SN – Substantia Nigra  
SOD1 – Superoxide dismutase 1  
Tf – Transferrin  
TFA – Trifluoroacetic acid  
TfR1 – Transferrin receptor 1  
TLC – Thin layer chromatography  
UV/Vis – Ultraviolet-visible

# Curriculum Vitae

Name: Carmen Rainer

Date of birth: 15 October 1989

Place of birth: Salzburg

Nationality: Austria

Address: Hardtgasse 32/2 1190 Vienna

## Education

September 1996 - June 2000	Elementary School, Volksschule Kreindlgasse 24, 1190 Vienna
September 2000 - June 2008	Secondary School, Döblinger Gymnasium, Gymnasiumstraße 83, 1190 Vienna

## Academic Studies

Since October 2008	Diploma Study Pharmacy at the University of Vienna, Althanstraße 1090 Vienna
February 2015 - July 2015	Erasmus study at King's College London, Franklin Wilkins Building, Waterloo Campus
	Diploma thesis research project

## Work Experience

September 2010 - January 2015 and September 2015 until now	Employee at Apotheke zum Heiligen Geist, 1010 Vienna
August 2015	Internship at Apotheke zum Lachenden Pinguin, 1120 Vienna

## Language Skills

English, fluent in speech and writing

Spanish, fluent in speech

French, moderate

German, native



## To Whom It May Concern by Professor R.C. Hider

School of Biomedical  
Sciences  
Institute of Pharmaceutical  
Science

Professor Robert Hider  
Emeritus Professor  
of Medicinal Chemistry

Franklin-Wilkins Building  
150 Stamford Street  
London SE1 9NH  
Tel +44 (0)20 7848 4882  
E-mail: robert.hider@kcl.ac.uk



27.11.2015

To whom it may concern

**Carmen Rainer**

Carmen Rainer worked with the Medicinal Chemistry Group at King's College London under the supervision of Professor R. C. Hider for the period February-July 2015. She joined a project centred on the design of iron sensitive fluorescence sensors. These compounds are being developed in order to quantify iron in the cytosol and mitochondrial matrix.

Carmen worked with enthusiasm in the laboratory and was unlucky not to isolate the hexadentate chelator. The bidentate fluorescent chelator, prepared and characterised for the first time by Carmen will be of considerable use to the Medical Chemistry Group at KCL. During her time here in London, she gained practical experience with fluorescence, NMR, HPLC and MS.

Her project work deserves a high rating.

A handwritten signature in black ink, appearing to be "R.C. Hider", written over a light blue grid background.

R C Hider  
Professor of Medicinal Chemistry